

STRUCTURE AND DYNAMIC PROPERTIES
OF TRABECULAR BONE

by

JAMES WHITWORTH PUGH

S.B., Massachusetts Institute of Technology

(1968)

Submitted in Partial Fulfillment of the Requirements

for the Degree of

DOCTOR OF PHILOSOPHY

at the

Massachusetts Institute of Technology

May 1972

Signature of Author . . .

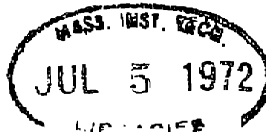
Department of Metallurgy and Materials Science
May 5, 1972

Certified by

Thesis Supervisor

Accepted by

Chairman, Departmental Committee on Graduate Students



STRUCTURE AND DYNAMIC PROPERTIES
OF TRABECULAR BONE

by

JAMES WHITWORTH PUGH

Submitted to the Department of Metallurgy and Materials Science
on May 5, 1972, in partial fulfillment of the requirements for
the degree of Doctor of Philosophy.

.....

ABSTRACT

Trabecular bone was studied both microscopically using metallographic techniques and mechanically, under cyclic sinusoidal loading at low strain-rates and small deformations. Special attention was paid to the function of trabecular bone as a stress distributor and shock-absorber, and to the relationship between structure-property changes in trabecular bone and the etiology of osteoarthritis.

Under conditions of very small deformation and low strain-rate, trabecular bone from the human knee behaves purely elastically in the low audio range, except at several sharp frequencies where it exhibits marked viscous behavior. These resonances are believed to be controlled by momentum-wave modes of calcium and phosphorous atoms in the lamellae of the trabeculae. Trabecular bone therefore can serve as a filter to reduce the amplitudes of certain frequencies present in force waves transmitted through the human skeleton. The elastic behavior is consistent with accepted rheological models for cortical bone, which is assumed to be the constituent material of trabecular bone.

The elastic modulus of trabecular bone is roughly 10^5 psi. The modulus varies about this value depending on the structure of the bone in the following manner: If the structure is comprised of uniform sheets of bone, the modulus is inversely proportional to the contiguity of the open spaces between the sheets. If the structure contains patches of dense bone, the modulus is proportional to the volume fraction of bone. The uniform structure deforms elastically by a plate-bending mechanism; the nonuniform structure deforms in a plate compression mode.

A model for trabecular bone is developed to investigate the mechanical behavior of the region just beneath the cartilage in the human knee. The stresses in the structure are calculated for a physiological static load using the finite-element method. In certain areas of the structure, the ultimate tensile and compressive strengths of the constituent material are exceeded. The modulus of the structure varies locally by a factor of ten. An

increase in thickness of a trabecula from 0.003 to 0.005 inch, as through normal remodelling, results in a fourfold increase in modulus.

Fracture is to be expected in trabecular bone. Buckling as well as Griffith-type brittle fracture are considered. Microfracture has been observed in samples of trabecular bone from rabbits and humans. It is reasoned that fatigue fracture is the most important mode of fracture in trabecular bone, and that the fatigue life of certain areas in the model is less than 10^3 cycles.

A proposed etiology for osteoarthritis is developed from studies of structure, properties, and cartilage degeneration in a group of twenty patients. Early arthritic joints contain trabecular bone that is significantly stiffer than that in normal or advanced arthritic joints. This stiffening is due to remodelling of the sheets of bone to resist the plate-bending deformation resulting from slightly increased impulsive loading. The bone remodels to decrease the contiguity of the open spaces. Increased stiffness implied decreased deflections of the bone under stress, and reduces its effectiveness as a shock-absorber. Under these conditions the cartilage loses mucopolysaccharides in the weight-bearing area, the first sign of the disease. The cartilage is severely damaged locally through increased punishment above dense patches of bone that form and serve as regions of increased local modulus as in the model. The bone subsequently undergoes fracture, necrosis, and resorption, resulting in lowered stiffness and progression of the disease.

Thesis Supervisor: Robert M. Rose
Professor of Metallurgy

TABLE OF CONTENTS

<u>Section Number</u>	<u>Page Number</u>
ABSTRACT	2
LIST OF FIGURES	5
LIST OF TABLES	11
ACKNOWLEDGEMENTS	12
I. General Introduction	15
II. Techniques for the Study of the Structure of Bone	17
III. Viscoelastic Properties of Human Trabecular Bone	36
IV. Structure-Property Relationships in Trabecular Bone	68
V. Structural Model for Trabecular Bone	127
VI. Speculations on the Etiology of Osteoarthritis	170
VII. General Conclusions	211
VIII. Suggestions for Future Work	212
IX. Appendices	
A. Response of the Human Frame to Physiological Mechanical Loads	215
B. Constants for Calculation of Modulus of Ceramic Test Specimen in Section IV	221
C. Sample Computer Run for a Simple Problem	222
D. Free-Body Diagram for Inclined Trabecula	223
X. References	225
Biographical Note	234

LIST OF FIGURES

<u>Figure Number</u>		<u>Page Number</u>
1	Automicroradiograph of human trabecular bone. 165X	21
2	Metallographic section of human cortical bone. 165X	23
3	Metallographic section of human trabecular bone. 165X	24
4	Thin decalcified section of human cortical bone. 165X	25
5	Thin decalcified section of human trabecular bone. 165X	26
6	Metallographic section of human trabecular bone. 330X	27
7	Thin decalcified section of human trabecular bone. 330X	28
8	Metallographic section of human cortical bone. 1330X	29
9	Thin decalcified section of human cortical bone. 1100X	30
10	Schematic of viscoelastometer used to measure viscoelastic properties of trabecular bone.	46
11A	Viscoelastometer.	47
11B	Closeup of sample in viscoelastometer	47
12A	Femoral location of samples of bone used in this study.	52
12B	Closeup of bone plugs used for viscoelastic measurements.	52
13	Oscilloscope photograph for natural rubber at 2400 Hz.	53
14	Viscoelastic properties of natural rubber as a function of frequency.	54

<u>Figure Number</u>		<u>Page Number</u>
15	Viscoelastic properties of PMMA as a function of frequency.	56
16	Elastic modulus for trabecular bone as a function of frequency.	58
17	Oscilloscope photograph for human trabecular bone at 1000 Hz.	59
18	Storage and loss moduli for human trabecular bone as a function of frequency.	62
19A	Apparatus for the measurement of relative stiffness.	78
19B	Closeup of sample in place in relative stiffness apparatus.	78
20	Detail of clamped elements in relative stiffness apparatus.	79
21	Schematic showing instrumentation used for measurement of relative stiffness.	81
22	Human bone section just beneath cartilage. 1.5X	83
23A	Sketch of rabbits on impacting table.	85
23B	Detail of rabbit with left and right legs in splints.	85
24	Modified stiffness apparatus.	87
25	Schematic of modified stiffness apparatus.	88
26	Applied voltage versus stress level for the relative stiffness apparatus.	91
27	Stress level versus preload at constant applied voltage.	92
28	Relative stiffness versus days run on impacting table for rabbits.	94
29	Photograph of cross-sections of left and right rabbit tibias. Ultraviolet illumination. 2.5X	97
30	Photomicrograph of weight-bearing area of left (control) leg of rabbit. 30X	98

<u>Figure Number</u>		<u>Page Number</u>
31	Photomicrograph of weight-bearing area of right (experimental) tibia of Group A rabbit (R.S.=1). 30X	99
32	Photomicrograph of weight-bearing area of right (experimental) tibia of Group B rabbit (R.S.=1.4). 30X	100
33	Photomicrograph of weight-bearing area of right (experimental) tibia of Group C rabbit (R.S.=2). 30X	101
34	Relative stiffness versus volume fraction bone for human trabecular bone.	104
35	Relative stiffness versus contiguity of holes for human trabecular bone.	106
36	Relative stiffness versus average trabecular thickness for human trabecular bone.	108
37	Relative stiffness versus average number of trabeculae per unit length for human trabecular bone.	109
38	Relative stiffness versus $V_V^{\text{Bone}}/C_{\text{Holes}}$ for human trabecular bone.	110
39A	Human trabecular bone showing uniform microstructure. 20X	113
39B	Human trabecular bone showing non-uniform microstructure. 20X	113
40	Relative stiffness versus contiguity of holes for human trabecular bone with uniform microstructure.	114
41	Relative stiffness versus volume fraction bone for human trabecular bone with non-uniform microstructure.	116
42	Schematic showing that the modulus of the uniform group of samples is controlled by a plate-bending type of deformation.	119
43	Idealized microstructures exhibiting contiguities of 0.5 and 0.	121
44A	Human trabecular bone with a C_H of 0.3. 20X	123
44B	Human trabecular bone with a C_H of 0.1. 20X	123

<u>Figure Number</u>		<u>Page Number</u>
45	Schematic showing that the modulus of the non-uniform group of samples is controlled by a plate compression mode of deformation.	124
46	Schematic of human knee joint.	129
47A	Non-zero stress components for an infinitesimal element of a sheet in plane stress.	134
47B	Stress resultants N and moment couples M of the type calculated by STRUDL II.	134
47C	A state of stress in a thin plate resolved into a bending component σ_B and a membrane component σ_M .	134
48A	Coordinates for calculation of stress concentration due to an elliptical hole in a thin sheet from equation (18).	138
48B	Coordinates for calculation of moment concentration due to an elliptical hole in a thin sheet from equation (19).	138
49A	Model for trabecular bone. 1/5X	142
49B	Transverse thin section, H & E stained, through human knee. 50X	142
50	Schematic of model	145
51A	The subchondral plate, plane 10, as divided into PBST finite elements.	148
51B	A vertical trabecula, plane 1, as divided into PBST finite elements.	148
52	Bending moment M_{yy} along plane 6 as a function of vertical distance Y beneath the subchondral plate, plane 10.	151
53	Position of local fracture around stress concentrator in an inclined trabecula.	153
54A	Trabecular microfracture in human bone. 180X	154
54B	Trabecular microfracture in rabbit bone. 260X	154
55	Thickening of trabeculae in rabbit tibia. 97X	156
56	Local deflections of the subchondral plate, viewed normal to plane 10, for the three models.	157

<u>Figure Number</u>		<u>Page Number</u>
57	Local modulus across the subchondral plate as calculated from the data in Figure 56.	159
58	Maximum stress versus cycles to failure for cortical bone.	175
59	Relative stiffness for each sample grouped according to degree of joint degeneracy.	183
60	Relative stiffness versus volume fraction bone for human samples with non-uniform microstructure.	185
61	Relative stiffness versus contiguity of holes for human samples with uniform microstructure.	188
62	Relative stiffness versus $V_V^{\text{Bone}}/C_{\text{Holes}}$ for human trabecular bone.	190
63	Relative stiffness data versus $V_V^{\text{Bone}}/C_{\text{Holes}}$ for human trabecular bone. Data from Figure 62 grouped schematically to indicate possible arthritic trends.	192
64A,B	Typical microstructures of Group 0 and Group I bone, respectively. 28X	195
65A,B	Typical microstructures of Group I bone from two different patients. 28X	196
66	Large patch of dense bone in a sample presumably undergoing transition from Group I to II. 28X	197
67A,B	Resorption areas in Group II bone. 110X	198
68	Typical Group III bone. 19X	200
69	Fractured trabecula showing no callus formation. 240X	204
70	Site of probable fracture with extensive callus formation evident. 120X	204
71	Site of probable fracture after significant remodelling has occurred. 240X	204
72	Site of probable fracture after extensive remodelling. 120X	204
73	Possible fatigue cracks in human trabecular bone. 220X	208

<u>Figure Number</u>		<u>Page Number</u>
74	Placement of accelerometer above left medial condyle of femur.	217
75	Schematic of instrumentation used in study.	218
76	Typical plot of voltage output from accelerometer versus time for one step during running.	219

LIST OF TABLES

<u>Table Number</u>		<u>Page Number</u>
1	Comparison of Metallographic and Thin Decalcified Sections	33
2A	Frequencies of Resonances for Trabecular Bone	65
2B	Two Sets of Resonances	65
3	Comparisons Between Model and Human Trabecular Bone	144
4	Stresses and Moments for INTACT Model	163
5	Stresses and Moments for FRACTURE Model	164
6	Stresses and Moments for CALLUS Model	165
7	Case Histories of Patients in Study	180
8	Relative Stiffness, Microstructure, and Degeneracy of Joint for Patients Used in Study	182
9	Proposed Etiology for Osteoarthritis	203

ACKNOWLEDGEMENTS

It would be very difficult to acknowledge all the people who made this endeavor possible. It is the culmination of years of education and many hours of discussion. I sincerely hope that the final product is worthy of the efforts of the many people that took part in it.

First of all, deep thanks go to my wife, Barbara, for providing encouragement and understanding when it was most needed, and for her many hours of work in preparing this manuscript. Thanks also go to my parents, for providing me with all the benefits of a secure home, love, and a fine education.

Professor Robert M. Rose originally suggested the possibilities of research in this area. I am deeply grateful to him for giving freely of his time when it was most needed, and for giving timely suggestions and words of encouragement. Without his guidance and patience, this work would have been impossible. His continual help with decisions in my professional life is also gratefully appreciated.

Special thanks go to Dr. Eric Radin for his criticisms and suggestions, and for his interaction with the thesis. The results of his work played a great role in the development and execution of the experiments described herein. It is through the efforts of Eric that I integrated myself into the Boston medical community and it is an understatement to say that I benefited from the interaction with him.

Thanks also go to Professor John Wulff for subtly guiding me into the Department of Metallurgy and Materials Science, and for

demonstrating his exemplary teaching methods both in and out of class. My love of teaching is due in great part to my association with Professor Wulff.

Mr. Irvin Puffer has always and will continue to receive my admiration, thanks, and respect for his deep understanding of experimentation and instrumentation and his willingness to give freely of his time and help me work out the details of a particular project, be it design, construction, or operation. Puff has saved me many hours of fruitless work merely with the point of a finger.

Dr. Alan Schiller has provided invaluable comments and suggestions concerning the pathology of bone and cartilage. His questions about the work have led to a deeper understanding of the mechanisms controlling the etiology of osteoarthritis. I am very grateful for his friendship and the many hours of discussion we have had.

Dr. Howard Parker provided the rabbit specimens used in this study. His untiring efforts and comments are also appreciated. Dr. Robert Steinberg also provided rabbits and comments when needed.

Nancy Hanafin and Edna MacLeod at the Children's Hospital Medical Center are to be commended for their patience and technique in preparing the thin stained sections of bone and cartilage used in this study. Without their assistance, I could never have completed one of the most interesting and fruitful parts of this thesis.

I want to thank Joe Stukas at Massachusetts General Hospital for providing the autopsy material used in this work. His conscientiousness has always and will continue to be appreciated.

I also want to thank Mr. Robert Miegel for the special projects he has performed during this research project. He has also spent many hours preparing samples and doing microscopy. The tetracycline work mentioned in this thesis is a direct result of his efforts.

Thanks also go to Mr. Tom Eagar for preparing several of the line drawings used in this paper; and to Miss Susan Sassano for her untiring help in preparing papers for publication and in executing administrative matters.

I also want to thank the other people with whom I have had informal discussions, and who have given me comments and encouragement. It is unfortunate that space is so limited.

I am grateful to the Department of Metallurgy and Materials Science for providing me with a Teaching Assistantship for three years of my graduate education.

This research was funded by grants from the National Science Foundation and the Office of Naval Research.

I. GENERAL INTRODUCTION

This thesis is part of a long-range study concerning the structure and properties of bone and the degeneration of the human frame, that has been undertaken jointly by groups in the MIT Department of Mechanical Engineering and the Department of Metallurgy and Materials Science. The work of the groups has also focused on the mechanical properties of cartilage, bio-mechanics of the human musculo-skeletal system, osteoarthritis, studies of wear of prostheses, and design of prosthetic devices. The work has been successful to a great extent because of the interaction of engineers and doctors in solving the particular problems encountered.

The impetus for this thesis was provided by a set of experiments originally performed by Radin, Paul, and Tolko⁶⁹ at MIT. This work suggested that there may be a relationship between the mechanical properties of bone in the joints and the development of osteoarthritis. Unfortunately, the data obtained did not readily lend itself to interpretation, and their work on the structural correlations did not show anything. Structure-property relations being the forte of the metallurgist, the researchers called in Robert M. Rose for consultation; and, later, I became interested in the problem.

Experiments of the type performed by Radin et al. are reported in this thesis, in addition to further work on mechanical properties and idealized models for the bone, in an effort to determine the validity of their findings and to place the structure-property relations in better perspective.

As in any work dealing with a biological system, it has been necessary to take occasional liberties with engineering and science in order to interpret results. It is hoped that the reader will bear with this.

In the literature, trabecular bone has also been referred to as cancellous bone, subchondral bone, and spongiosa. All of these are synonymous. I have chosen to use the word "trabecular" because the definition of the singular noun "trabecula" best describes its true structure and function: a little beam; used in anatomical nomenclature as a general term to designate a supporting or anchoring strand of connective tissue, as such a strand extending from a capsule into the substance of the enclosed organ.⁸³ Trabecular bone is typically found in the cranium, the ends of the long bones such as the femur, the vertebral bodies, and any place where the mechanical function deems this bone necessary.

Section II of this thesis describes the structure of different types of bone, and the different techniques preferred for microscopic study. The sections that follow deal with the interrelations between the structure and the mechanical properties. Section VI attempts to synthesize the data and to relate the conclusions of the previous sections to the behavior of bone in the human body.

II. TECHNIQUES FOR THE STUDY OF THE STRUCTURE OF BONE

Introduction

Recently the identification of three-dimensional structure from single sections of biological samples was discussed.¹ Reference was made to the opacity of metals and the consequent necessity of using reflected-light microscopy (metallography) for studying the structure of metals and alloys. Since bone is opaque and hard, it is also ideally suited for examination by reflected-light. No mention was made of this; no metallographic sections were presented. Only thin sections were shown. Unfortunately, most scientists in the biological and materials sciences are unaware of how easily and effectively the metallography of bone is accomplished.

There has been only sporadic use of metallographic sections of bone in the medical literature. A recent study² of fracture of bone included metallographic sections. A renowned textbook on histology³ even shows a macrophotograph of a metallographic section of a whole femur to illustrate the two major types of bone: cortical, the dense bone of which the shafts of the long bones are comprised; and trabecular, the spongy bone present in the ends of the long bones, the cranium, and the vertebrae. However, they do not show any photomicrographs of metallographic sections.

The major problem with the most extensively used techniques for studies of the microstructure of bone is that the structural integrity is often not preserved. These techniques involve grinding a very thin section between sheets of silicon carbide paper.

The samples are so fragile that artifacts are very difficult to avoid. Another method requires decalcification of the bone to render it pliable and subsequent slicing on a microtome. Again, the structure is not preserved. The sample shrinks during decalcification, and structural components are often rearranged during the remainder of the processing. Resolution in these techniques is often poor. Features such as microfractures often do not show up at all. In addition these methods are very time-consuming.

Materials and Methods

Trabecular bone was obtained at autopsy from the distal end of the human femur (the knee joint), and cortical bone from the midshaft of the femur. Samples for metallography were immediately immersed in ethyl alcohol, and those for decalcified thin sections were fixed in neutral buffered formalin. Samples for automicro-radiography were obtained from the proximal end of the human tibia (the knee joint) and immediately immersed in ethyl alcohol.

Metallographic Sections

After about two days in the ethyl alcohol, the fatty tissues in the bone have been dissolved. The samples are then immersed in solutions of alcohol and methyl-methacrylate monomer, under vacuum, to get rid of any small bubbles of air that can get trapped in the plastic during polymerization which is effected by the combination of a catalyst (benzoyl peroxide) and ultraviolet light. The whole process takes about a week. During this time, only about one man-hour is required for twenty specimens. After the methyl-methacrylate has fully polymerized, flats are polished on

the samples by standard metallographic techniques:⁴ finer and finer grit silicon carbide papers, 0.3 micron alumina in distilled water, 0.05 micron alumina in distilled water, and finally an alcohol rinse. No stains are used. The sample is ready for reflected-light microscopy and photography immediately. The total time to polish twenty samples is of the order of one hour, frequently less.

Thin Sections of Decalcified Bone

The bone is fixed in the neutral buffered formalin for two days. The samples are then decalcified in 25% buffered formic acid for 16 hours. After embedding in paraffin, sections are cut 6 microns thick on a microtome. These are then stained with hematoxylin and eosin and mounted on glass slides for observation with the transmitted light microscope. The time expended in preparing twenty specimens is typically ten man-hours over a period of a week.

Automicroradiography

Thin sections, roughly 1 mm are cut from the bone embedded in methyl-methacrylate. These are ground between sheets of silicon carbide paper to a thickness of about 10 microns or less. Automicroradiographs are obtained and mounted on glass slides for observation by transmitted light.

Thin Ground Sections of Undecalcified Bone

Fresh bone is sectioned into 1 mm thick slabs. These sections are ground on silicon carbide paper to a final thickness of 6 - 10 microns. Stains can then be used on the sections, and the

samples are ready for transmitted-light microscopy. Twenty specimens can be prepared in this manner in about 3 hours. An alternative method consists of first embedding the bone in methyl-methacrylate to provide mechanical stability and then sectioning and grinding.

Microscopy

The samples were all studied with a Reichert microscope that has provisions for both reflected and transmitted light. Unpolarized tungsten illumination was used for all samples. Polaroid positive/negatives were taken with a green filter by a variable bellows attachment fitted with a Polaroid 4 x 5 sheet film back. The transmissivity and reflectivity of the samples and the sensitivity of the film were such that exposures of 15 to 200 seconds were necessary.

Results

The use of automicroradiographs is standard practice in most medical research centers to determine the relative calcium content of different areas of bone. The morphological features that show up in trabecular bone through this technique are essentially the position of the trabeculae and the lacunae, which are spaces occupied by bone cells (osteocytes). The lacunae show up as tiny holes in the trabeculae (Figure 1).

Studies of decalcified sections of bone are also commonplace in the medical world. The same general structural features show up both in the metallographic sections and in the thin decalcified sections. The Haversian systems, concentric rings of bone,



Figure 1: Automicroradiograph of human trabecular bone. Longitudinal section. Small holes in the bone structure are lacunae. Differences in relative calcium content of adjacent areas show up as variations in photographic density. 165X



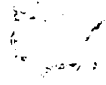
lacunae, and canaliculi are evident in the cortical bone. Lamellae and lacunae in the trabecular bone are also evident. Osteoid (not yet completely calcified bone, or new bone) is also identifiable. However, these features show up much better in the metallographic sections (Figures 2 - 9). Thus, metallographic sections are preferred in studies of structural morphology.

The lacunae in the ground sections invariably appear empty, while the presence of osteocytes in the lacunae of the thin sections is verified. In all probability, the bone cells are removed from the ground section by the polishing operation. One of the easiest methods to ascertain if the bone is living or dead involves determining whether or not the lacunae are occupied. This proves to be very difficult in metallographic sections. Therefore, the authors prefer to use thin sections for studies of cellular activity. In addition, the soft tissues within the Haversian canals and between trabeculae are retained in the thin decalcified sections (Figure 9).

The excellent contrast in the metallographic sections arises from the presence of slight relief ground into the surface as a result of the variation in hardness of the various structural components of the bone. An increase in resolution over the thin section techniques results from the plane of zero thickness of the metallographic sections. One of the basic principles of stereology⁵ is that a bias in measurement of desired quantities and a lack of resolution result from failure to observe a true two-dimensional section. The thin sections actually have a



Figure 2: Metallographic section of human cortical bone. Transverse section. The Haversian canals are the large holes surrounded by the concentric rings of bone. The Haversian systems contain many lacunae. 165X



Human cortical ...

... analysis ...

P

1000
1000
1000

1000

1000

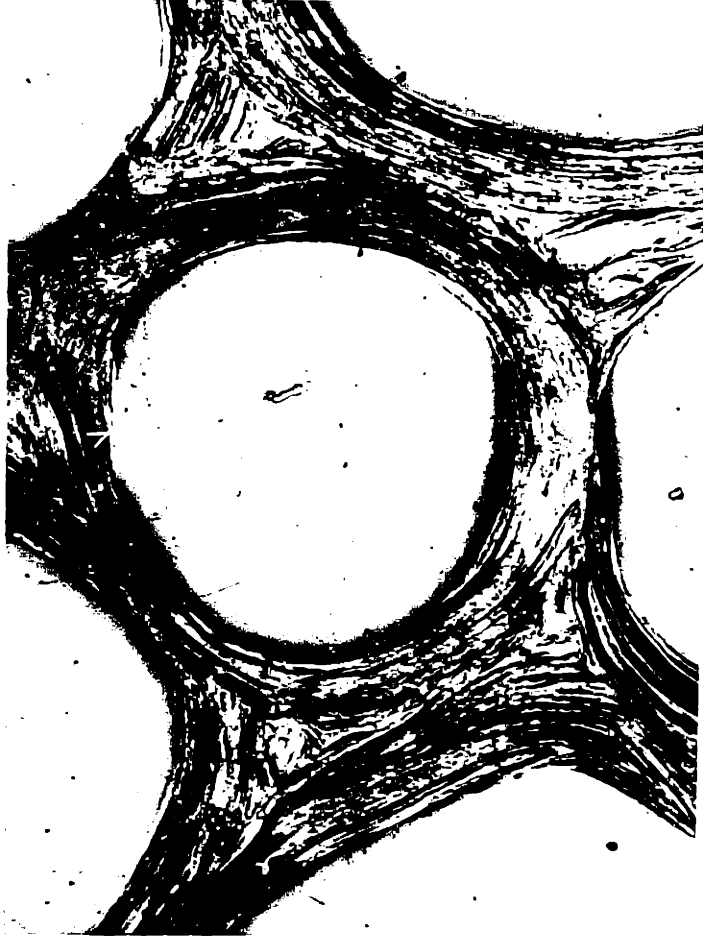


Figure 3: Metallographic section of human trabecular bone. Transverse section. The lamellar nature of the interconnected trabeculae is evident. The structure of trabecular bone is clearly a system of interconnected sheets. 165X



Figure 4: Thin decalcified section of human cortical bone. Transverse section, H & E stained. Haversian systems and lacunae are evident. Some of the lacunae are occupied by osteocytes, which appear as black dots. 165X



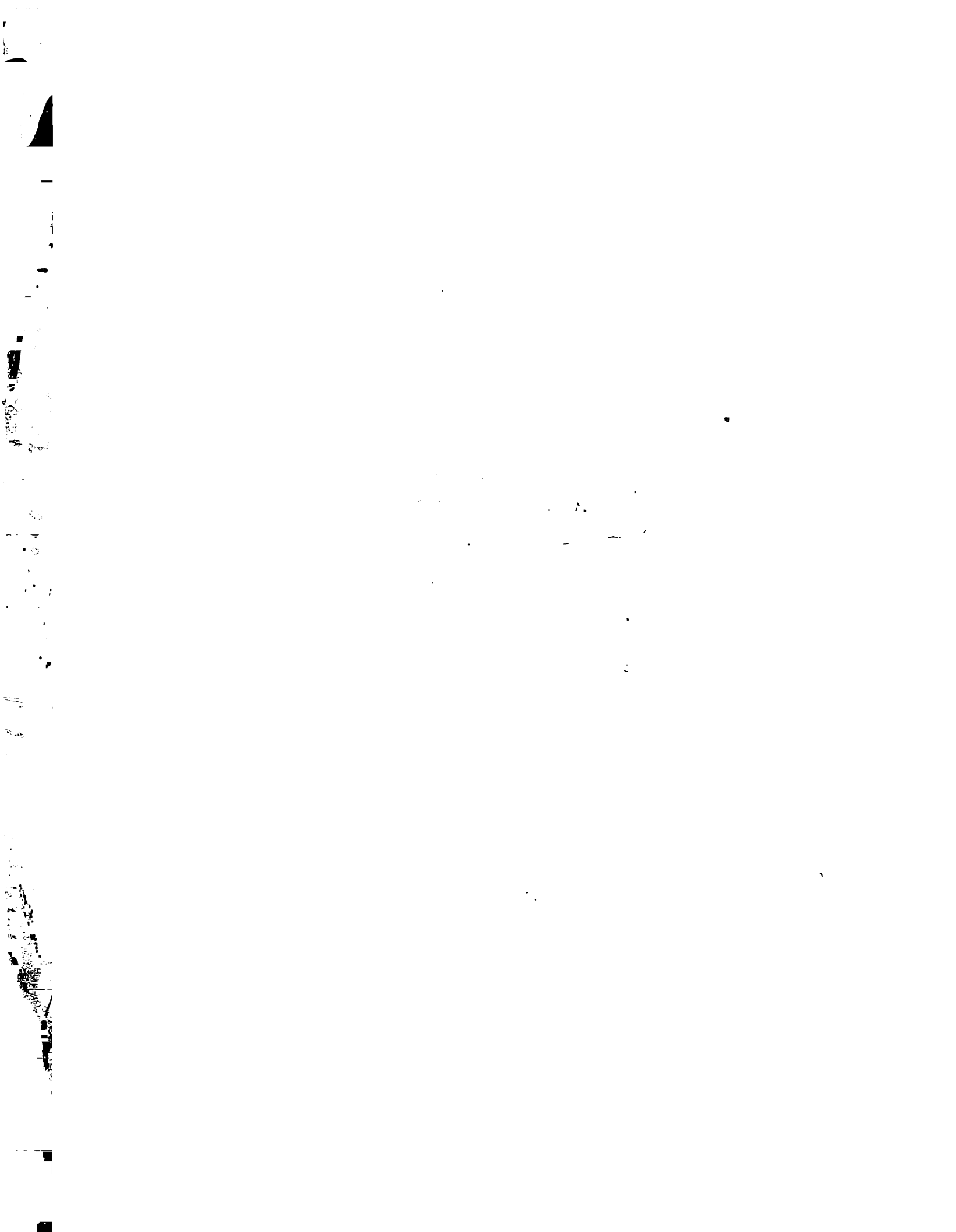




Figure 5: Thin decalcified section of human trabecular bone. Transverse section, H & E stained. The lamellae and lacunae are evident. Some networks of soft tissue are present in the open spaces. 165X



Figure 6: Metallographic section of human trabecular bone. Transverse section. Notice the non-lamellar osteoid present on the trabecula. The older bone in the center is lamellar; the osteoid is not completely calcified and therefore not lamellar. Lacunae are evident in the osteoid. 330X







Figure 7: Thin decalcified section of human trabecular bone. Transverse section, H & E stained. An area of osteoid is separated from the older bone by a thin line and is darker than the older bone. A proliferation of osteocytes (occupied lacunae) is evident in the osteoid. A few occupied lacunae are in the older part of the bone. 330X



Figure 8: Metallographic section of human cortical bone. Transverse section. The lacunae appear empty. A central Haversian canal is at the upper left. The concentric rings of bone are evident, as well as the smaller interconnecting canaliculi, which run outward radially from the Haversian canal and tend to connect the lacunae. 1330X



...rectory ...
...the lac...
...at the ...
...vident...
...licu... w...
...na' ... t...





Figure 9: Thin decalcified section of human cortical bone. Transverse section, H & E stained. The lacunae are occupied by osteocytes (black dots). The Haversian canal with its concentric rings of bone and the interconnecting canaliculi radiating outwardly are evident. The soft tissue and blood cells in the Haversian canal are retained. 1100X

finite thickness of 6 - 10 microns. The metallographic sections, even with the slight relief ground in, have a plane of polish (the only plane observed) that approaches the two-dimensional limit. Thus the metallographic section is very nearly a plane of zero thickness. This is a very important consideration when selecting a microscopic technique for quantitative measurements. The metallographic technique is definitely superior in this respect.

Thin ground sections of bone that have been stained and viewed with transmitted light show the same general features as the metallographic and the thin decalcified sections. For representative photomicrographs, the reader is referred elsewhere.^{6,7} A severe drawback of this technique is the fragility of the very thin sections of bone. Since the bone is very brittle, even if it is embedded in methyl-methacrylate, artifacts such as cracks are very difficult to avoid. Furthermore the undesirable effects of finite sample thickness are present. Therefore the author does not recommend this technique for structural studies.

Conclusions

Table 1 summarizes the relative advantages and disadvantages of the use of metallographic and thin decalcified sections, for the study of bone. The author prefers to use these two techniques as complementary. For studies of the structural composition of bone such as lamellae, lacunae, osteoid, canaliculi, and microfractures, he prefers metallography. If one happens to be interested, for example, in locating the osteocytes to positively

identify whether the bone is living or dead, the thin decalcified sections are used. The author believes that these two techniques, if used in such a manner can reveal many more phenomena in bone than either technique used alone.

Table 1

Comparison of metallographic and thin decalcified sections

<u>Thin Sections</u>	<u>Metallographic Sections</u>
1. Specimens viewed with transmitted light.	Reflected light.
2. Thin sections, 6 microns.	Bulk specimens with a single plane of observation.
3. Process time-consuming. Requires 10 man-hours for 20 specimens.	Much less time-consuming. 20 specimens can be done in 2 man-hours.
4. Samples must be decalcified.	Decalcification not necessary.
5. Because of tissue shrinkage during decalcification, only relative measurements (volume fractions, etc.) can be made without corrections.	No apparent shrinkage. Absolute (thickness of a trabecula) as well as relative measurements are directly made.
6. Folding of the thin section is often a problem. Trabeculae can be rearranged during processing.	Structural integrity preserved throughout the process.
7. As long as the features to be studied are large compared to the thickness of the section, this technique will suffice stereologically.	Plane of zero thickness is mathematically superior. The resolution on the metallographic sections is thus much better.
8. Details such as microfractures of bone are difficult to identify because of thickness of section.	These defects are easily identified if they are within the limit of resolution of the microscope.
9. Orientation of the specimen for cutting is difficult after embedding in paraffin. Uncertainties in orientation of the thin section frequently result.	Specimen is embedded in a completely transparent plastic. The plane of polish can be selected with full knowledge of its orientation.

Table, continued

<u>Thin Sections</u>	<u>Metallographic Sections</u>
10. Studies of three perpendicular planes require three separate slides. Morphological studies are thus difficult because of orientation problems.	Three perpendicular planes of polish can be made on one specimen. The point where these three planes meet can be studied, thus facilitating studies of morphology.
11. Serial sections are easily taken and each individually mounted for comparison or for future reference.	Serial sections can be viewed by repeatedly polishing and photographing, but this destroys part of the specimen. Referral back to earlier planes of polish is impossible except through photographs.
12. Only soft tissue such as decalcified bone can be processed. Metal prostheses must be removed before sectioning.	Studies of bones with metal prostheses in situ are very simple. Any material can be studied metallographically. Bone reactions to prostheses can be studied with the appliance in place.
13. Stains necessary for contrast.	Better contrast in general is obtained without stains.
14. Useful for studies of cells such as osteocytes, since these are stained and retained in the finite thickness of the section.	Cells are usually not observed. They are probably polished off of the surface.
15. Osteoid distinguished from older bone by a line of demarcation and slight differences in staining and cellular activity.	Osteoid easily differentiable from older bone on basis of photographic contrast alone.
16. Useful for getting structural and cellular information on bone with cartilage, or other soft tissue, attached (see cover)	Soft tissues generally do not show up well.
17. Soft tissue between	

Table, continued

Thin Sections

trabeculae (including blood cells) can be stained and studied.

18. Lamellar nature of bone visible and enhanced by polarizing microscope. Use of polarized light will increase contrast, but not resolution.

Metallographic Sections

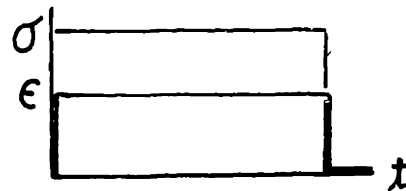
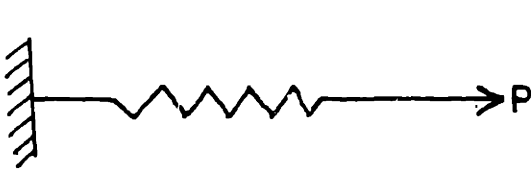
Polarization not necessary. Lamellae distinctly visible.

III. VISCOELASTIC PROPERTIES OF HUMAN TRABECULAR BONE

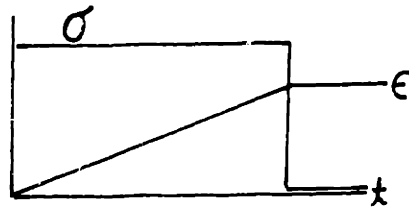
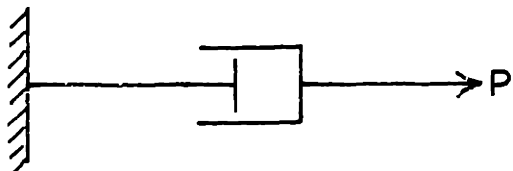
Introduction

Rheology

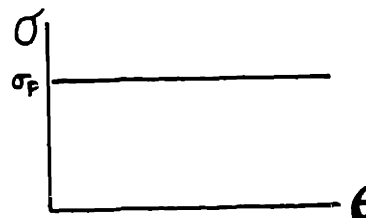
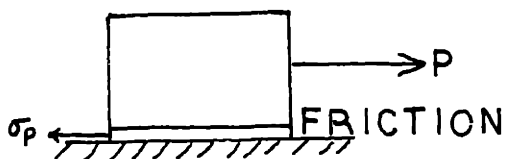
Rheological models have been developed to explain the static viscoelastic behavior of materials⁸⁻¹⁰. These models involve a combination of a variety of the following elements: perfectly elastic solid or Hookean body (spring), perfectly viscous substance or Newtonian body (dashpot), and rigid plastic substance or St. Venant body (sliding weight). The characteristic mechanical behavior of each of these elements is shown as follows:



The Hookean elastic body is seen to deform instantaneously, and, upon release of the load, the original shape is regained.

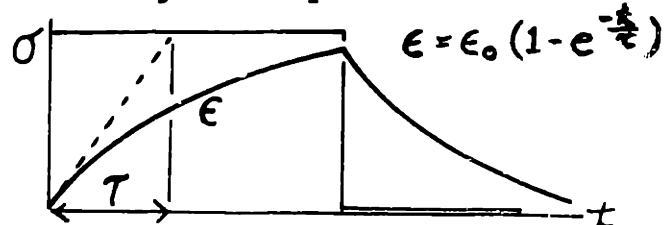
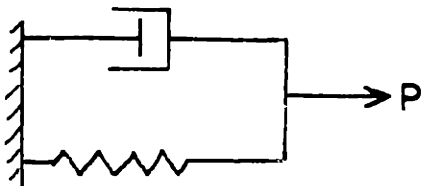


The Newtonian viscous body is time-dependent; application of a load does not result in instantaneous deformation but the strain is proportional to the time of application of the load. The relationship between stress and rate of strain in the Newtonian body is expressed as $\sigma = \eta \frac{d\epsilon}{dt}$ where η is the effective viscosity.

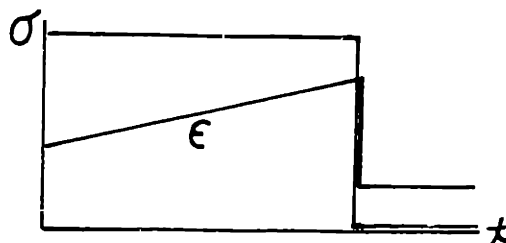
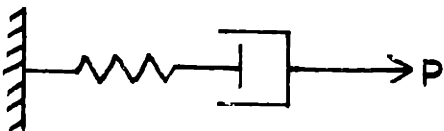


The St. Venant body is used to explain plasticity of a material. The symbol for this is a weight resting on a flat surface with a solid friction between them. Below the yield point σ_p no deformation occurs. When the stress becomes equal to σ_p the material flows indefinitely. When the stress is relaxed, the deformation remains.

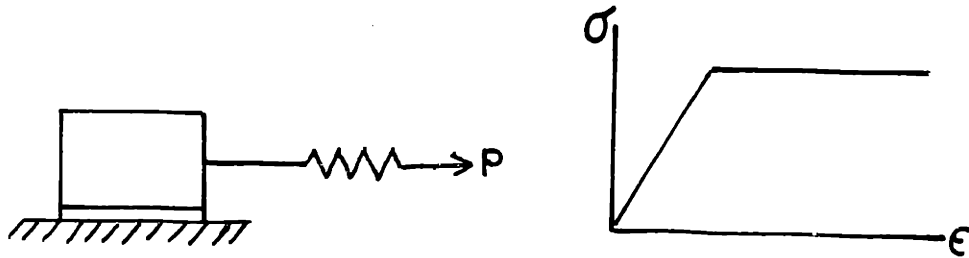
Combinations of these elements may be used to approximate the mechanical behavior of real materials. When the elements are combined in series, the stress in each element is the same. If the elements are combined in parallel, the strains in each element are identical. The Voigt model utilizes a spring and dashpot in parallel. The response with time is exponential, and, upon release of the stress, the strain gradually returns to zero:



The Maxwell model uses a spring and dashpot in series. The initial elastic deformation is due to the spring, the dashpot providing time-dependent behavior. Upon release of the stress, a permanent set remains:



The Prandtl model is used to explain the mechanical behavior of the perfectly plastic body, which behaves elastically up to the yield point, at which its behavior is purely plastic:

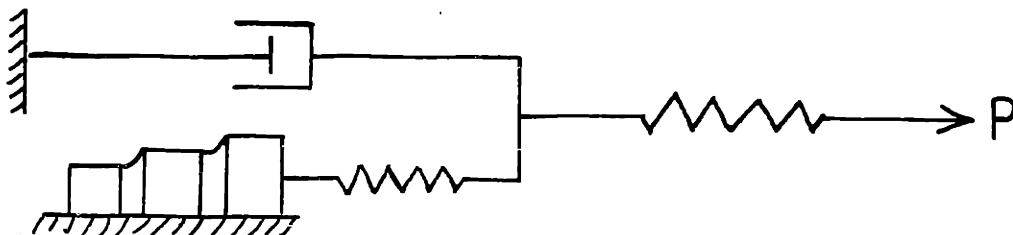


A permanent strain remains when the stress is relaxed.

Previous Work

Much has been written on the mechanical properties of bone.¹¹ There have been some data¹² gathered through static measurement of such properties as Young's modulus, yield strength, ultimate strength of bovine cortical bone as a function of strain rate. Other studies^{13,14} focused attention on mechanical properties of human trabecular bone. These were tests conducted under large-displacement static conditions; that is, the specimens were placed in an Instron-type apparatus and strained to fracture, or impacted to fracture. Reference to Appendix A shows that static measurement of properties is questionable from a physiological standpoint. There have also been recent studies utilizing ultrasonics¹⁵ in the measurement of mechanical properties of bone^{16,17}. These tests give reasonable data, but the frequencies of application of the small stresses are much higher than those encountered physiologically.

A rheological model developed by Sedlin¹⁸ for cortical bone utilizes combinations of the elements and models discussed above:



This model was developed to explain the results of different static and cyclic tests that Sedlin performed on cortical bone sections from the human femur. It must be emphasized that these tests were large-displacement, high-stress tests; and it comes as no surprise that a complex model is needed to explain the non-linear behavior of cortical bone in these tests. The behavior of the model below the yield point may be represented by the following equation:

$$\sigma = A \frac{d\epsilon}{dt} \left(1 - e^{-\left\{ \frac{B}{d\epsilon} \right\} \cdot \epsilon} \right) + C\epsilon$$

At low strain-rates, $\frac{d\epsilon}{dt} \approx 0$, the stress-strain relationship is seen to be linear and time-independent, $\sigma = C\epsilon$. This agrees with the experimental observation that the hysteresis loops close with very low strain-rates. In this regime the response of cortical bone is purely elastic.

There are only very small amounts of data¹⁹ in addition to those of Sedlin concerning the true viscoelastic properties of bone, and this is only for cortical bone. The only data presented here are static tests in which a load is applied to the specimen and the deflection as a function of time is recorded. These data are also of questionable value in a physiological sense as they are an indication only of the static or quasi-static properties of bone.

McElhaney and Byars²⁰ went so far as to entitle their paper "Dynamic Response of Biological Materials." The samples were not really tested in a dynamic manner; they were merely static-tested at a variety of strain-rates. It will be instructive to differentiate here between these tests and true dynamic tests. For the purposes of this thesis "dynamic" will refer to conditions of

There have been dynamic measurements done on intact long bones. Jurist²¹ has measured the ulnar resonant frequency using an electromagnetic force generator and plotting acceleration of the bone as a function of frequency for the range 200 to 1000 Hz. Campbell and Jurist²² have measured the mechanical impedance of the femur using similar techniques. In both cases, the long bones exhibited resonances corresponding to viscous (energy-dissipating) response in the low audio range.

Swanson and Freeman²³ addressed the question of hydraulic strengthening of bone, the effect of fluid in the open spaces between trabeculae, up to 2 Hz. They measured no viscous component in the elastic response either for a femur with empty intertrabecular spaces or for one filled with a viscous fluid. The conclusion was that bone, both cortical and trabecular, behaves purely elastically up to 2 Hz.

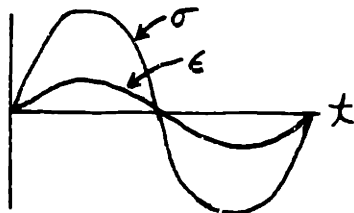
Reasonable viscoelastic properties are usually measured in a small-displacement apparatus which gives data as a function of frequency.²⁴ The preferred methods of measurement of viscoelastic properties generally involve application of a sinusoidal stress and simultaneous measurement of the resulting sinusoidal strain, paying proper attention to amplitudes and the phase angle between stress and strain.

Fitzgerald²⁵ has measured the viscoelastic response of intervertebral disks at audiofrequencies. He gives justification for the use of such a small-displacement apparatus and dynamic measurement at audiofrequencies. Dynamic measurement can be "expected to lead eventually to significant correlations with the

cellular and subcellular structures of tissues, and perhaps even to a quantitative measurement of the mechanical differences between healthy and diseased tissue."²⁶ High sensitivity and precision are attainable in such an apparatus even at low stress and strain amplitudes. Such an apparatus allows measurement of the properties in the linear region of the response and are entirely non-destructive. Appendix A gives additional justification for the choice of dynamic measurement of properties at audiofrequencies.

General Theory of Dynamic Viscoelasticity²⁷

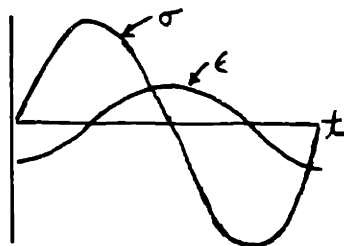
It is instructive to recall the concept of an ideal elastic material and an ideal viscous material, and to apply these to the case of a material under sinusoidal loading. The ideal elastic material responds to a stress with an instantaneous strain. Furthermore, the strain is completely and instantaneously recoverable when the stress is removed. The dynamic response of an ideal elastic material is shown as follows:



$$\sigma(t) = \sigma_{MAX} \sin \omega t$$

$$\epsilon(t) = \epsilon_{MAX} \sin \omega t$$

An ideal viscous material responds with delayed strain to an applied stress. Under steady loads, the strain increases indefinitely with time and remains when the stress is removed. For sinusoidal loading the completely viscous dynamic response is shown below:

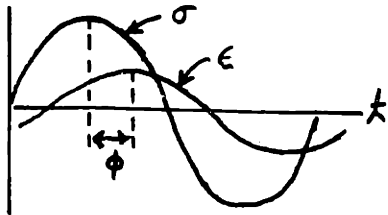


$$\sigma(t) = \sigma_{MAX} \sin \omega t$$

$$\begin{aligned} \epsilon(t) &= \epsilon_{MAX} \sin(\omega t - 90^\circ) \\ &= -\epsilon_{MAX} \cos \omega t \end{aligned}$$

Notice that the response of an ideally viscous material to an applied sinusoidal stress is a strain 90° out of phase with that stress.

Real materials, especially living tissue, generally respond in a manner that is both elastic and viscous. Part of the strain is instantaneous and part is delayed, as follows:



$$\sigma(t) = \sigma_{MAX} \sin \omega t$$

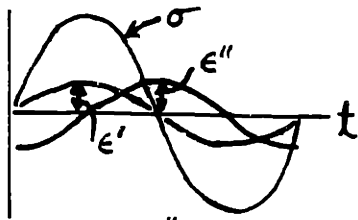
$$\epsilon(t) = \epsilon_{MAX} \sin(\omega t - \phi)$$

where ϕ is less than 90° . The equation for the strain can be rewritten as:

$$\epsilon(t) = \epsilon_{MAX} \cos \phi \sin \omega t - \epsilon_{MAX} \sin \phi \cos \omega t$$

$$\epsilon(t) = \epsilon' \sin \omega t - \epsilon'' \cos \omega t$$

Graphically, this can be represented as



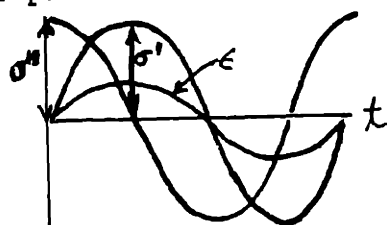
where ϵ' and ϵ'' are the components of the strain in phase and 90° out of phase with the stress.

The storage compliance, S' is then defined as the strain in a sinusoidal deformation in phase with the stress divided by the stress, or $S' = \frac{\epsilon'}{\sigma_{MAX}}$. This represents the elastic part of the compliance and is a measure of the energy stored and recovered per cycle. The loss compliance, S'' is defined as the strain 90° out of phase with the stress divided by the stress, or $S'' = \frac{\epsilon''}{\sigma_{MAX}}$. A very useful parameter is the loss tangent, $\tan \phi$, which is dimensionless and conveys no physical magnitude but is a measure

of the ratio of the energy lost to the energy stored in a cyclic deformation. It is defined by the following:

$$\tan \phi = \frac{S''}{S'}$$

The storage modulus E' is the stress in phase with the strain divided by the strain. The loss modulus E'' is the stress 90° out of phase with the strain divided by the strain.



$$E' = \frac{\sigma'}{\epsilon_{\text{MAX}}}$$

$$E'' = \frac{\sigma''}{\epsilon_{\text{MAX}}}$$

$$\tan \phi = E''/E'$$

Thus the compliances and moduli are complex quantities:

$$S^* = S' + iS''$$

$$E^* = E' + iE''$$

Although $S^* = 1/E^*$, the individual components are not reciprocally related, but are connected by the following equations:

$$S' = \frac{1/E'}{1 + \tan^2 \phi}$$

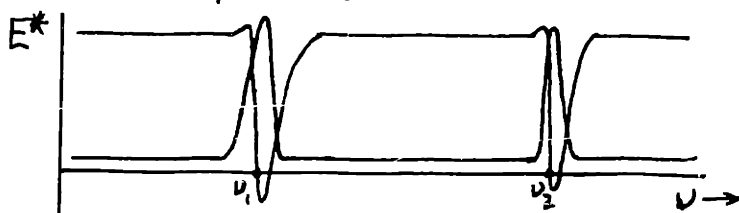
$$S'' = \frac{1/E''}{1 + (\tan^2 \phi)^{-1}}$$

In general, the compliance for a viscoelastic material decreases with increasing frequency. Thus, the modulus increases with increasing frequency. The loss tangent generally increases or decreases uniformly with increasing frequency, but occasionally, like for polymethylmethacrylate, the $\tan \phi$ function peaks (at about 50 Hz, for example PMMA).²⁸

Resonance Dispersion

Fitzgerald has found that crystalline polymers,^{29,30} polycrystalline solids³¹ including metals³² and some single crystals³³

exhibit unusual response to cyclic mechanical stress under certain conditions. More recently³⁴ he has shown that biological materials such as intervertebral disks exhibit this response, which is a frequency dependence of the complex compliance that has the characteristics of a resonance dispersion, illustrated schematically for resonances at ν_1 and ν_2 as follows:



As depicted above, the loss modulus E'' goes through a very sharp maximum while the storage modulus E' goes through a maximum and a minimum and can even go negative. Even a metal, which for all practical purposes is purely elastic, can exhibit completely viscous behavior at particular frequencies.

Fitzgerald³⁵ has presented a theory to explain such resonance dispersions. In it he uses wave mechanics as the basis for a new theory of deformation. The basis for this is the hypothesis that, under mechanical loads, some of the atoms in a crystal move through sections of the crystal lattice as waves rather than as classical particles. A macroscopic deformation results after large numbers of atoms have moved through the crystal. After a wave mechanical treatment, he obtains the equation:

$$\nu_p \approx \frac{h}{8mS^2} q^2$$

where ν_p = a set of frequencies where resonances occur

h = Planck's constant

m = the mass of the atom responsible for the resonance

S = some geometric constant in the material (segment length)

q = an integer (1, 2, 3, ...)

Fitzgerald³⁶ states that there is a preponderance of evidence that S is about 10^{-4} cm in many cases of low audio frequency resonances. Particle-wave modes have been measured in the low audio range for metals known to have a dislocation cell size of 10^{-4} cm. The occurrence of these inelastic vibrations is shown to result from the presence of net oscillating forces and torques acting on lattice segments during particle-wave propagation.

Experimental Methods

Equipment

A viscoelastimeter was constructed to measure the viscoelastic properties of trabecular bone in longitudinal compression. Schematics and photographs of the complete apparatus are given in Figures 10 and 11. In the design of this unit, particular care was given to the following:

1. The specimens must be measurable when wet; that is, as soon as possible after dissection and in a physiological state of hydration. No cements can be used on the sample because of this.
2. The viscoelastometer must be entirely non-destructive. This means the utilization of small stress and small displacements. High sensitivity is therefore necessary. This ensures that the specimens, after measurement, can be examined microscopically to obtain non-artifactual structural parameters.
3. The viscoelastometer must have good response throughout the low audio frequency range.

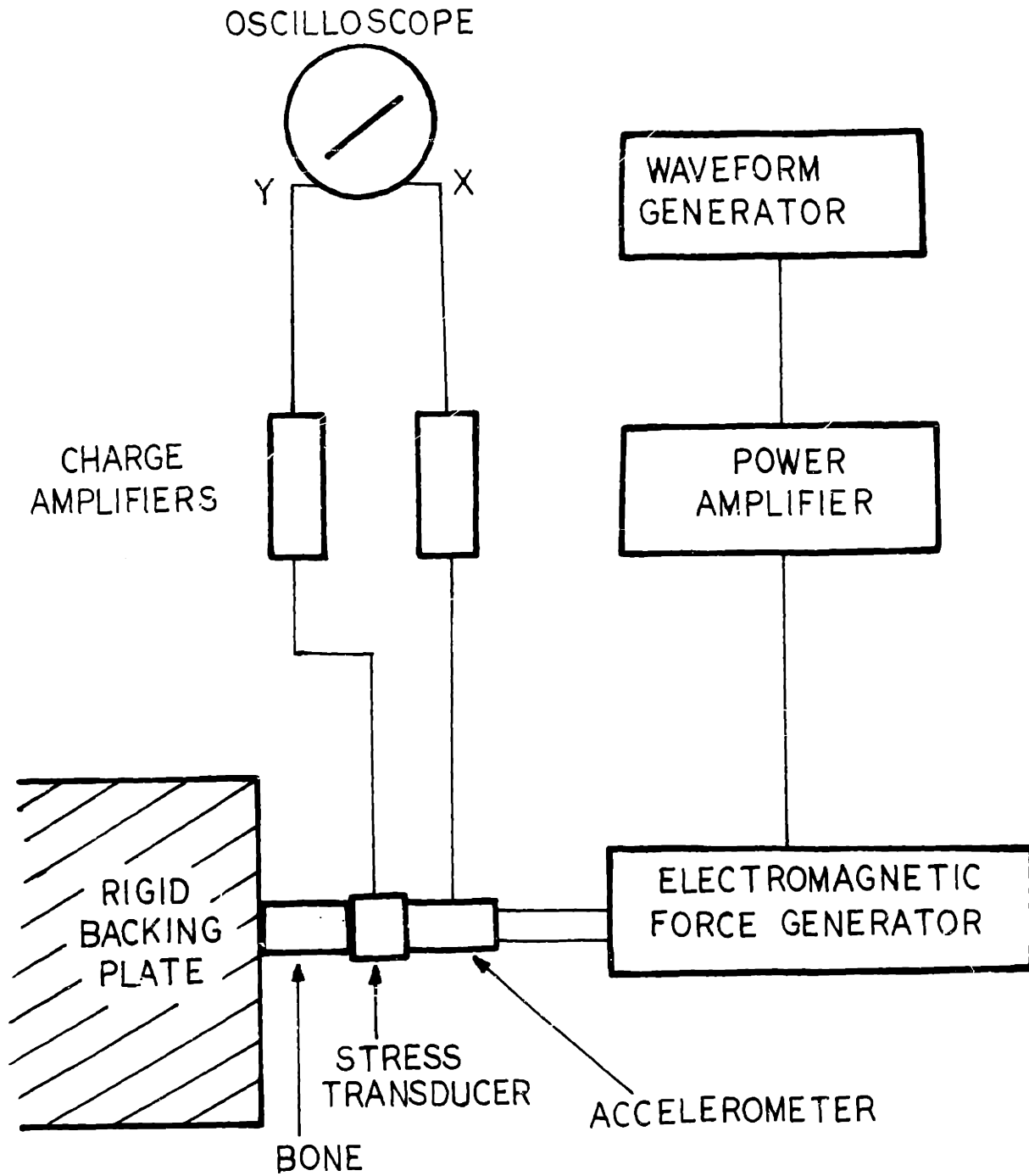


Figure 10: Schematic of viscoelastometer used to measure the viscoelastic properties of trabecular bone.

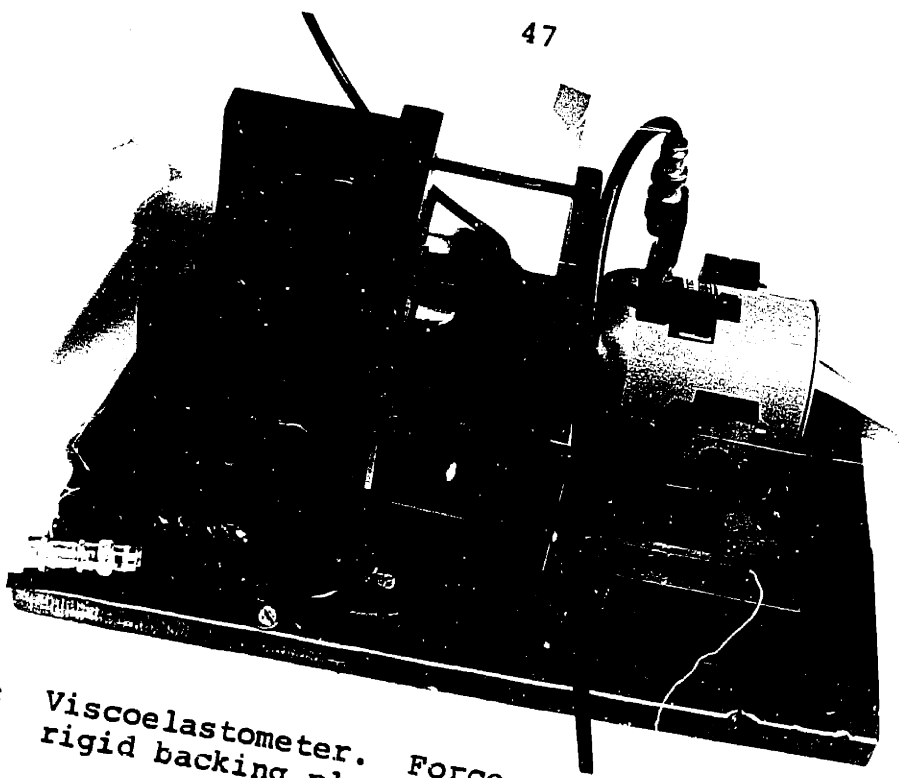


Figure 11A: Viscoelastometer. Force generator is at right and rigid backing plate to left.

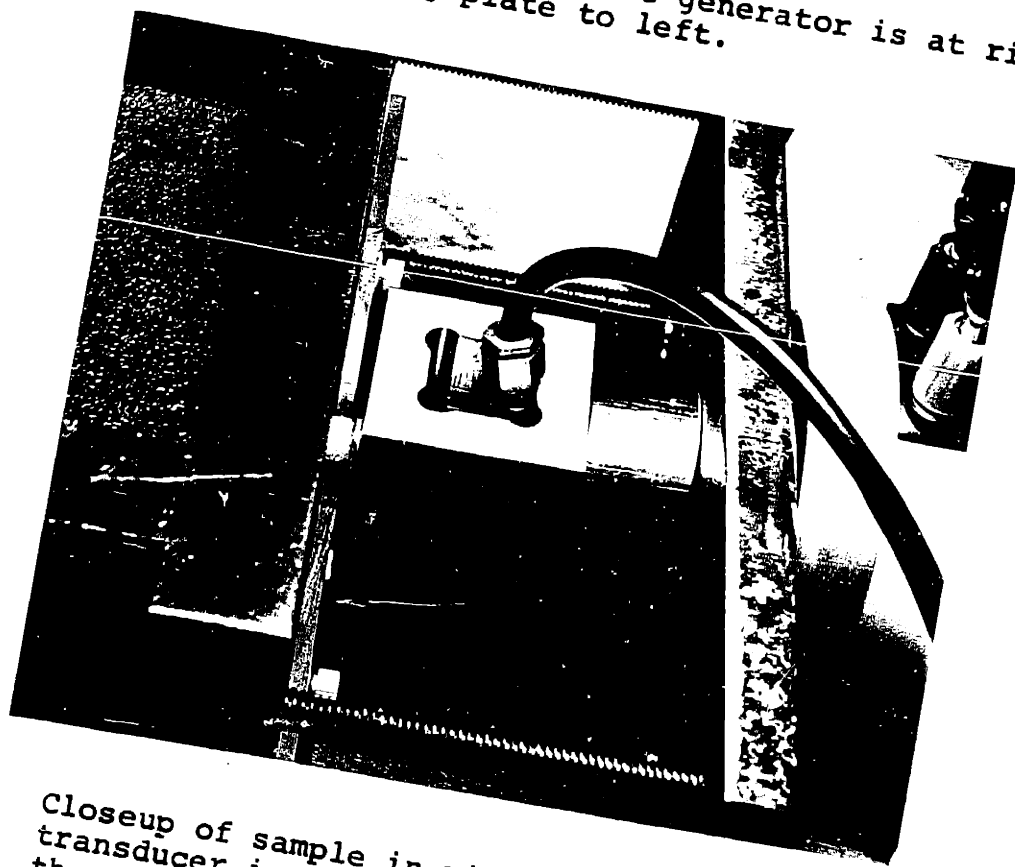
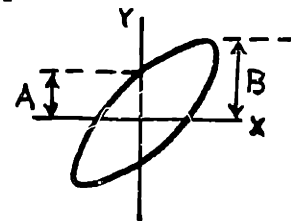


Figure 11B: Closeup of sample in viscoelastometer. The stress transducer is sandwiched between the bone plug and the steel box containing the accelerometer.



As shown in the diagrams, an electrical transducer capable of generating sinusoidal forces was used. A piezoelectric stress transducer was chosen for its high rigidity and good frequency response. A piezoelectric titanate zirconate variety because of the high rigidity requirement. A piezoelectric accelerometer was used for strain data. This was chosen because of the high acceleration transducers compared to displacement transducers. In addition, the electrical characteristics (frequency response, phase shifting, etc.) were better than those of the stress transducer. The signals from the transducers were fed into two Kistler charge amplifiers (with their own electrical characteristics) and subsequently connected to a scope to produce a Lissajou figure. The polarity of the signals was such that, for a purely elastic material, the stress and strain were in phase. Thus the acceleration and strain were shifted 180° with respect to the stress. The scope screen displayed stress versus strain $\times \omega^2$ (see Figure 37 for discussion). Amplitudes and phase relationships were determined from the scope screen:³⁷



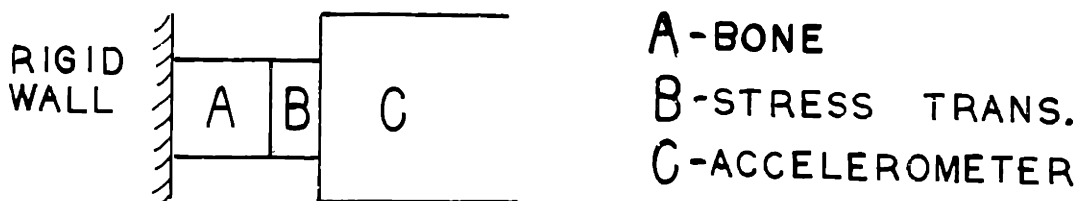
$\sin \phi :$

Both the stress transducer and accelerometer were connected to a vibration standard that puts out a sinusoidal wave at 100 Hz. For the stress transducer, a known force was applied to a surface and the assembly placed on the v

$F=ma$, the known force applied to the transducer can be compared to the voltage output for an accurate calibration. For the accelerometer, the voltage output was measured for the known acceleration of 1 g rms applied. Both of these devices have a flat frequency response over the range of frequencies used, so the calibration at 100 Hz is useful for frequencies up to 5000 Hz approximately.

The accelerometer was enclosed in a steel box to increase its effective rigidity. A thin sheet of Saran wrap was placed between the bone and the stress transducer to keep the moisture of the sample from shorting the leads of that unit. The bone, stress transducer, and accelerometer unit were clamped in a yoke assembly against a heavy, rigid backing plate. The force generator was coupled mechanically to this yoke. The geometry was such and the system was stiff enough that the stresses and accelerations measured were those experienced by the bone specimen. The diameter of the stress transducer was the same as that of the bone sections. This transducer therefore gives a good measure of the force on the cross-section of the bone. The accelerometer measures the acceleration of the bone-stress transducer interface, since the stress transducer is so rigid that its strain is negligible ($E=10^7$ psi).

The geometry is shown below:



The applied and measured stresses were of the form:

The accelerations measured were of the form

$$a(t) = -a_{\max} \sin(\omega t - \phi)$$

After two integrations, one obtains

$$x(t) = \frac{a_{\max}}{\omega^2} \sin(\omega t - \phi)$$

Division by the sample thickness gives the strain

$$\epsilon(t) = \frac{a_{\max}}{l\omega^2} \sin(\omega t - \phi)$$

Notice that a change in sign of the acceleration $a(t)$, which corresponds to a phase shift of 180° , gives

$$a(t) = a_{\max} \sin(\omega t - \phi)$$

and division of both sides by $l\omega^2$ gives the strain. An oscilloscope display of $\sigma(t)$ versus $a(t)$ is therefore equivalent to $\sigma(t)$ versus $l\omega^2\epsilon(t)$. It is obvious that measurement of the acceleration $a(t)$ gives an amplitude that is a factor of ω^2 greater than a measurement of the displacement $x(t)$. Typical stresses were of the order of 1 psi. Typical strains were of the order of 10^{-5} or 0.001%. Subsequent microscopic examination attested to the nondestructive nature of these measurements.

Unfortunately, the phase angle ϕ could not be measured if it was smaller than about 3° . Measurements of very small values of the loss tangent (less than 0.08) are thus impossible with this equipment. Polymethylmethacrylate (PMMA) and natural rubber were measured to ascertain if the equipment was performing as designed.

Material

The distal end of human femurs from four patients were obtained at autopsy. Transverse sheets 5 mm thick were machined

from the condyles (Figure 12A) on a high-speed cutoff wheel with a coolant used to prevent heating of the bone. Parallel cuts were easily made on the apparatus. 3/8-inch diameter plugs of trabecular bone were produced from these sheets by turning the sheets on a lathe with a very sharp cutting tool. The amount of bone removed on each pass was small enough to prevent excessive deformation of the cylindrical specimen. Figure 12B shows the final sample of trabecular bone produced in this manner. In all instances, the viscoelastic properties of the bone were measured wet and within 48 hours of death of the patient.

A typical measurement consisted of placing a cylindrical sample, with dimensions 3/8-inch diameter by 5 mm thick between the stress transducer and backing plate, and recording manually from the oscilloscope trace the amplitudes of stress and acceleration and the phase angle. This was done in a frequency sweep from 100 to 2000 Hz.

Results and Discussion

Viscoelastic Properties of Rubber and PMMA

Figure 13 is an oscilloscope photograph for the sample of natural rubber at 2400 Hz. The phase angle here is 49° . Ferry³⁸ gives the loss tangent of natural rubber as approximately 1 over the range of frequencies 100 - 2000 Hz. This is in good agreement with the measurements in this study. There is more discrepancy in the modulus as shown in Figure 14. This is attributed to the necessity of clamping the rubber firmly in the apparatus, which resulted in a compression of 50 - 100%. It is well known that

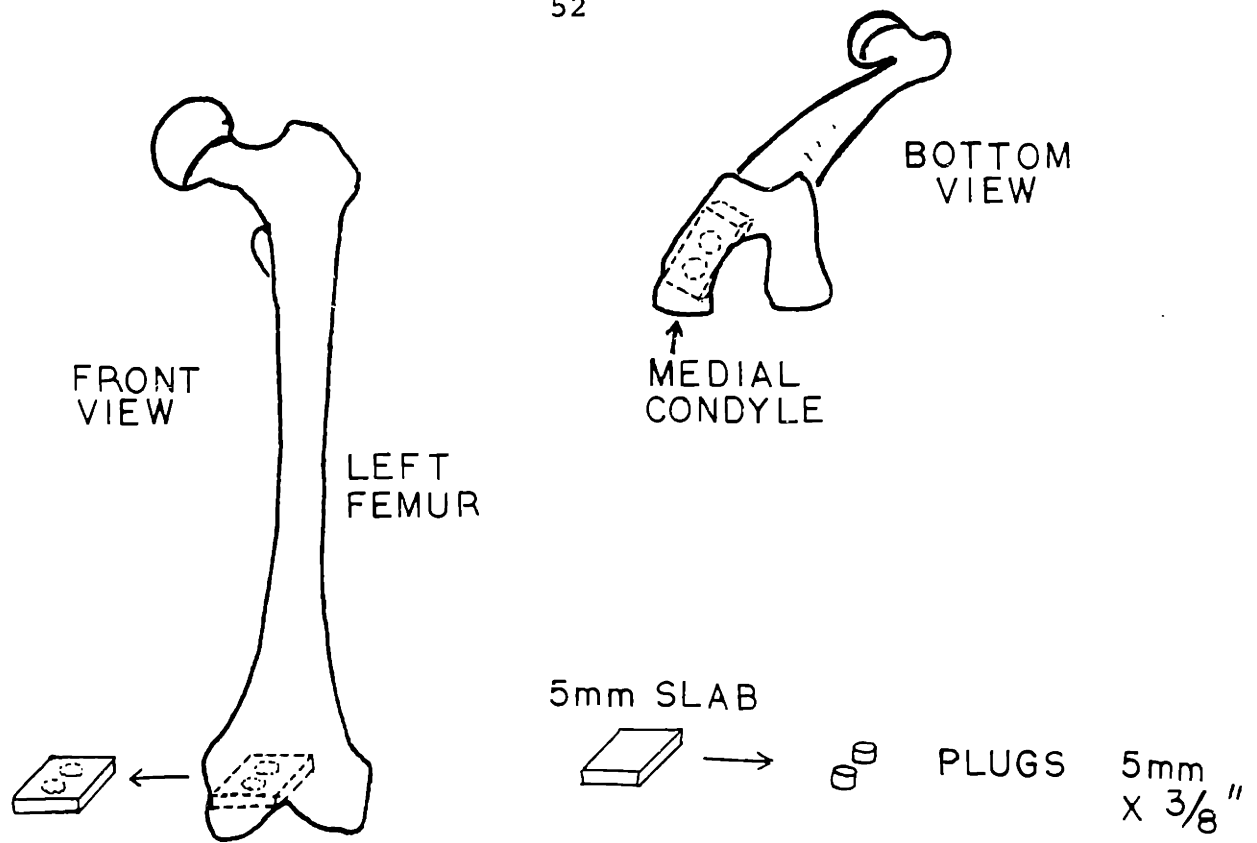


Figure 12A: Femoral location of samples of bone used in this study.

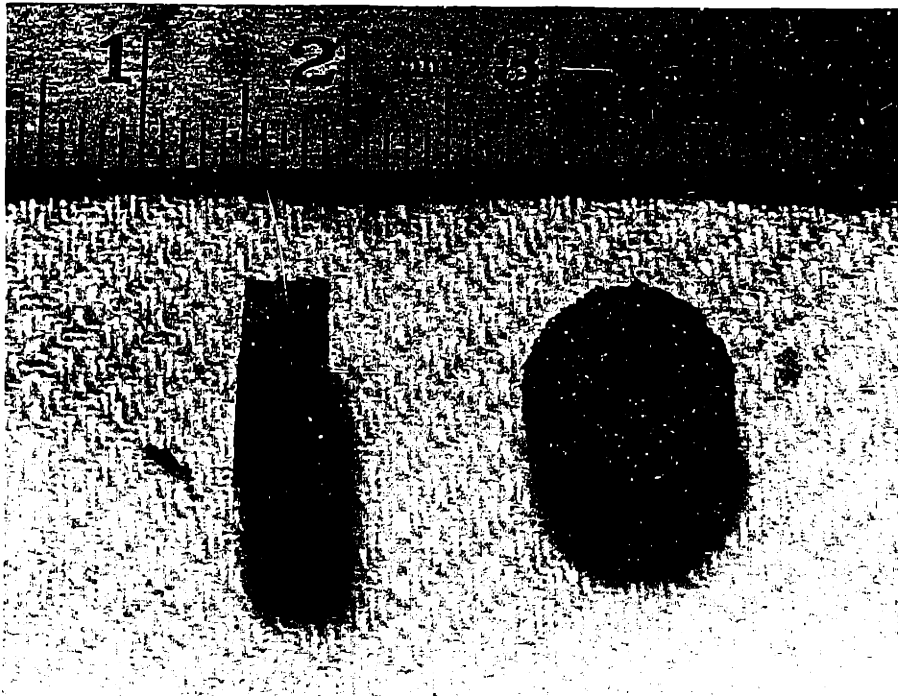


Figure 12B: Closeup of bone plugs used for viscoelastic measurements.

12



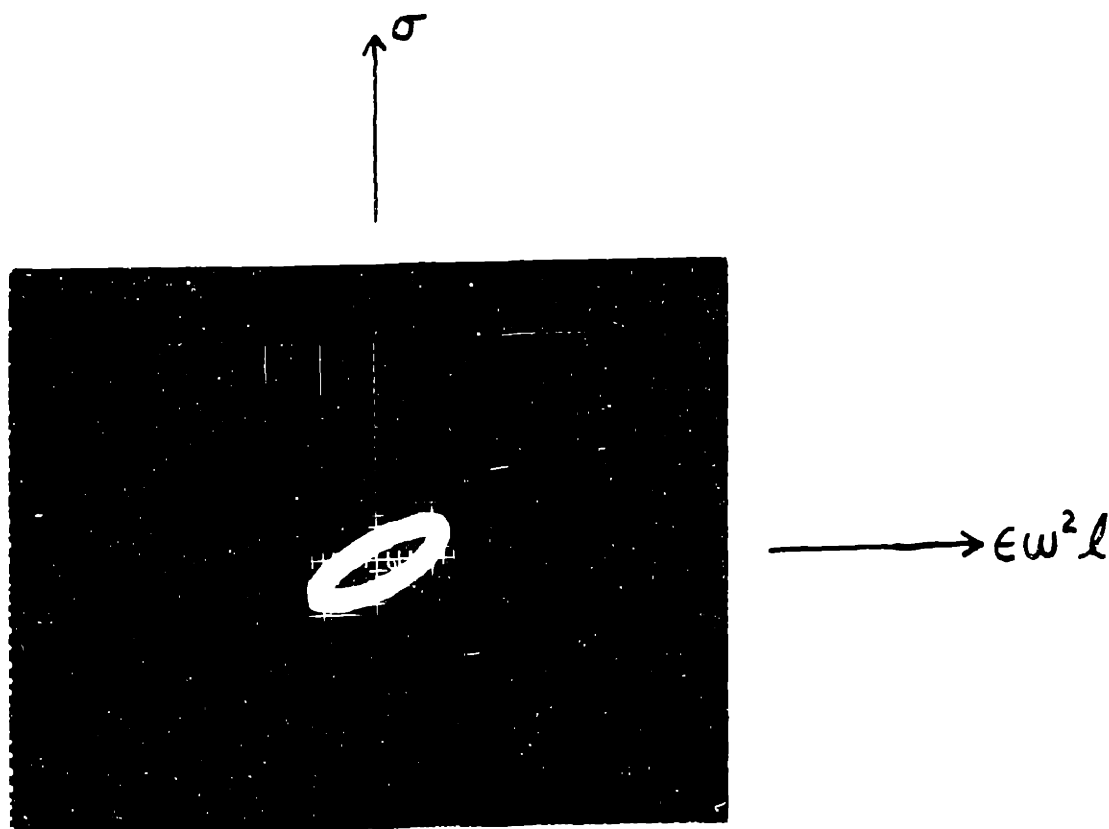


Figure 13: Oscilloscope photograph for natural rubber at 2400 Hz. There is a phase angle of 49° between stress and strain, the loss tangent being slightly greater than 1. This shows considerable viscous response.

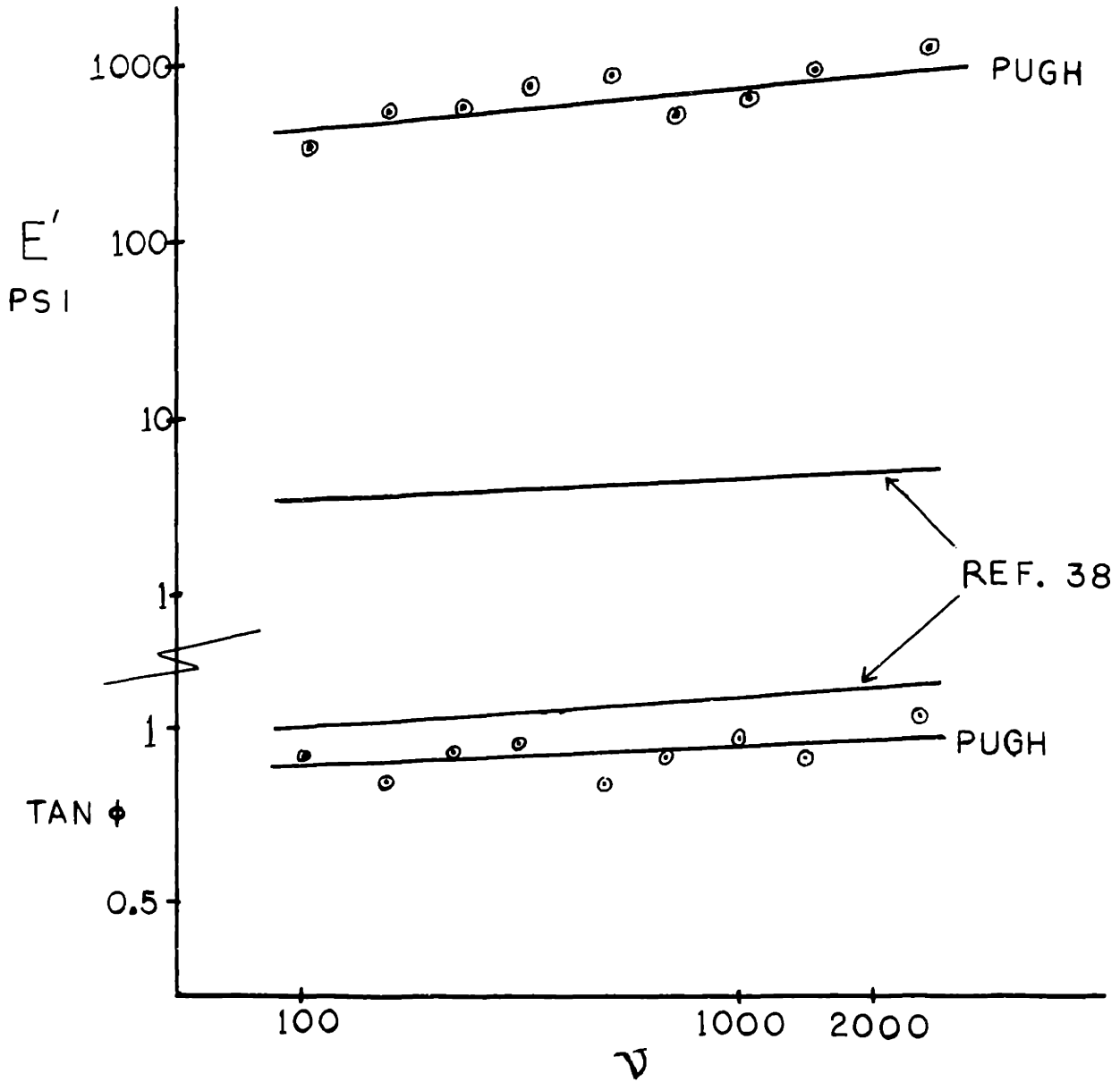


Figure 14: Viscoelastic properties of natural rubber as a function of frequency.

the mechanical properties of polymers change drastically with preload.³⁹ There is nevertheless good general agreement with the data of Ferry in the dependence of modulus with frequency for natural rubber.

The agreement of data obtained for PMMA with published data is much better, as Figure 15 shows. The published values for $\tan \phi$ go from 0.1 to 0.04 at 100 and 1000 Hz respectively. The experimental values for $\tan \phi$ were not measurable on this apparatus except at 100 and 200 Hz, where the values agree with those of Ferry.⁴⁰

The data presented in Figures 14 and 15 show that the viscoelastometer constructed is capable of producing data consistent with previously published data. The data for PMMA is much better than that for natural rubber, since the viscoelastometer was designed to measure properties of hard solids (such as PMMA and bone) in a compression mode.

In comparison with the published data for the PMMA, the modulus measurements from present equipment tend to be slightly low, by perhaps a factor of 2 to 5. This could be due to slight nonlinearities in amplifier response, or in the accelerometer actually measuring strains slightly larger than that in the bone. It is possible that the backing plate of the viscoelastometer is buckling slightly during testing, even though this was stiffened by a heavy cast iron plate. Nevertheless, the two data points for $\tan \phi$ in Figure 15 show that the measurement of this quantity is exactly where it should be. (Values of $\tan \phi$ lower than 0.08 are unmeasurable on the oscilloscope.) Thus, even if the

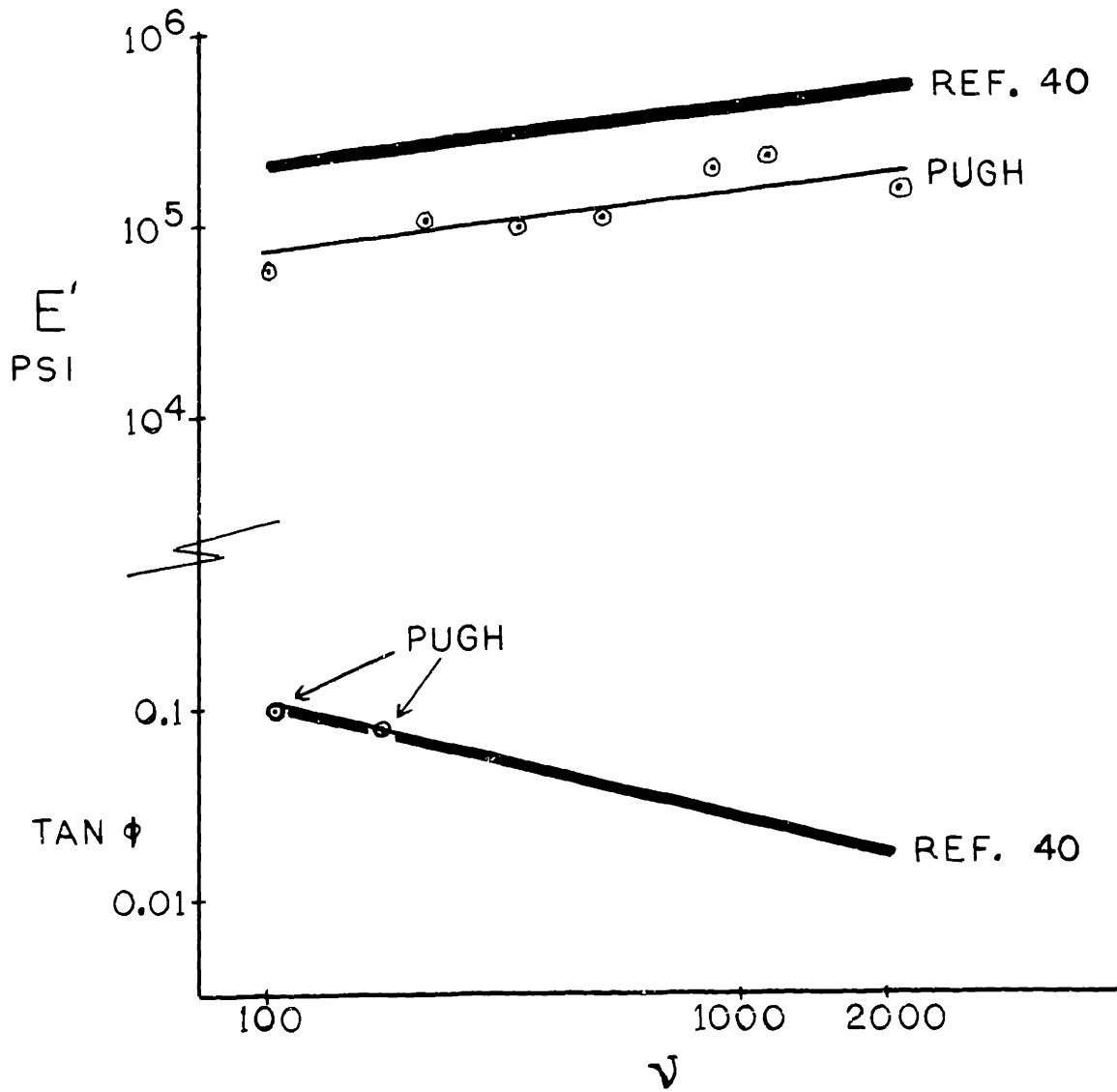


Figure 15: Viscoelastic properties of PMMA as a function of frequency.

magnitude of the modulus as measured is low, the loss tangent can be measured with some certainty if it is above a certain level. Therefore, faith can be put in the data for the relative values of the loss (viscous) and the storage (elastic) components of the complex compliances or moduli.

Viscoelastic Properties of Trabecular Bone

The experimentally measured data for transverse sections of trabecular bone from the medial condyle of human femur are given in Figure 16. The data are roughly around 10^5 psi for the modulus (storage). In plotting these data, resonances were avoided in order to get an overall picture of the elastic component of the modulus as a function of frequency. The phase angle between stress and strain was unmeasurable over this range of frequencies. An oscilloscope photograph for trabecular bone at 1000 Hz is shown in Figure 17. The linearity shows that the phase angle ϕ and the loss tangent are close to zero.

The data for the elastic modulus of trabecular bone in Figure 16 shows some spread around 10^5 psi, from a low of 0.8×10^5 at 100 Hz to a high of 1.5×10^5 at 3000 Hz. Note that the spread of the values for the different specimens is roughly a factor of 2 (the limits of the dashed lines in the figure). This is ascribed to the extreme variability of structure in the bone from the different patients (this will be verified in Section IV). (A most interesting discussion of the scatter in mechanical properties data for human bone is given by Wall, Chatterji and Jeffrey.⁴¹) These data were all measured away

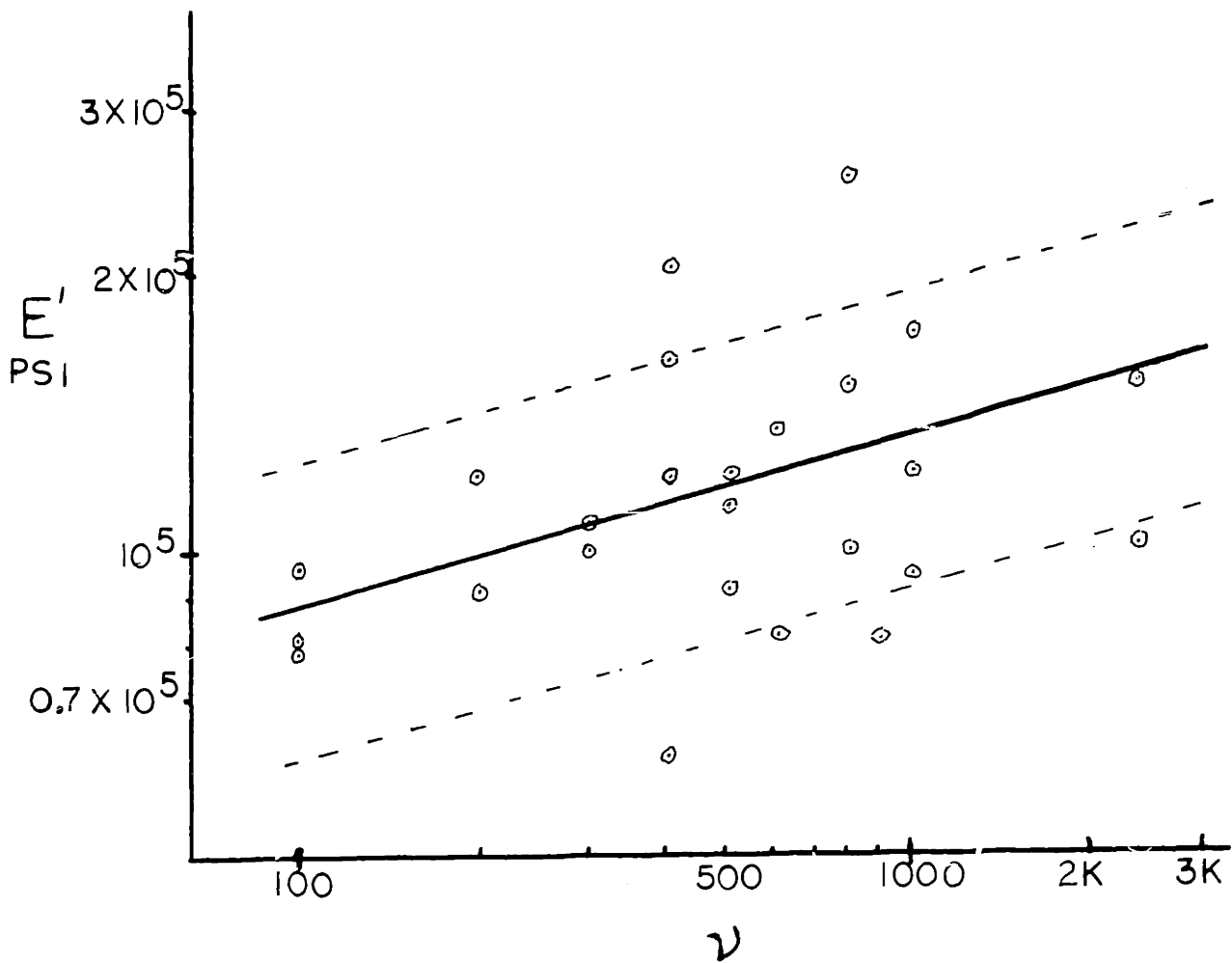


Figure 16: Elastic modulus for human trabecular bone as a function of frequency. The dashed lines represent a factor of 2 spread about the heavy line.

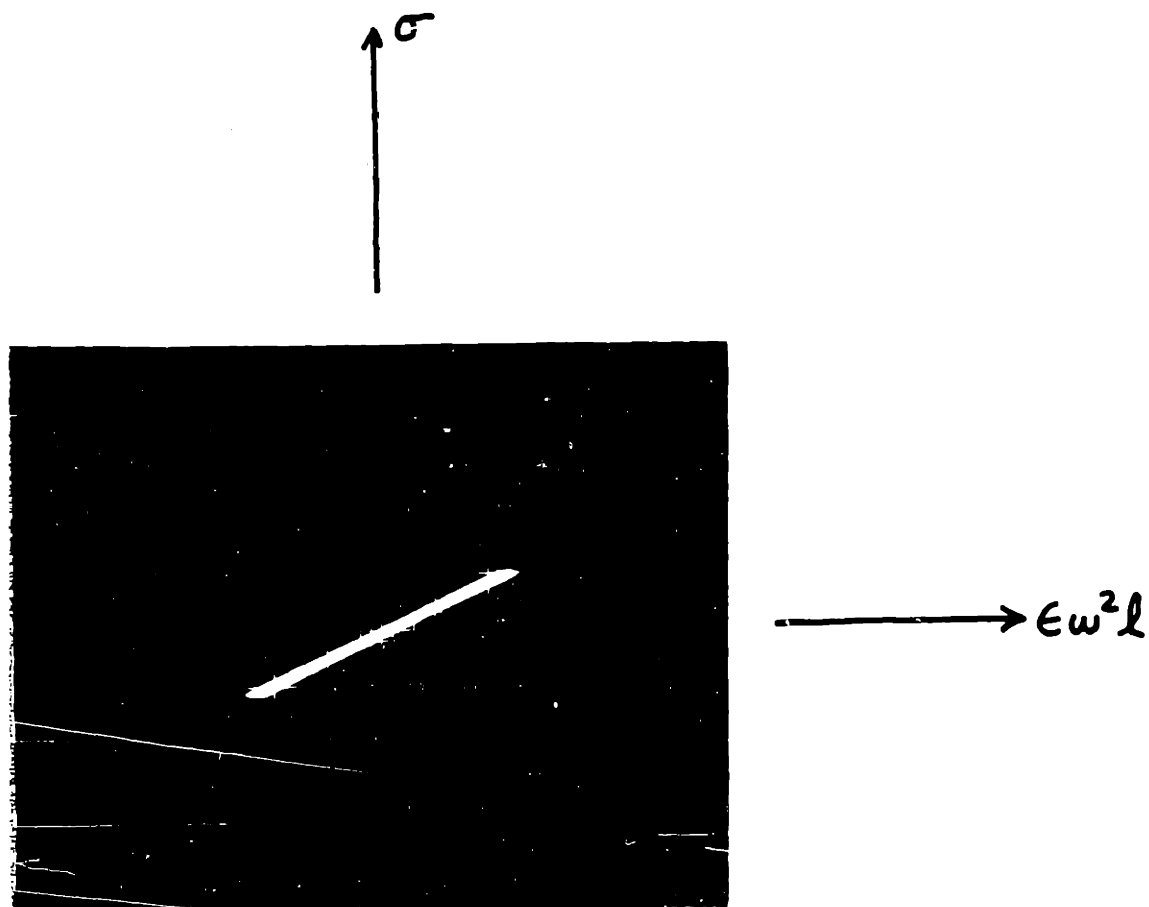
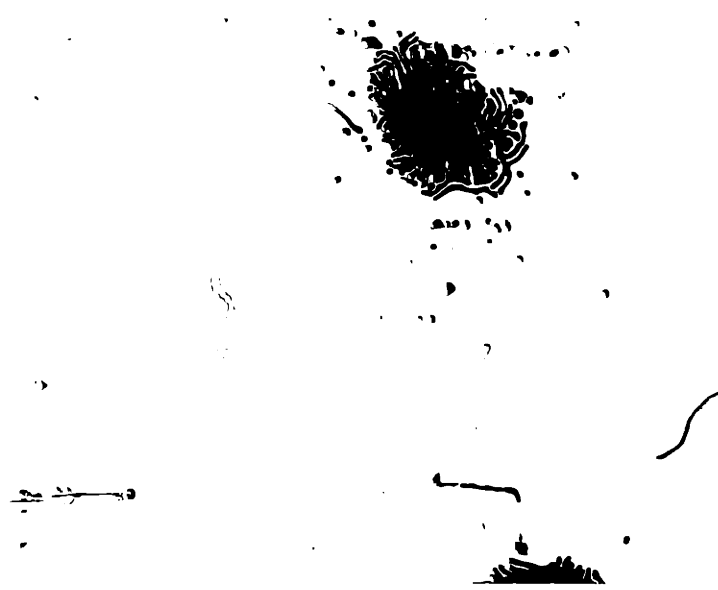


Figure 17: Oscilloscope photograph for human trabecular bone at 1000 Hz. The linearity shows that, at this frequency, trabecular bone behaves purely elastically.



from the resonant points encountered in the frequency spectrum for the bone, and therefore show a linear response with frequency. At all points the viscous component of the modulus was zero (linear trace on the oscilloscope as shown in Figure 17). This agrees with the conclusions of Swanson and Freeman discussed in the introduction.

The data obtained for the modulus of trabecular bone in the femoral condyles compares favorably with the data of McElhaney, Alem and Roberts.⁴² Their data referred to vertebral bodies and cranial bone and varied from 2.2×10^5 to 3.5×10^5 psi respectively. There is very little data in the literature in addition to this on the elasticity of trabecular bone. There has been much work done on the compressive strength of trabecular bone, but the elasticity data is sparse. It is well-known that the modulus of cortical bone is of the order of 10^6 psi⁴³⁻⁵⁰, and it is generally believed that the modulus of trabecular bone is an order of magnitude lower.⁵¹

Strain Rate Effects

It is of interest to note the strain rates used in this study. The strains are of the order of 10^{-5} and are applied at frequencies of 100 to 1000 Hz. The maximum strain is achieved in 1/4 cycle, so the effective strain rates are of the order of 0.004 to 0.04/second. These are very low strain rates by engineering standards. The data presented by McElhaney and Byars⁵² and by Sedlin⁵³ for cortical bone show only slight strain rate dependence for these strain rates at small strains. It is suggested that the increasing modulus with frequency observed in this study is a reflection of

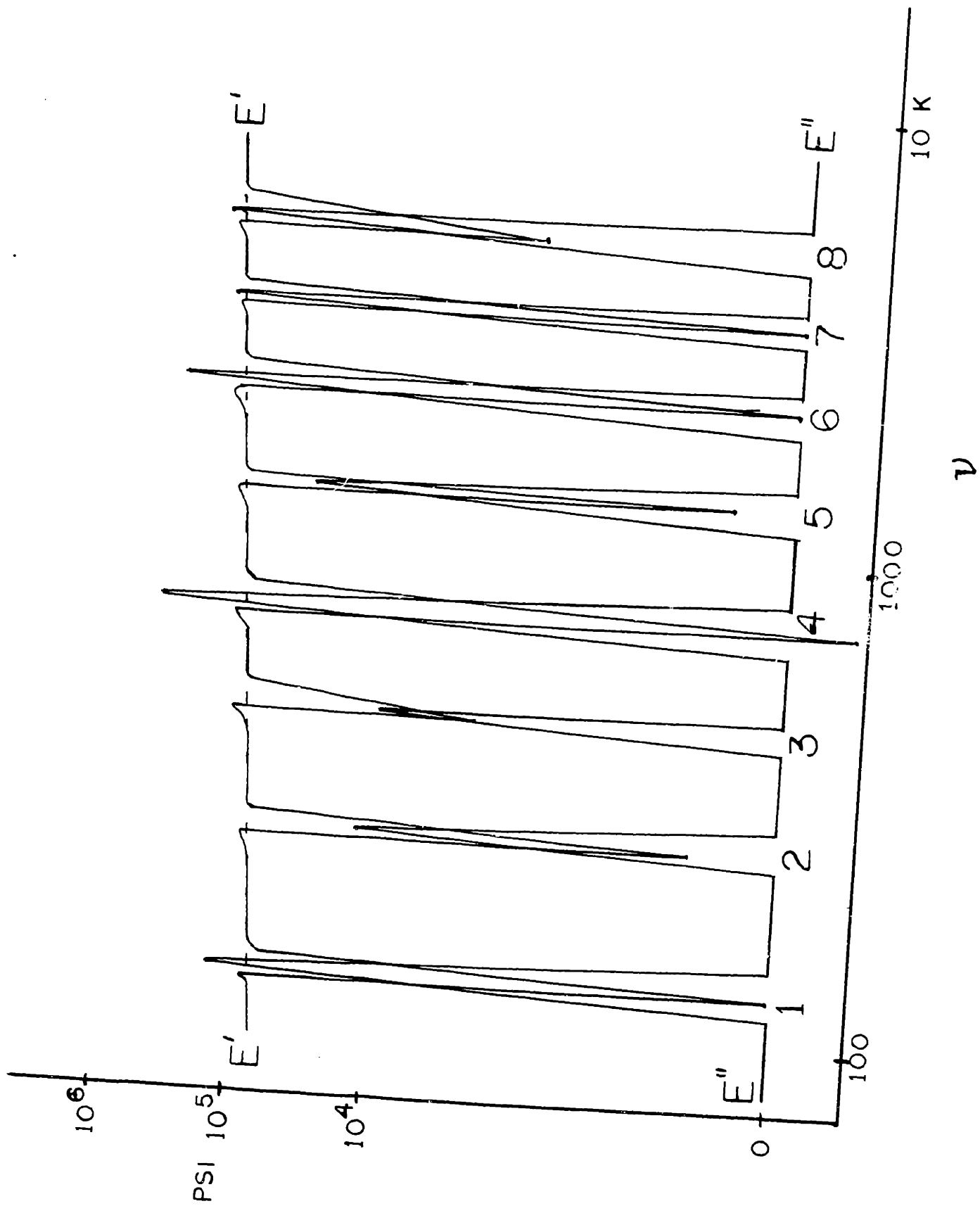
the small strain rate dependence of trabecular bone. In addition, part of the spread in data at particular frequencies could be due to the measurement of the modulus of different samples at different strain rates but at the same frequency of mechanical loading. Although care was taken to ensure that all measurements were made under the same conditions (constant voltage input to the force generator), the construction of the yoke and slight differences in geometry of the samples caused some variation in strains (and therefore in strain rate) that was unavoidable. If the yoke resonated at a particular frequency, the stresses and strains produced in the viscoelastometer were slightly higher than normal, although, from the construction of the unit, only the response of the bone was measured and the stress and strain were still in phase. Resonances of the yoke were found only to have these strain rate effects. In retrospect, it would probably have been advantageous to have measured the properties at constant strain rather than at constant input to the force generator.

Resonance Dispersion Measurements

The data in Figure 18 show the resonance dispersion spectrum for a sample of human trabecular bone (from the same group used for the data in Figure 17) after a very careful frequency sweep through the observed resonances.

The figure is necessarily distorted for clarity. Particular attention was focused on the relative levels of the viscous and elastic components of the modulus at the resonant

Figure 18: Storage and loss moduli for human trabecular bone as a function of frequency. The data show sharp resonances at certain frequencies between 100 and 4000 Hz.



frequencies. These data are reproduced exactly. The elastic component drops to zero at frequencies 1, 6, and 7; and it even goes slightly negative at frequency 4. At each of these frequencies it is interesting to note that the viscous component climbs either above or close to the average value of the elastic component.

Table 2A summarizes the frequencies at which resonance occurred. Table 2B shows these frequencies separated into two sets. If the ratios of the higher frequencies to the first frequency in each set are calculated:

$$\begin{array}{ll} \nu_{4c} / \nu_{1c} = 15.9 \approx 16 & \nu_{4p} / \nu_{1p} = 15.9 \approx 16 \\ \nu_{3c} / \nu_{1c} = 9.3 \approx 9 & \nu_{3p} / \nu_{1p} = 9.4 \approx 9 \\ \nu_{2c} / \nu_{1c} = 3.9 \approx 4 & \nu_{2p} / \nu_{1p} = 3.85 \approx 4 \end{array}$$

one finds that, roughly, the ratios go as q^2 where q is an integer. The columns marked "calculated" are the set of frequencies one would calculate from ν_1 assuming a q^2 relationship. The agreement between the experimental and calculated values is remarkably good. The equation governing this behavior is given by:

$$\nu_p \approx \frac{h}{8\pi m S^2} q^2$$

from the introduction to this section. Since the mass of the atom responsible for the wave modes appears in the expression, one would expect a discrete set of frequencies for each type of atom in the structure. Bone is approximately 65% inorganic matter by weight, the major constituent being a type of calcium phosphate, hydroxyapatite, with a formula similar to

TABLE 2A

Frequencies of Resonance for Trabecular Bone

(from Figure 18)

1	145
2	203
3	570
4	780
5	1350
6	1900
7	2310
8	3230

TABLE 2B

Two Sets of Resonances

$c a^{40}$		p^{31}	
Calc.	Exp.	Calc.	Exp.
145	145	203	203
580	570	812	780
1300	1350	1827	1900
2320	2310	3248	3230

$[Ca_{10}(PO_4)_6(OH)_2]$ ⁵⁴. The likely candidates for the observed resonances would therefore be calcium and phosphorous. The set of modes for each atom would then be as follows:

$$v_{qCa} \cong \frac{h}{8m_{Ca}S^2} q^2 \qquad v_{qP} \cong \frac{h}{8m_P S^2} q^2$$

Therefore, the ratios of the q modes for each atom would be:

$$\begin{array}{l} q = 1 \\ \vdots \\ q = n \end{array} \qquad \begin{array}{l} v_{1Ca} : v_{1P} = m_P : m_{Ca} \\ \vdots \\ v_{nCa} : v_{nP} = m_P : m_{Ca} \end{array}$$

The q=2 frequencies for calcium and phosphorus are 570 and 780, respectively. Calculating the ratios:

$$\begin{aligned} v_{2Ca} : v_{2P} &= 570 : 780 = 0.731 \\ m_P : m_{Ca} &= 30.97 : 40.08 = 0.773 \end{aligned}$$

The agreement here is good, indicating that the choices of calcium and phosphorous are probably correct.

Using the formula $v_{2Ca} = \frac{h(2)^2}{8m_{Ca}S^2}$, the value of S calculates to 2.96×10^{-4} cm or roughly 10^{-4} inches. This corresponds (see photographs in Section I of this thesis) to the thickness of a lamella in trabecular bone. It seems highly probable that the momentum wave modes set up in the lamellae of trabecular bone by the calcium and phosphorous atoms are responsible for the observed resonances. The slight deviations in the experimental data from that calculated are probably due to a range of segments lengths being responsible for the momentum-wave modes.

The data taken by Jurist and Campbell⁵⁵ show that the femur exhibits resonances at 100, 200, 700, 1200, and 3000 Hz. The ulnar resonant frequencies⁵⁶ are at 250 and 450 Hz. It is suggested that, in addition to geometric considerations, the

resonances observed in these intact long bones may be influenced by the resonance spectrum of the trabecular bone present in the ends of the bones. Thus, the overall mechanical behavior of the long bones is probably controlled to some extent by the mechanical behavior of the trabecular bone contained therein.

Conclusions

1. The viscoelastometer constructed for this study is capable of giving good data for modulus and compliance, and excellent data for the loss tangent.
2. Trabecular bone behaves purely elastically throughout the frequency range 100 to 4000 Hz, except at several frequencies where it sharply exhibits marked viscous behavior. The elastic modulus for trabecular bone in the absence of resonances is 10^5 psi throughout this range.
3. It is hypothesized that there exist two discrete sets of resonant frequencies: one set for calcium and one for phosphorous in the bone. It is highly probable that the critical parameter S in the Fitzgerald equation corresponds to a lamellar spacing in trabecular bone (approximately 10^{-4} inches).

IV. STRUCTURE-PROPERTY RELATIONSHIPS IN TRABECULAR BONE

Introduction

Previous Work

The results of Section III indicate that there is a spread in the data for the elastic modulus of trabecular bone, and that a part of this spread could be due to slight differences in structure of the trabecular bone. It is well-known⁵⁷ that structure-property relationships exist for metals, polymers, and ceramics. The only data^{58,59} that exist for trabecular bone merely relates the compressive strength to the ash weight or porosity (volume fraction bone). The data furthermore relate only to vertebrae or cranial bone. There has been virtually no work done on the relationship between stiffness and microstructure measured on a quantitative stereological⁶⁰ basis. It has been suggested⁶¹ that no simple correlation exists between volume fraction bone and stiffness of human trabecular bone in the knee.

There has been much work done concerning the role of stress in controlling the structure of bone.⁶² The basic rule governing this is best summarized by Wolff's Law⁶³: a change in stress produces a change in structure. If the stresses in a bone increase, the bone thickens so as to be able to support this increased stress. If the stresses decrease, the amount of bone present decreases because it is no longer needed. It is well-known that bones lose mass through disuse.⁶⁴

Stereology

Several very important relationships have been derived to aid in the measurement of stereological parameters. The most basic⁶⁵ is probably

$$V_V = L_L$$

which states that the volume fraction of a particular phase in a structure is statistically equal to the fraction of a random line that lies on cross-sections of that phase in a random two-dimensional section. The second most basic⁶⁶ is

$$S_V = 2N_L$$

which allows one to calculate the surface area of a phase per unit volume by measuring the number of intercepts that surface makes with a random line drawn on a random two-dimensional cross-section. A useful extension of this is the contiguity ratio⁶⁷

$$C_t = \frac{2S_V^{\alpha\alpha}}{S_V^{\alpha\beta} + 2S_V^{\alpha\alpha}}$$

which is an indication of the average degree of contact of two phases α and β . C_t is the fraction of the total boundary area of a phase α shared by particles of the same phase. The factors of 2 arise because each $\alpha\alpha$ interface is associated with 2 particles of α , but the $\alpha\beta$ interfaces involve only 1 particle of β . "The calculations of contiguity do not require any assumption as to volume fraction, particle size, or particle shape."⁶⁸ The contiguity ratio varies from 0 to 1 as the phase α changes from a completely dispersed state to one of complete agglomeration.

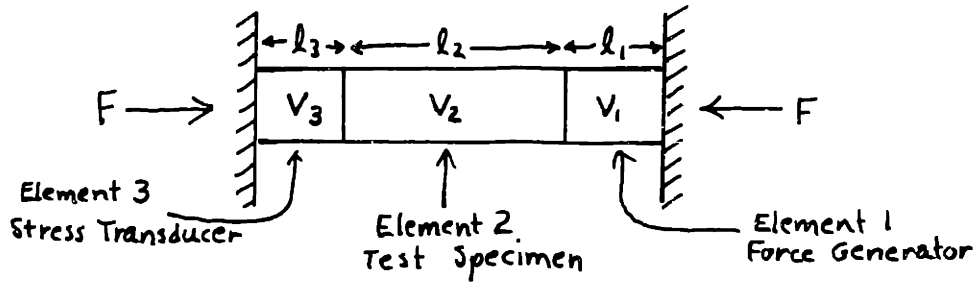
Equipment

To facilitate the rapid and accurate measurement of the moduli of different samples of trabecular bone from various animals, an apparatus was designed to measure the relative stiffness of specimens at physiologically meaningful frequencies. Relative stiffness measurements have been generally accepted as meaningful and have been in use for years in several different types of apparatus.⁶⁹

The following design criteria were observed in construction of the apparatus:

1. The loading must be of a dynamic nature and at low levels of stress and strain to avoid damaging the bone and to remain in the linear elastic region.
(The advantages to these techniques have been discussed in Sections III and Appendix A.)
2. No cements should be used, since these can penetrate the bone and change the properties. The sample should be held in place by a small static compressive load.
3. The particular frequency chosen for the measurements should be physiological and well away from the observed resonances in Section III.
4. The design must be simple and allow reproducible measurement of stiffness in a matter of minutes.

In keeping with the above guidelines, an apparatus was designed according to the following diagram:



The sample to be measured elastically is clamped with a force F between two rigid walls. A transducer is clamped between each end of the test specimen and the wall. A sinusoidal voltage is applied to the forcing transducer. Because all the elements are assumed to be purely elastic, this can be equated as a ramp voltage for 1/4 cycle with no loss of rigor. Since the transducer is piezoelectric, it generates a ramp force that is picked up by the stress transducer. This is an incremental force in addition to the clamping force F . The stress transducer thus measures the stress in the linear chain of three elements.

The forcing transducer is a very high-impedance ($10^9 \Omega$) unit. It therefore acts as a parallel-plate capacitor with the area between the plates filled by a dielectric. The capacitance of such a unit is given by the following:⁷⁰

$$C = \frac{\epsilon_0 K A_1}{l_1} \quad (1)$$

Where ϵ_0 is the permittivity of free space, K is the dielectric constant of the transducer material, A_1 is the cross-sectional area of the transducer, and l_1 is the length of the transducer (the distance between the plates of the capacitor). The energy input to the capacitor as a function of the voltage applied between the plates is:⁷¹

$$\mathcal{E}'' = \frac{1}{2} C V^2 \quad (2)$$

If the initial energy state \mathcal{E}' of the transducer is taken as that at zero voltage, then the energy state \mathcal{E}'' after application of the voltage is given by equation (2) and the energy change is:

$$\begin{aligned}\mathcal{E} &= \mathcal{E}' - \mathcal{E}'' = 0 - \frac{1}{2}CV^2 \\ \mathcal{E} &= -\frac{1}{2}CV^2\end{aligned}\quad (3)$$

Of course, the capacitor expands or contracts under the applied voltage. The amount of this change in length, Δl_1 , is very small compared to the original length l_1 (10^{-5} and 10^{-1} inch respectively). Therefore the change in capacitance upon expansion or contraction is neglected.

The energy term given by equation (3) must be equal to the energy transferred to or work done on the material comprising elements 1, 2 and 3. The force transducer expands due to the voltage V , and the energy \mathcal{E} put into the transducer goes into the strain energies of the three elements:

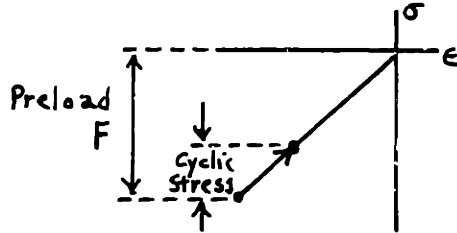
$$\mathcal{E} = \mathcal{E}_1 + \mathcal{E}_2 + \mathcal{E}_3 \quad (4)$$

assuming purely elastic behavior of the three elements. Because of the compressive preload F , when the forcing transducer expands, it reduces its strain energy, and elements 2 and 3 increase their strain energy. Elements 2 and 3 must compress when element 1 expands. The strain energy per unit volume of material is given by:⁷²

$$\mathcal{E}_S = \frac{1}{2}\sigma\epsilon = \frac{1}{2}\frac{\sigma^2}{E} = \frac{1}{2}\epsilon^2 E \quad (5)$$

The three relationships in equation (5) are equivalent because the modulus E equals $\frac{\sigma}{\epsilon}$.

The calculation of the terms in equation (4) is best facilitated by considering the state of stress of each element. For element 1 the stress-strain relationship looks like the following:



The transducer expands due to the voltage V , and the σ - ϵ curve moves in the direction of the arrow. The term \mathcal{E}_1 is given by the difference in strain energies before and after expansion. Following the convention used in deriving equation (3), \mathcal{E}' is the strain energy before the voltage is developed, and \mathcal{E}'' is that after application of the voltage and the resulting expansion. Therefore, one may write:

$$\mathcal{E}_1 = \mathcal{E}' - \mathcal{E}'' \quad (6)$$

The force in the system before the ramp stress develops is due to the preload F , so the stress in any element is given by:

$$\sigma_i = \frac{F}{A_i}$$

where A_i is the cross-sectional area of the element. Equation (6) can then be written:

$$\mathcal{E}_1 = \frac{1}{2E_1} \left(\frac{F}{A_1} \right)^2 V_1 - \frac{1}{2E_1} \left(\frac{F}{A_1} - \Delta\sigma_1 \right)^2 V_1 \quad (7)$$

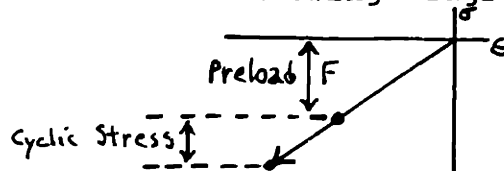
$\Delta\sigma_1$, is calculated from the change in length of the force transducer, Δl_1 , and is given by:

$$\Delta\sigma_1 = \frac{E_1 \Delta l_1}{l_1} \quad (\Delta\sigma = E \Delta\epsilon) \quad (8)$$

from equation (5). Substituting, and cancelling terms

$$\epsilon_1 = \frac{1}{2E_1} \left[\frac{2FE_1 \Delta l_1}{A_1 l_1} - E_1^2 \left(\frac{\Delta l_1}{l_1} \right)^2 \right] V_1 \quad (9)$$

The strain energy changes for elements 2 and 3 may be calculated from the following diagram:



Both these elements are compressed an amount in addition to that due to the preload. The terms ϵ_2 and ϵ_3 are given by:

$$\epsilon_2 = \frac{1}{2E_2} \left(\frac{F}{A_2} \right)^2 V_2 - \frac{1}{2E_2} \left(\frac{F}{A_2} + \sigma \right)^2 V_2 \quad (10)$$

$$\epsilon_3 = \frac{1}{2E_3} \left(\frac{F}{A_3} \right)^2 V_3 - \frac{1}{2E_3} \left(\frac{F}{A_3} + \sigma \right)^2 V_3 \quad (11)$$

In this case, σ is the stress measured by the force transducer, element 3. Cancelling terms,

$$\epsilon_2 = -\frac{1}{2E_2} \left[\frac{2F\sigma}{A_2} + \sigma^2 \right] V_2 \quad (12)$$

$$\epsilon_3 = -\frac{1}{2E_3} \left[\frac{2F\sigma}{A_3} + \sigma^2 \right] V_3 \quad (13)$$

The expansion of the force transducer has to be taken up by the compression of the elements 2 and 3, so

$$\Delta l_1 = \epsilon_2 l_2 + \epsilon_3 l_3 \quad (14)$$

The amount these elements strain, ϵ_i , equals $\frac{F\sigma}{E_i}$ from equation (5). Substituting in equation (14)

$$\Delta l_1 = \frac{\sigma}{E_2} l_2 + \frac{\sigma}{E_3} l_3 \quad (15)$$

The modulus of the transducer material, E_3 is 7.7×10^6 psi,⁷³ l_2 is one inch and l_3 is 0.080 inch. Therefore the second term in (15) is at least 3 orders of magnitude smaller than the first term, assuming the modulus of the test specimen is of the order of 10^5 psi. Therefore, (15) can be rewritten

$$\Delta l_1 \approx \frac{\sigma l_2}{E_2} \quad (16)$$

Substituting this term in (9) and (9), (12), and (13) in (4), one obtains:

$$\begin{aligned} \mathcal{E} = & \frac{F\sigma l_2}{E_2} - \frac{E_1 V_1}{2} \left(\frac{\sigma l_2}{E_2 l_1} \right)^2 - \frac{F\sigma l_2}{E_2} \\ & - \frac{\sigma^2 V_2}{2E_2} - \frac{F\sigma l_3}{E_3} - \frac{\sigma^2 V_3}{2E_3} \end{aligned}$$

Cancelling terms, and substituting equation (3)

$$\frac{1}{2} CV^2 = \frac{E_1 V_1}{2} \sigma^2 \left(\frac{l_2}{l_1} \right)^2 \frac{1}{E_1^2} + \frac{\sigma^2 V_2}{2E_2} + \frac{F\sigma l_3}{E_3} + \frac{\sigma^2 V_3}{2E_3}$$

Multiplying through by E_2^2 and rearranging

$$\left(\frac{1}{2} CV^2 - \frac{F\sigma l_3}{E_3} - \frac{\sigma^2 V_3}{2E_3} \right) E_2^2 - \frac{\sigma^2 V_2}{2} E_2 - \frac{E_1 V_1}{2} \sigma^2 \left(\frac{l_2}{l_1} \right)^2 = 0$$

The relevant terms in this equation are given in Appendix B.

The second two terms in the coefficient of E_2^2 are negligible compared to the first. Solving the resulting equation quadratically,

$$E_2 = \frac{\sigma^2 V_2}{2} \pm \sqrt{\left(\frac{\sigma^2 V_2}{2}\right)^2 + 4\left(\frac{1}{2} CV^2\right) \left[\frac{E_1 V_1}{2} \sigma^2 \left(\frac{l_2}{l_1}\right)^2\right]}$$

$$2 \cdot \frac{1}{2} CV^2$$

In this equation, the first term in the numerator, and the first term under the radical are negligible, leading to

$$E_2 \approx \frac{\sqrt{4\left(\frac{1}{2} CV^2\right) \left[\frac{E_1 V_1}{2} \sigma^2 \left(\frac{l_2}{l_1}\right)^2\right]}}{2 \cdot \frac{1}{2} CV^2} \quad (17)$$

This is the final equation for calculation of the modulus from the experimental data.

Implications of the Operation of the Equipment

Notice that

$$E_2 \propto \sigma \quad (18)$$

The stress as measured by the stress transducer is thus directly proportional to the modulus of the test specimen, all other things being equal, provided the unknown modulus is of the order of 10^5 psi or less. Relative values for the moduli of different specimens are easily obtained by measuring the stress level or voltage output from the stress transducer for each sample and relating this back to the values for the other samples.

It is interesting that equation (17) does not contain the term F. Therefore the modulus measurements are independent of the preload, if the modulus itself is linear. Furthermore, from (17)

$$E_2 \propto \frac{\sigma}{V} \quad (19)$$

A very important consequence of these relationships is that the preload need not be reproducible, once it is above a level necessary for good coupling of the interfaces between elements 1, 2, and 3 and the rigid walls. In addition, the measurements need not be made at the same voltage input, as long as this voltage is noted. It must be reemphasized that these considerations are true if the sample exhibits purely elastic behavior and if its modulus is linear up to the chosen preload.

Experimental Procedure

Operation of Equipment

A photograph of the relative stiffness apparatus is shown in Figure 19A. The clamping device was a vise with a free-sliding clamp. The clamping force was applied reproducibly by using a very accurate torque wrench, and closing the vise to the same torque for each measurement. The clamping force-torque relationship was obtained by measuring the spring constant of a system of springs on the Instron in compression and then placing the system in the vise and measuring the torque-displacement relationship. A clamping force of 85 pounds was used throughout this study because it was only slightly above the minimum force necessary for good coupling of the buffer-bone interfaces shown in Figure 20.

The buffers were high modulus (10^6 psi) ceramics chosen for their stiffness and electrical insulating abilities. The piezoelectric transducers were of the lead-zirconate titanate variety to provide high stiffness and high sensitivity. The electronics

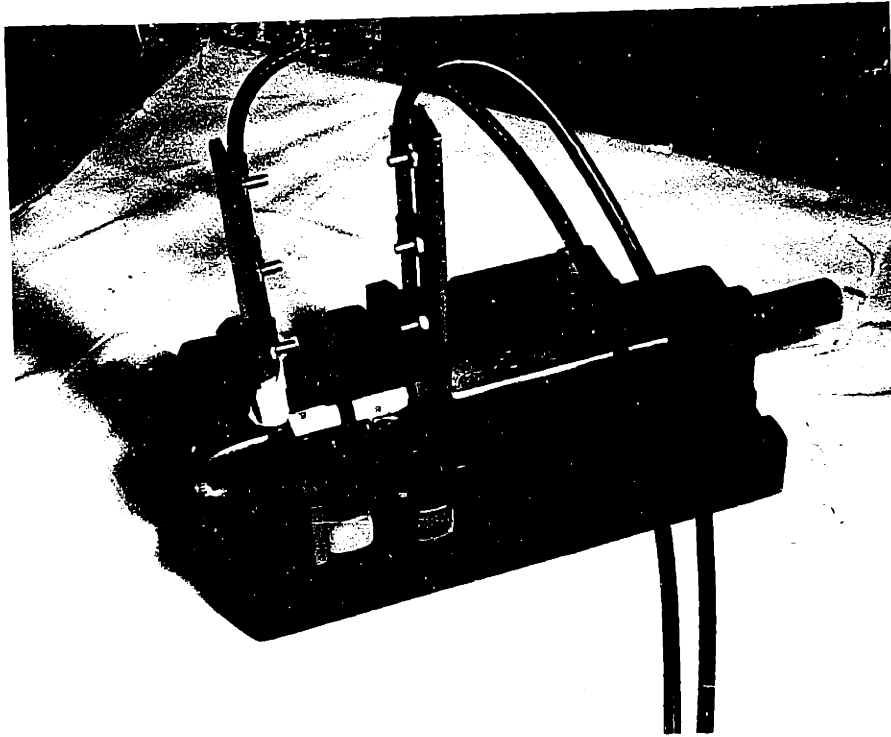


Figure 19A: Apparatus for the measurement of relative stiffness.

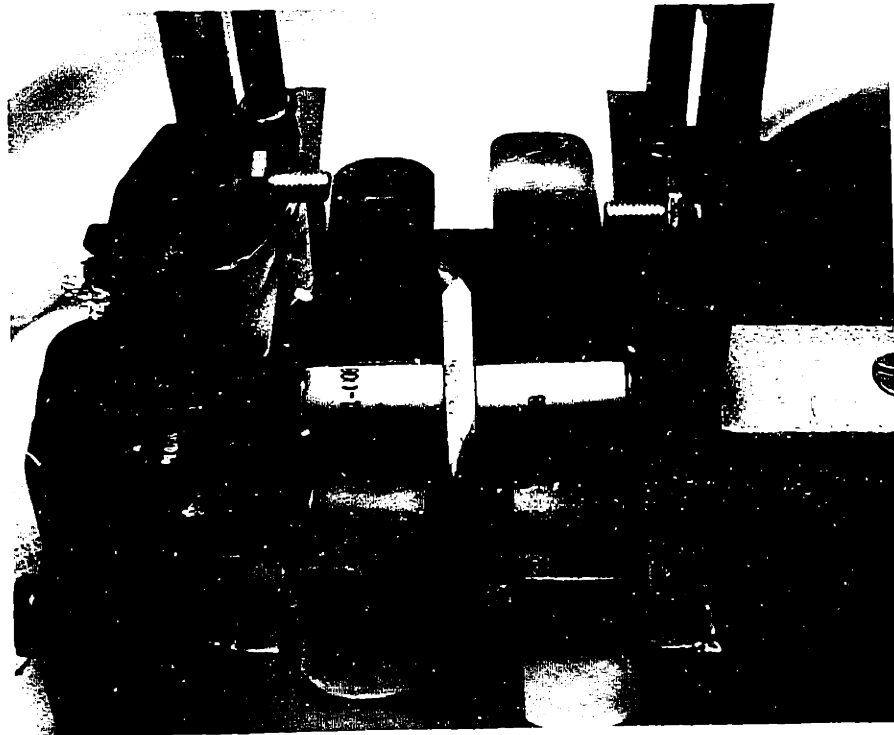
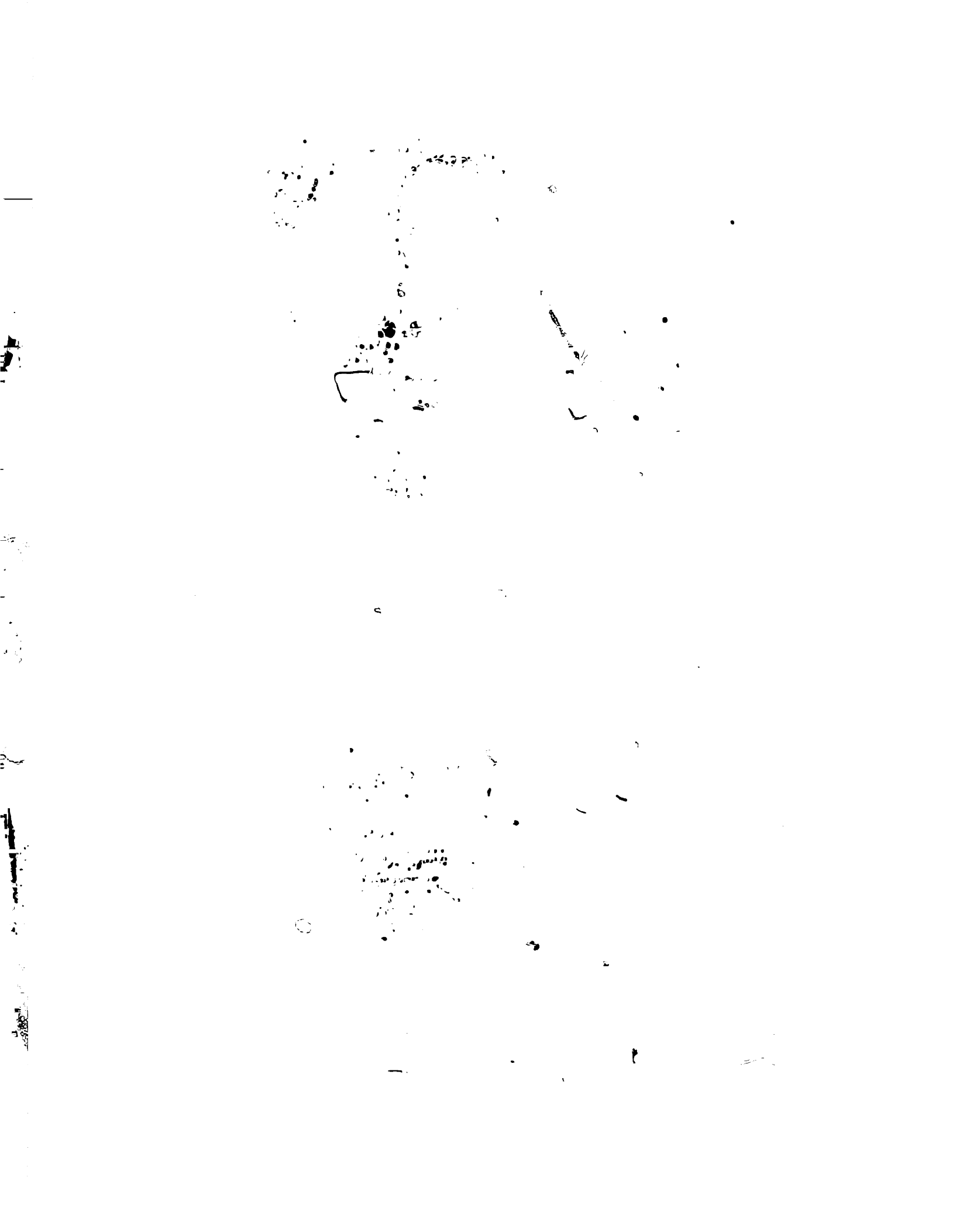


Figure 19B: Closeup of sample in place in relative stiffness apparatus.



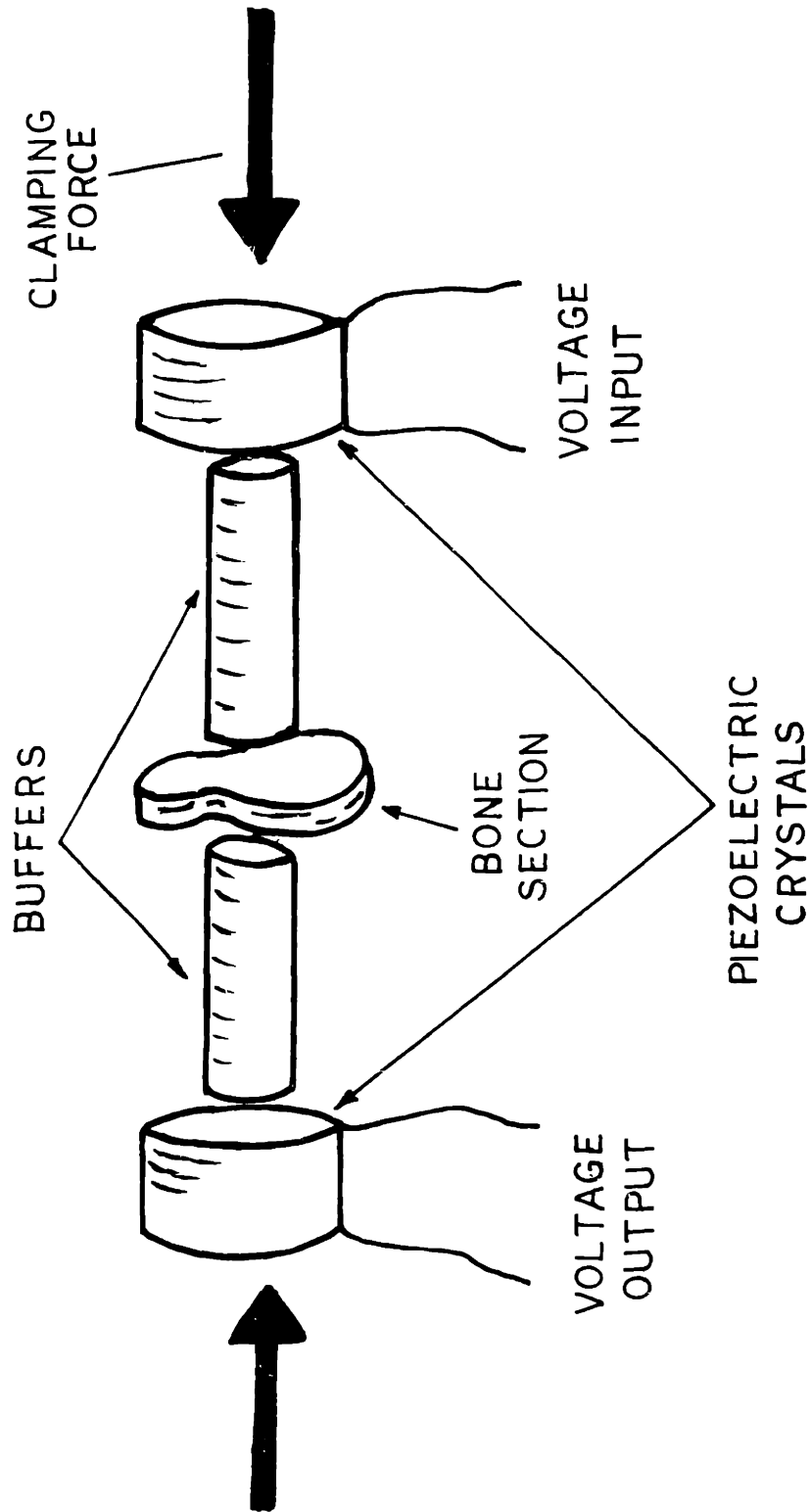


Figure 20: Detail of clamped elements in relative stiffness apparatus. Notice that the outside rim of bone on the sample is not machined off; and that, because of this, the sample has a diameter greater than that of the buffers.

were set up as in Figure 21. A photograph of a sample of bone in place is shown in Figure 19B.

A frequency of 400 Hz was chosen for all the measurements because of its physiological significance (see Appendix A) and because this frequency is well away from the dispersion resonances encountered (see Section III).

A typical measurement consisted of clamping a section of bone between the two buffers, applying a 400 Hz, 134 volt amplitude signal to the force transducer, and recording the amplitude of stress indicated by the stress transducer. (The stress transducer itself had been calibrated through use of a vibration standard and a seismic mass as in Section III.) This was typically done several times for each sample of bone to determine the most reproducible value of the stress output. The accuracy of measurement of the stress was roughly 10%.

This deviation was probably due to repositioning the sample in an area with slightly different properties from that of the original area. The choice of a constant preload is necessary because the mechanical behavior of bone is generally nonlinear.⁷⁴ Part of the 10% deviation could therefore be due to slight irreproducibility of the preload, since the modulus of bone is expected to vary slightly with preload.

Material

The distal ends of human femurs were obtained at autopsy. The left medial condyle was used for this study as shown in Figure 12A in Section III. The cartilage was cut off of the weight-

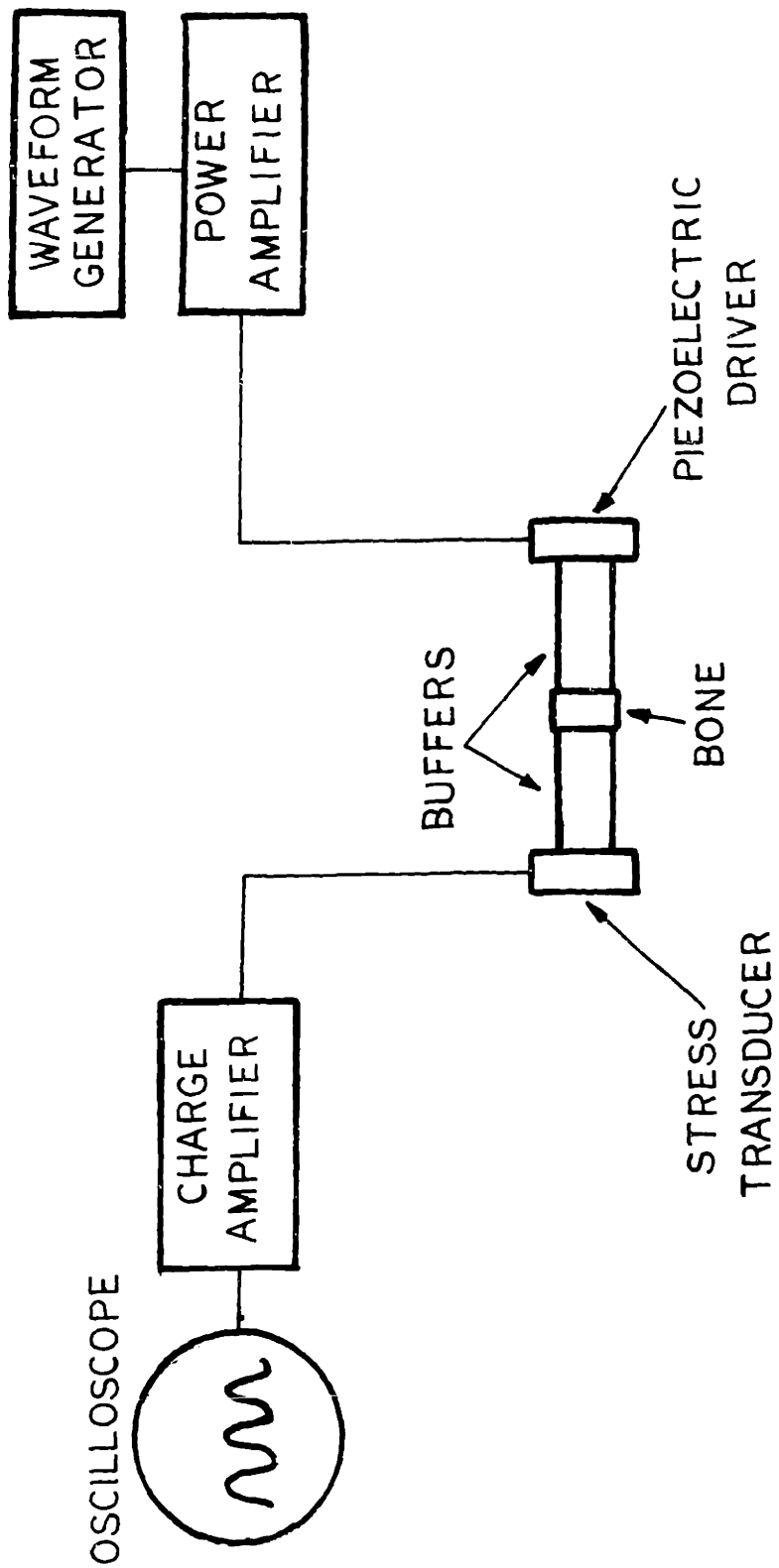


Figure 21: Schematic showing instrumentation used for measurement of relative stiffness.

bearing area using a high-speed cutoff wheel with a coolant to avoid heating the sample. Care was taken to slice just beneath the subchondral plate and to expose a small ring about 3/4 inch in diameter of trabecular bone. A transverse section of trabecular bone was cut 5 mm thick just beneath the cartilage that had been removed. A photograph of a typical sample of human trabecular bone is shown in Figure 22. The buffers in Figure 20 were clamped in the center of the 3/4 inch ring of exposed trabecular bone. Care was taken to ensure that this area was indeed the weight-bearing area of the knee. The relative stiffness was measured only in this area for each patient used in the study. The sections were then mounted and examined microscopically as described in Section II. L_L and N_L were measured for each sample so that the volume fraction bone, contiguity ratios, and trabecular thickness and spacing could be calculated using relationships in the introduction.

The right lower limbs of male New Zealand white rabbits weighing between eight and ten pounds were loaded impulsively with a force approximately equal to their body weight at a rate of sixty times per minute for one hour daily. The reason for doing this lies in Wolff's Law. By changing the stress in the right leg, it was hoped that resultant changes in structure (and properties) could be produced. The right leg was held in a polymethylmethacrylate splint so that its knee was in an attitude of maximum extension. The dynamic force (which incidentally contained a high frequency peak and a broader peak similar to the traces in Appendix A) was delivered to the splint

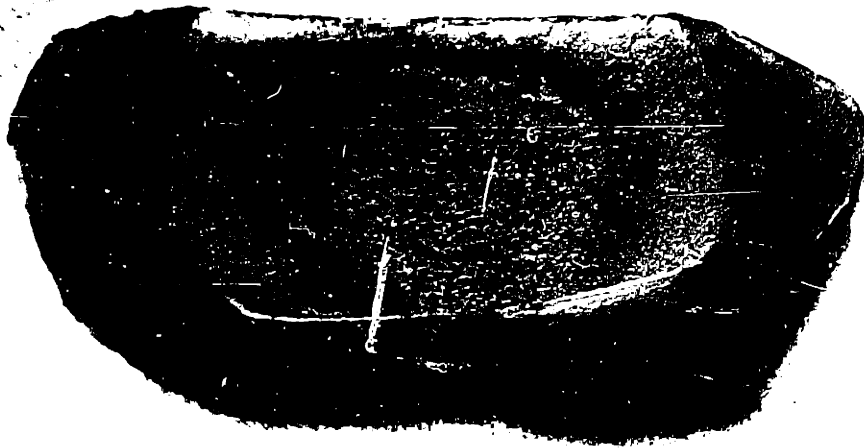


Figure 22: Human bone section just beneath cartilage. The trabecular bone is evident in the center, with a ring of thick cartilage surrounding it. Approximately 1.5X.



.

.

.

.

.

.

.

.

.

.

.

.

.

.

1. 2. 3.

4. 5. 6.

7. 8. 9.

10. 11. 12.

13. 14. 15.

by a traveller connected to a motor-driven cam. The left limb acted as a control, since it was held in an identical splint but was not subjected to the impulse loading. The apparatus was constructed so that the animal was suspended over the cam by a rack which had holes in it for the extremities (see Figures 23A and B).⁷⁵ Groups of rabbits were sacrificed at two day intervals for a period of a month. Transverse sections 2 mm thick were machined from beneath the left and right tibial plateaus. The relative stiffness was measured for these samples on each rabbit. The sections were subsequently mounted and examined microscopically as described in Section II. Two of the rabbits were injected with tetracycline in a dose of 1.4 mg/kg body weight intramuscularly every eight hours for two days, three days prior to sacrificing. This was not administered to all of the rabbits because of the reported effect of tetracycline on mechanical properties of bone.⁷⁶ Tetracycline is known to be deposited in areas of new bone formation and it was hoped to be able to locate the weight-bearing areas in the rabbit tibias through the use of tetracycline fluorescence.

Several cats were also examined by the same techniques as for the rabbits, after they had been impacted for a number of days.

Bone samples of the type used in this study have the advantage of avoidance of edge effects. The cross-section is much larger than the plunger used to load the sample. Unfortunately, the geometric advantages are offset by an inability to calculate a meaningful modulus. Relative moduli are easily measured. Therefore the data for bone in this section are only relative. Samples

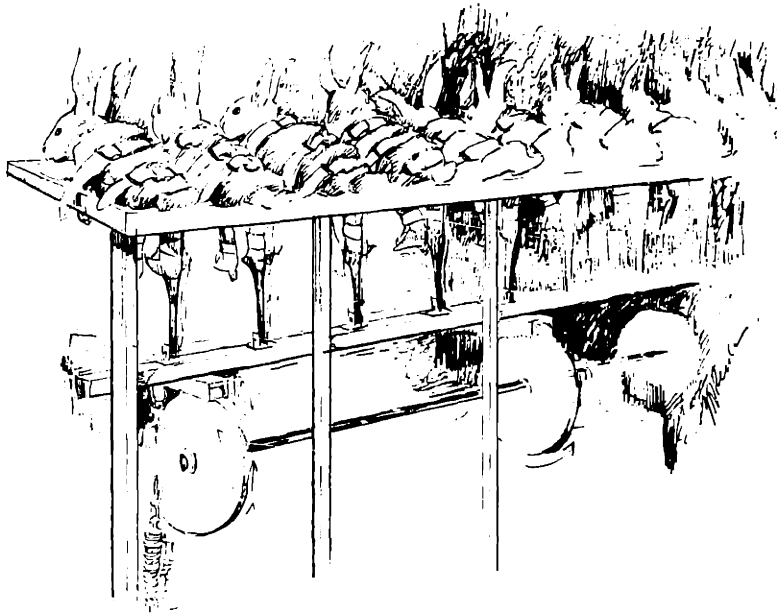


Figure 23A: Sketch of rabbits on impacting table. The cams rotate and cause the impacting.

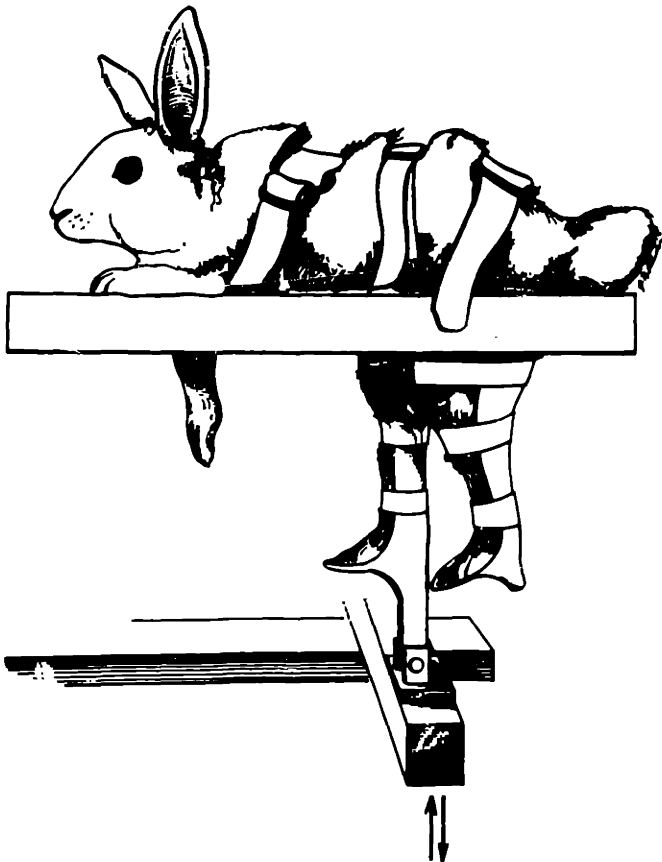


Figure 23B: Detail of rabbit with right and left legs in splints. Only the right leg received the impact, the left leg serving as a control.

of similar geometry have been used for measurements of relative compressive strength of cancellous bone in the femur.⁷⁷

All Samples were measured wet, and within 48 hours of death.

Results and Discussion

Performance of the Equipment

To check the validity of the equations (17), (18), (19), and (20) derived above, a piece of material one inch long with a cross-section of 0.1 inch² (a hollow piece of ceramic) was compressed elastically in the Instron. The modulus at a strain rate of 0.05/min was found to be 2.0×10^5 psi (just about at the upper limit for the measurement of modulus in the apparatus). The modulus at 400 Hz as measured through direct readings of the stress and strain by means of the slightly modified apparatus in Figures 24 and 25 was 5.16×10^5 psi. This apparatus utilized two phono styli--velocity transducers--to give the information on the strain in the sample. The subtraction of the amplitude of the lower trace on the oscilloscope from that of the upper trace, after one integration with respect to time, gives the relative motion of the two ends of the sample, and consequently, the strain. (This proved to be a very tedious and time-consuming measurement and was the only measurement attempted on the modified equipment.)

The cyclic stress level in the relative stiffness apparatus on the ceramic test sample was 0.58 psi. Using equation (17) with the values in Appendix B and $\sigma = 0.58$ psi,

$$E = 4.17 \times 10^5 \text{ psi}$$

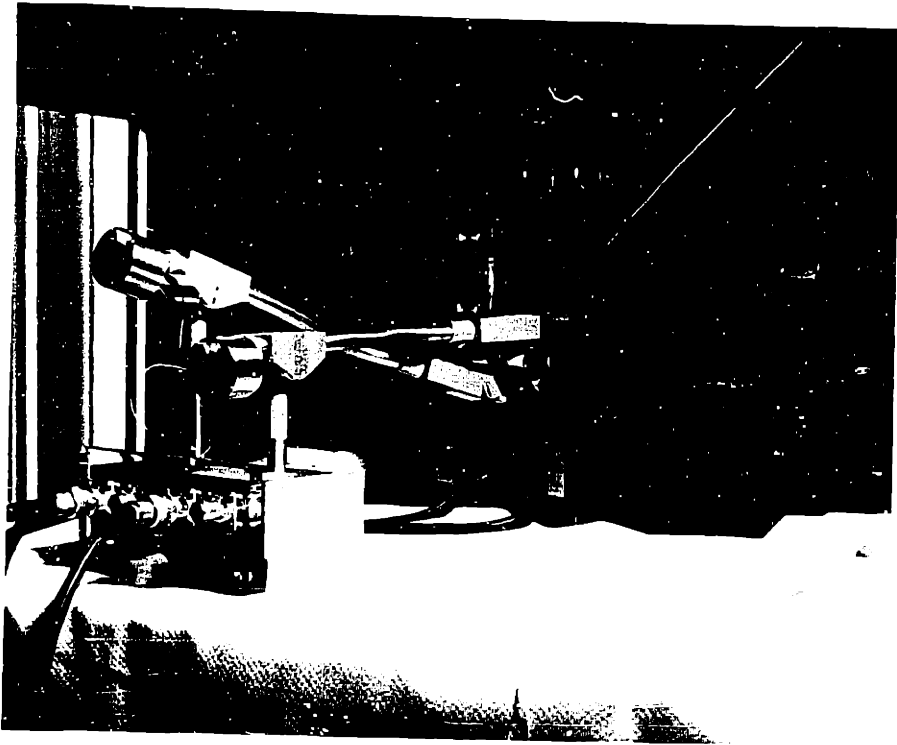
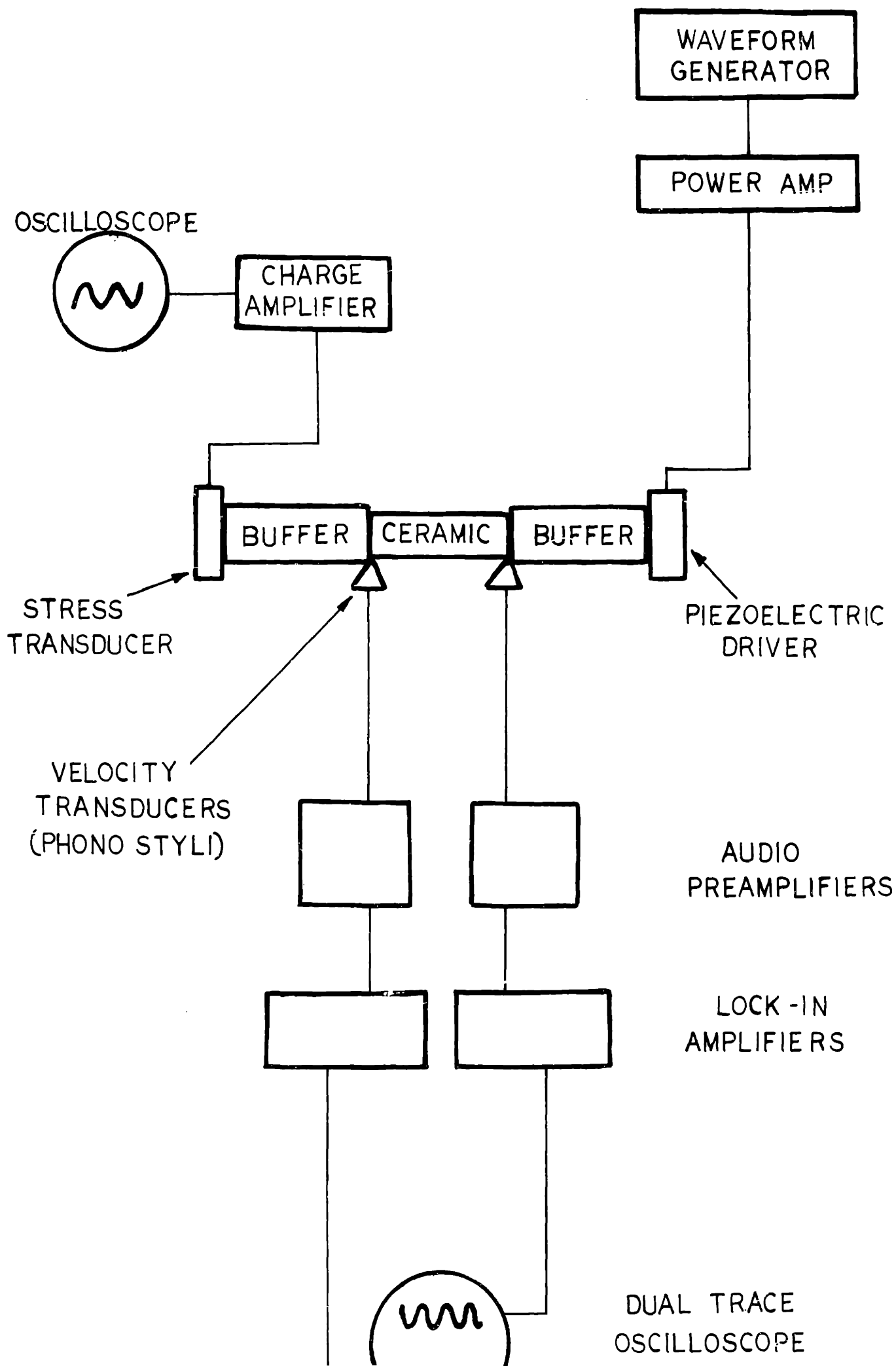


Figure 24: Modified stiffness apparatus. This utilizes two phono styli and a stress transducer to determine the modulus of a test piece through direct measurement of stress and strain.



Figure 25: Schematic of modified stiffness apparatus. Lock-in amplifiers were necessary to retrieve the low-level signals coming from the styli.



This is in good agreement with the value measured on the modified equipment and is only a factor of 2 greater than the Instron modulus. A possible explanation for this deviation is that the modulus increases with increasing frequency (Section III).

The ceramic test sample was clamped with a preload of 85 pounds and the voltage input to the force transducer was increased over the range 0 to 70 volts. The stress from the stress transducer, σ , was recorded for selected values of V . These data are plotted in Figure 26. There is a linear relationship here for V versus σ , attesting to the validity of equation (2). The voltage input at higher levels gives proportionally higher values of σ . (In the case above $V = 134\text{v}$ and $\sigma = 0.58$ psi. This point falls on the extrapolation of the line in Figure 26.)

Finally, the voltage input to the transducer was set at 134 volts and the preload was increased gradually from 0 to 150 pounds. The resulting stress level measured by the stress transducer is given in Figure 27 as a function of the preload F . Notice that the value of σ is constant after a preload of about 50 pounds. At lower values of F there is much scatter in the data, indicating coupling problems between the interfaces in the linear chain of elements in the relative stiffness apparatus. After the coupling is effected, the value of σ is seen to be independent of F , indicating that equation (18) is correct.

All of these measurements on the ceramic test piece show that the equations governing the behavior of the relative stiffness apparatus are correct. The predicted dependence of V versus σ

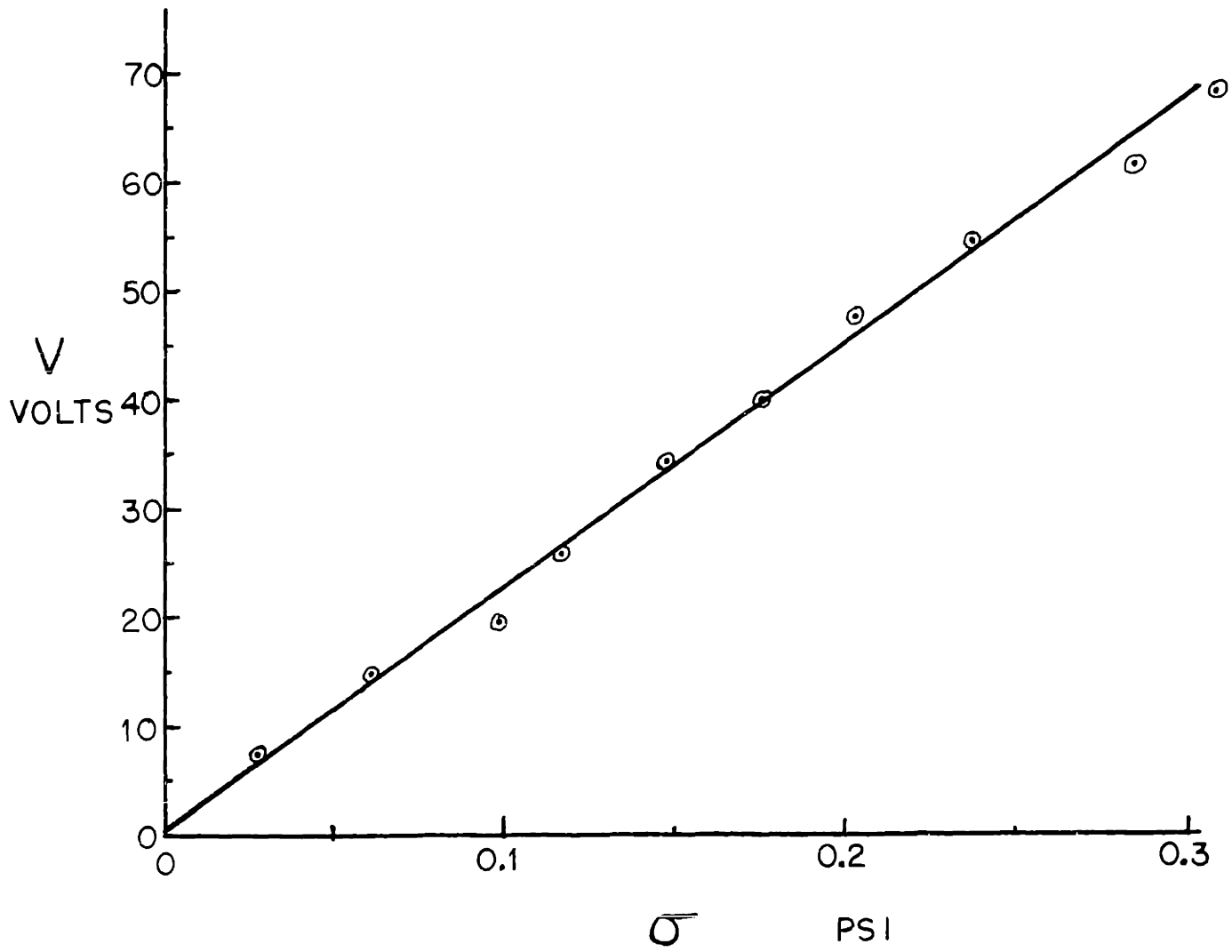


Figure 26: Applied voltage versus stress level for the relative stiffness apparatus.

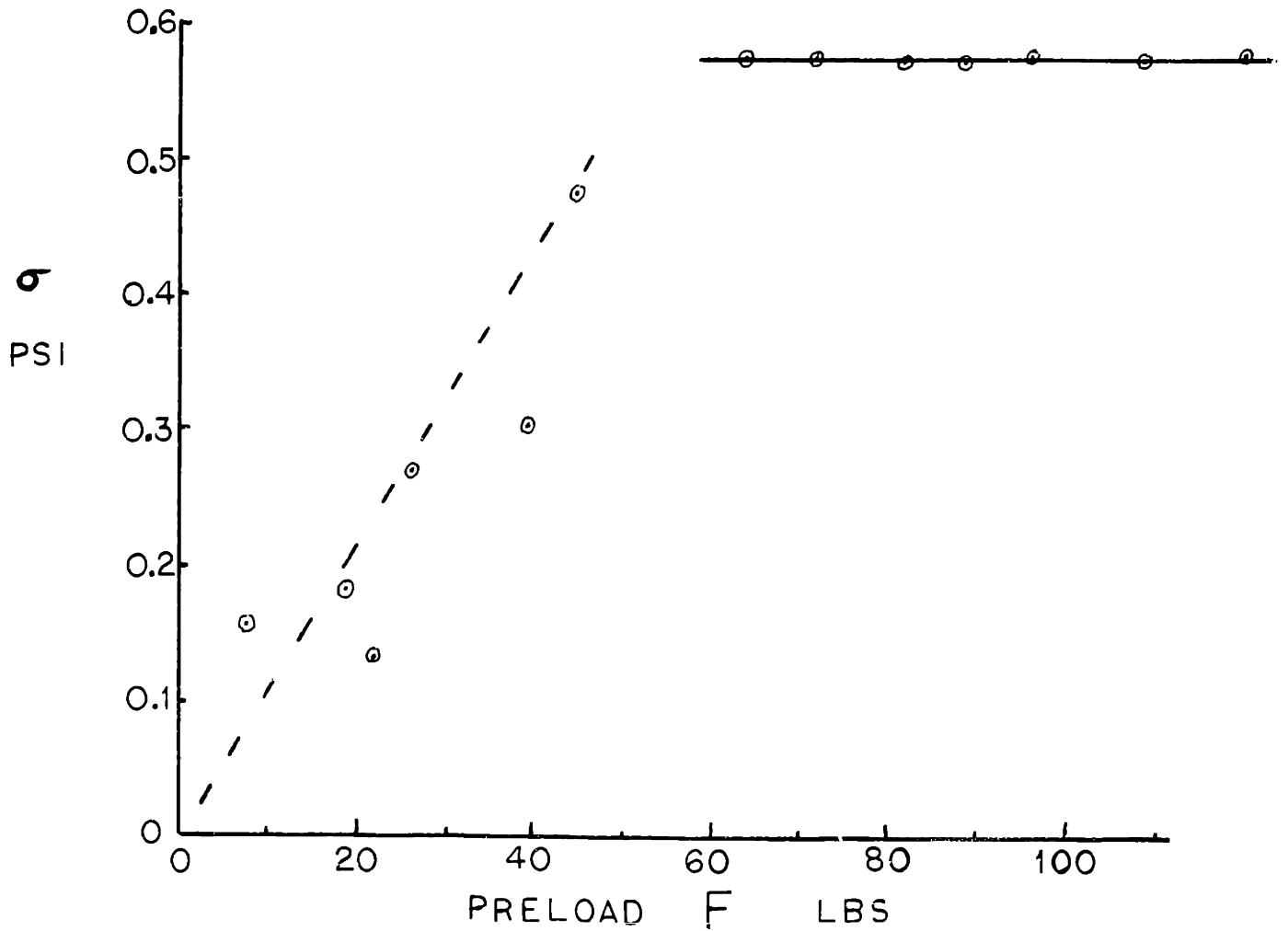


Figure 27: Stress level versus preload at constant applied voltage for relative stiffness apparatus. σ is independent of F above 50 pounds. The scatter below 50 pounds is due to interface coupling problems.

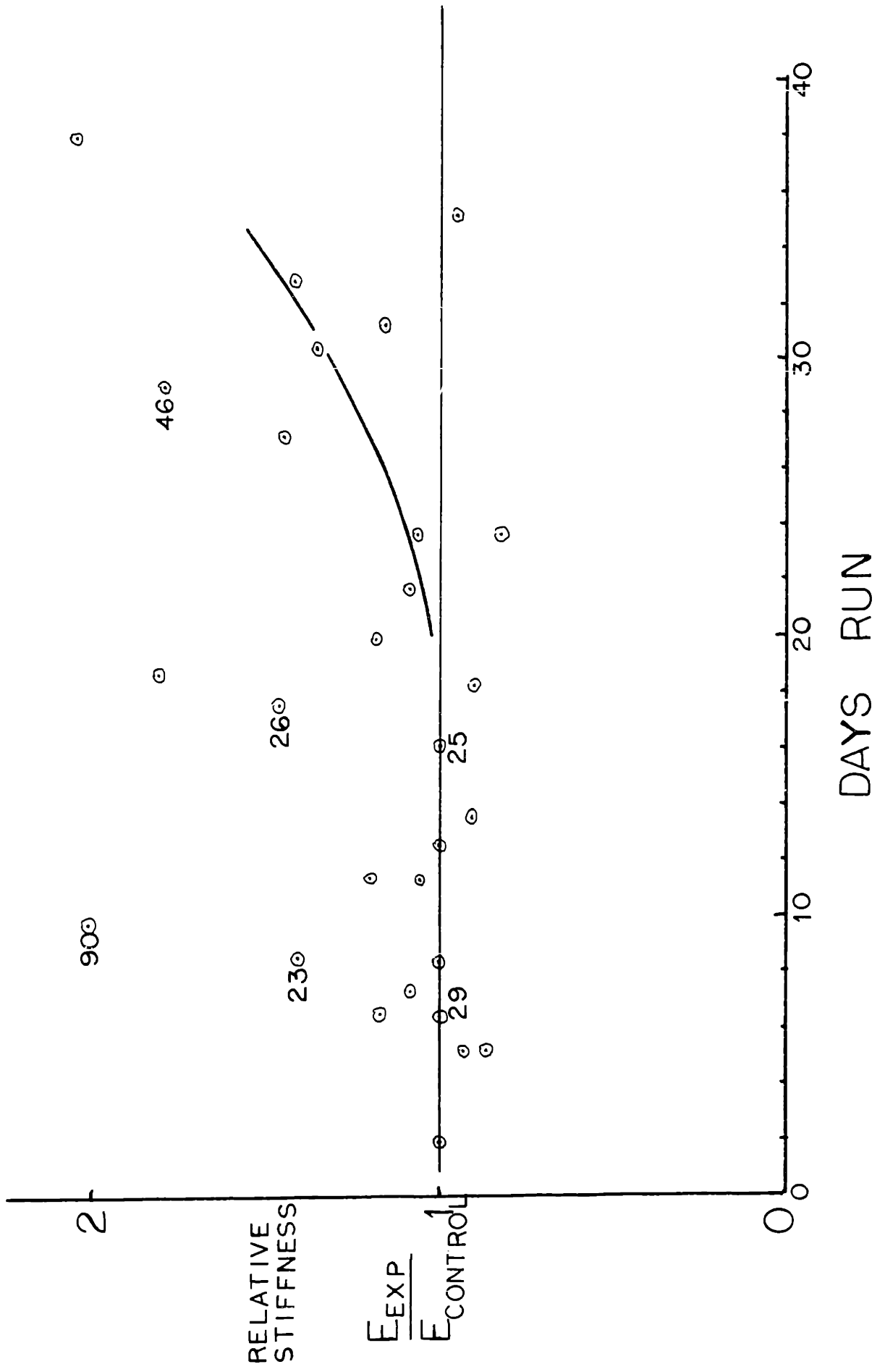
for constant E and the independence of σ on preload are verified. The modulus measured on this apparatus agrees with the static value within a factor of 2, and with the dynamic value measured on a separate apparatus within a factor of 1.25.

Rabbit Samples

The data for 28 rabbits is given in Figure 28 as relative stiffness versus days impacted. The relative stiffness here is the ratio of the modulus of the trabecular bone in the right leg (experimental side) to that of the left leg (control side). Notice that the data are generally clustered about a relative stiffness (R.S.) of 1. Several rabbits in the period 0 to 20 days show marked stiffening of the bone in the experimental leg. After 20 days, however, the points are not clustered near the horizontal line representing a R.S. of 1. There is a definite upward trend towards uniformly increasing R.S., as indicated by the curved line beginning at 20 days.

Force traces obtained by strain gauging the splints of the rabbits as they were run indicated that the forces applied were not reproducible from cycle to cycle, or even from rabbit to rabbit.⁷⁸ There were additional problems encountered in splinting the legs of the rabbits so they were held in an attitude of maximum extension. The scatter in the data is probably due to these problems. Some rabbits received a more severe impact than others. Therefore the mechanical properties of the bone vary greatly from rabbit to rabbit although they were impacted the same number of days in some cases.

Figure 28: Relative stiffness versus days run on impacting table for rabbits. Significant stiffening begins at day 20. The scatter is due to problems encountered in splinting the rabbits and in impacting them reproducibly.



The data points in Figure 28 with the numbers beside them represent samples that were examined microscopically to see if there were any structural differences in specimens possessing different mechanical properties. Samples 25 and 29 (Group A) were selected as exhibiting no change in modulus from left to right side (R.S. = 1). Samples 23 and 26 (Group B) exhibit moderate changes (R.S. \cong 1.4), and Samples 90 and 46 show extreme changes in properties (R.S. \cong 2).

To select the relevant area in the cross-sections to study microscopically, the tetracycline-injected rabbits were processed similarly to the rest of the group. Figure 29 shows a photograph taken with ultraviolet illumination of the cross sections of the tibias of one of these rabbits. The cross-section of the right leg is glowing in a very localized region, while the left leg seems to show no tetracycline fluorescence at all in the subchondral region. The fluorescence is indicative of cellular activity in the bone, and since Wolff's law predicts that bone remodels in response to stress, this area of fluorescence should be the weight-bearing area (the region of maximum stress) in this rabbit.

When the cross-sections of the samples (the same cross-sections as used for R.S. measurements) from Groups A, B, and C were examined, the structure of the trabecular bone seemed identical for all of them, except in the weight-bearing region. Figures 30 through 33 show typical structures in the weight-bearing area of the right tibias of a control, a Group A, a Group B, and a Group C respectively. There is good qualitative correlation here between R.S. and the



Figure 29: Photograph of cross sections of left and right rabbit tibias. Ultraviolet illumination. The rabbit was injected with tetracycline. Areas of new bone formation are shown to fluoresce. Only the cortex in the control leg at left shows bone growth. The subchondral region on the right side (experimental side) also fluoresces, indicating the weight-bearing area during impacting.





Photograph of weight-bearing leg of rabbit. The leg appears normal. The bones in the plantar region are disregarded.



Figure 30: Photomicrograph of weight-bearing area of left (control) leg of rabbit. Transverse Section. Trabeculae appear normal. 30X. (The black spots are holes in the plastic mounting material and should be disregarded.)

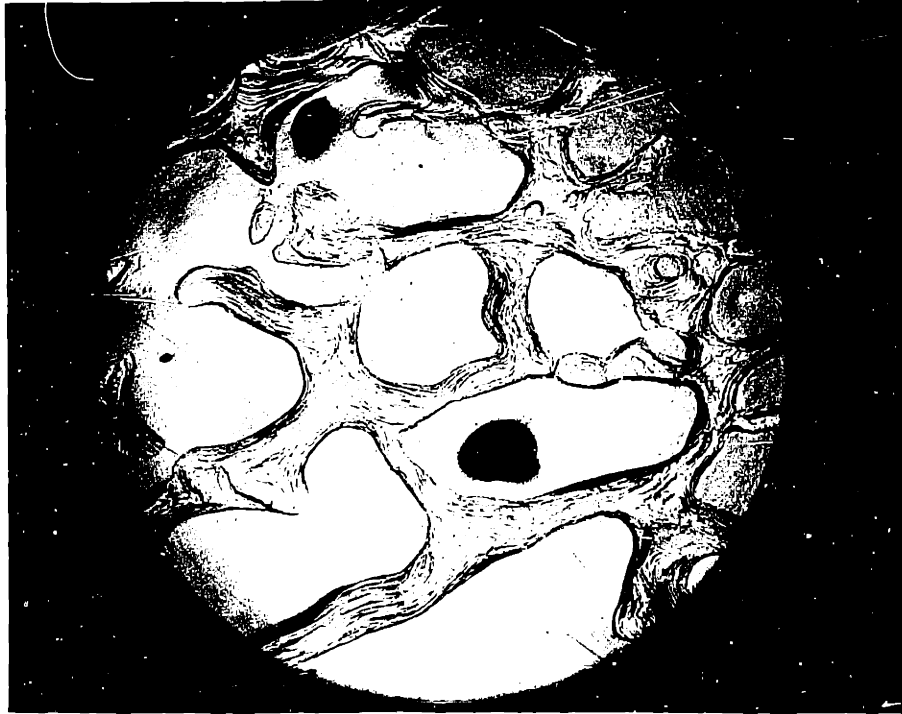


Figure 31: Photomicrograph of weight-bearing area of right (experimental) tibia of Group A rabbit (R.S. = 1). Transverse section. This appears very similar to the control in Figure 30 except for a small amount of resorption. 30X



Fig. 1

Fig. 2





Figure 32: Photomicrograph of weight-bearing (experimental) tibia of Gro mouse. Transverse Section. Trabeculae, and microfractures are

ght
= 1.4).
resorp-

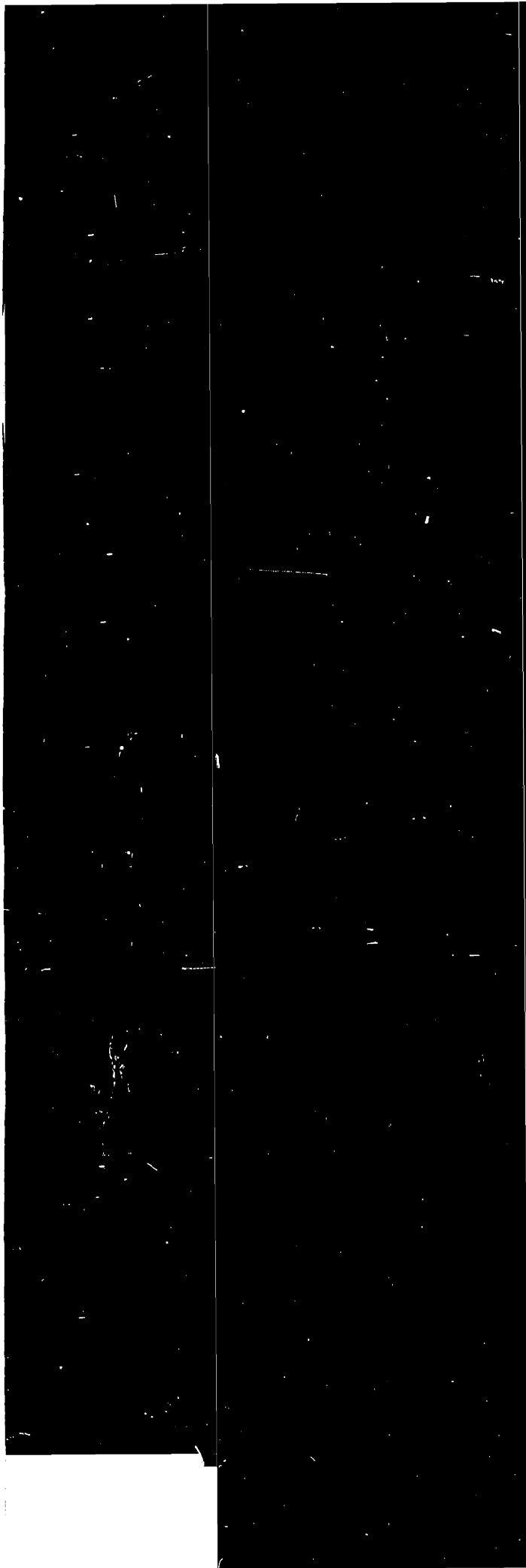
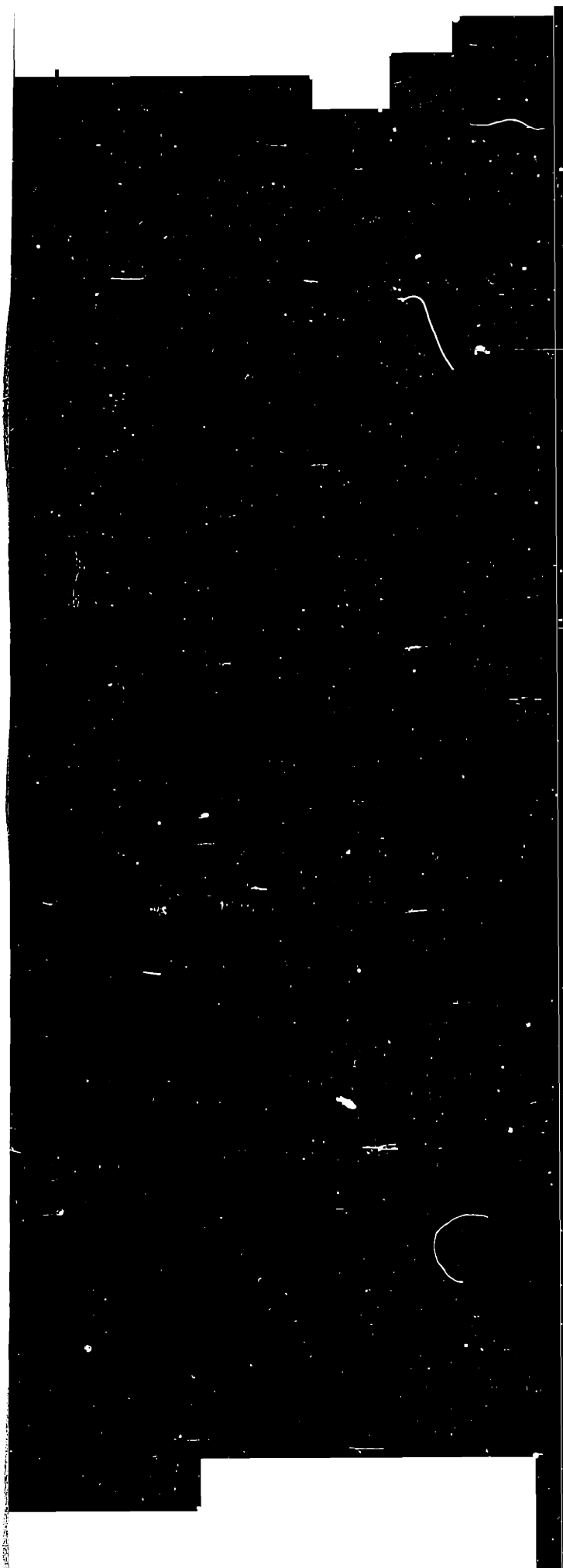


Figure 33: Photom:
(exper:
Transv
is note



ight-bearing area of right
of Group C rabbit (R.S. = 2).
Gross thickening of trabeculae



changes in structure of the trabecular bone. The Group A's were virtually undifferentiable from controls. Group B's showed such changes as thickening of trabeculae, callus formation around probable areas of microfracture, and resorption. (The suggestion is made that the resorption is due to the Law of Weinmann and Sicher, discussed in Section VI. The spread of data above and below $R.S. = 1$ in Figure 28 can also be explained through this law. Some rabbits received much more punishment than others. Resorption is expected in the former and lowered stiffness.) Group C's showed the greatest changes of all. There were large amounts of new bone formation, callus response to microfractures, and the resulting trabecular thickening. No quantitative measurements were attempted on the microstructures because there were not enough trabeculae in the affected areas to get statistically meaningful results. The qualitative differences between the photographs in Figures 30 through 33 are striking just taken at face value.

It appeared that, from studying the microstructures of the cross-sections of the balance of the samples used for the R.S. measurements, that there is extreme variability in the changes that occurred. Massive areas of resorption were observed in the weight-bearing areas of some of these rabbits. The trabeculae seemed to be much thicker in these rabbits than in those not exhibiting much resorption. It was almost as if the trabeculae had thickened up as in Group C, and then the bone had died. The resorption areas are an attempt to remove the dead bone and replace it with new bone. This variability in structure and

properties is believed to be due to the problems with impacting discussed previously.

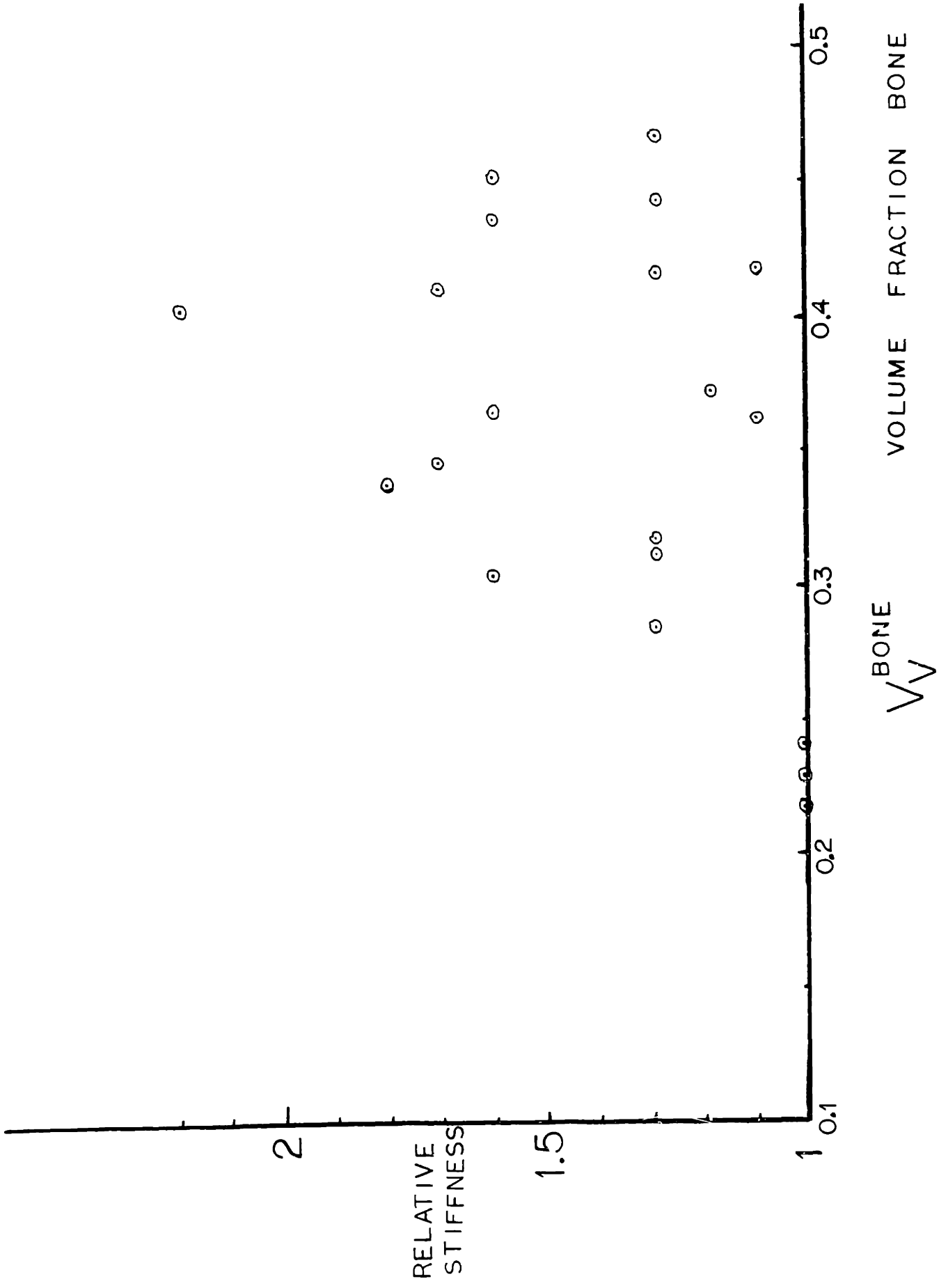
Human Samples

Condyles from twenty random patients were obtained at autopsy for this part of the study. The only requirements for selection were that the patients have no history of degenerative joint disease, that they be less than 65 years of age, and that they be male (Section VI). In such a random population, it is certain that the patients will have very different life styles and different levels of physical activity. The combination of this with differences in body weight leads to the conclusion that the structure and properties of the bone in the twenty patients will vary considerably through Wolff's Law considerations.

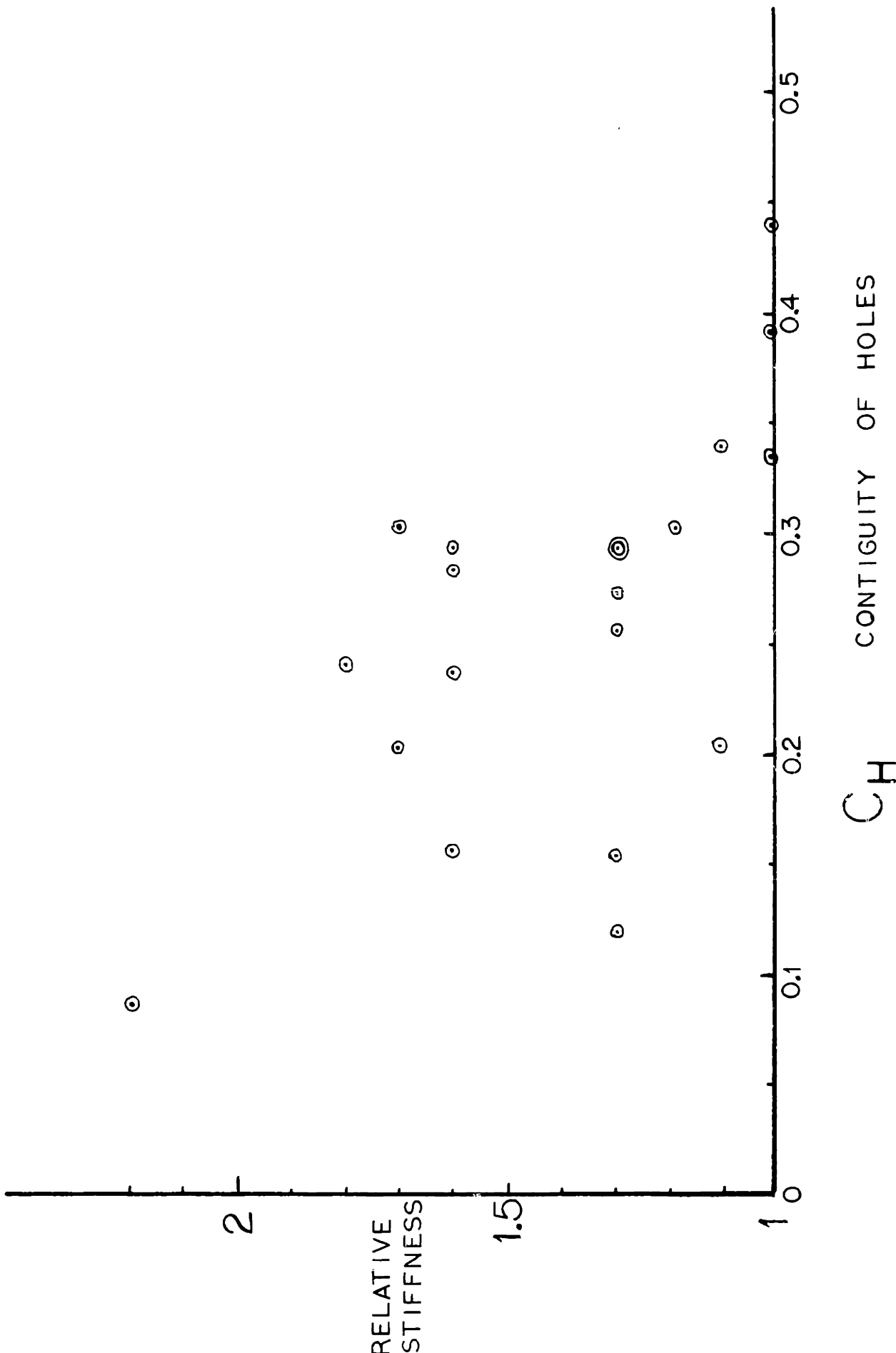
Transverse planes of section were examined for the twenty specimens that had been machined and that had had relative stiffness measurements made on them. The same area was examined and photographed as had been in contact with the buffers in the R.S. apparatus. Several quantities were measured from these photographs: the volume fraction of bone present, the contiguity of the holes in the bone, the average thickness of the trabeculae, and the average trabecular spacing (or the number of trabeculae per unit length). These data are related to the R.S. measured for each sample in Figures 34 through 37.

The wide variation in the stereological quantities indicates that the assumption that the bone from the random patients would be different is verified. The R.S. data also show great variation,

Figure 34: Relative stiffness versus volume fraction
bone for human trabecular bone.



**Figure 35: Relative stiffness versus contiguity of holes
for human trabecular bone.**



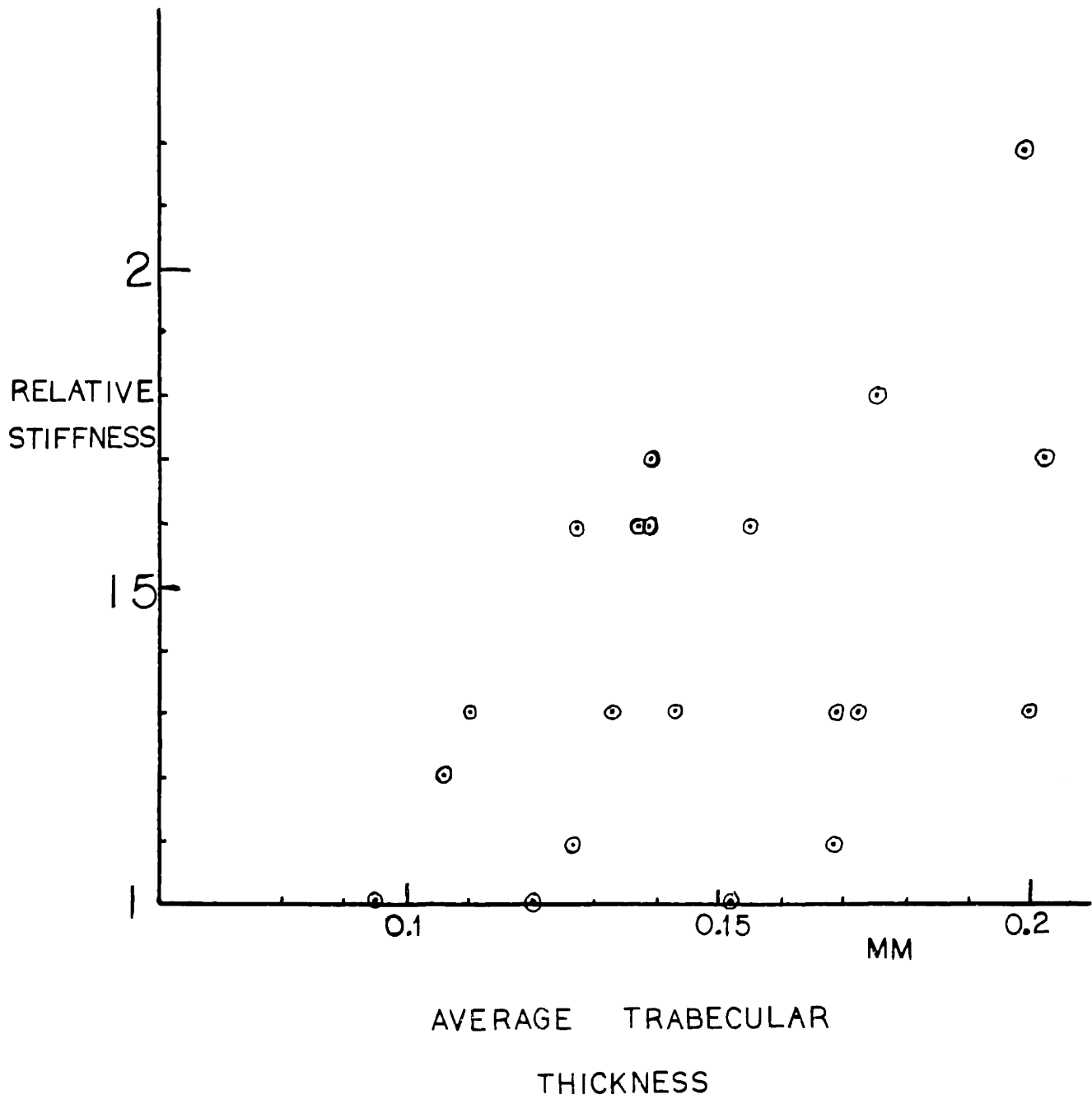


Figure 36: Relative stiffness versus average trabecular thickness for human trabecular bone.

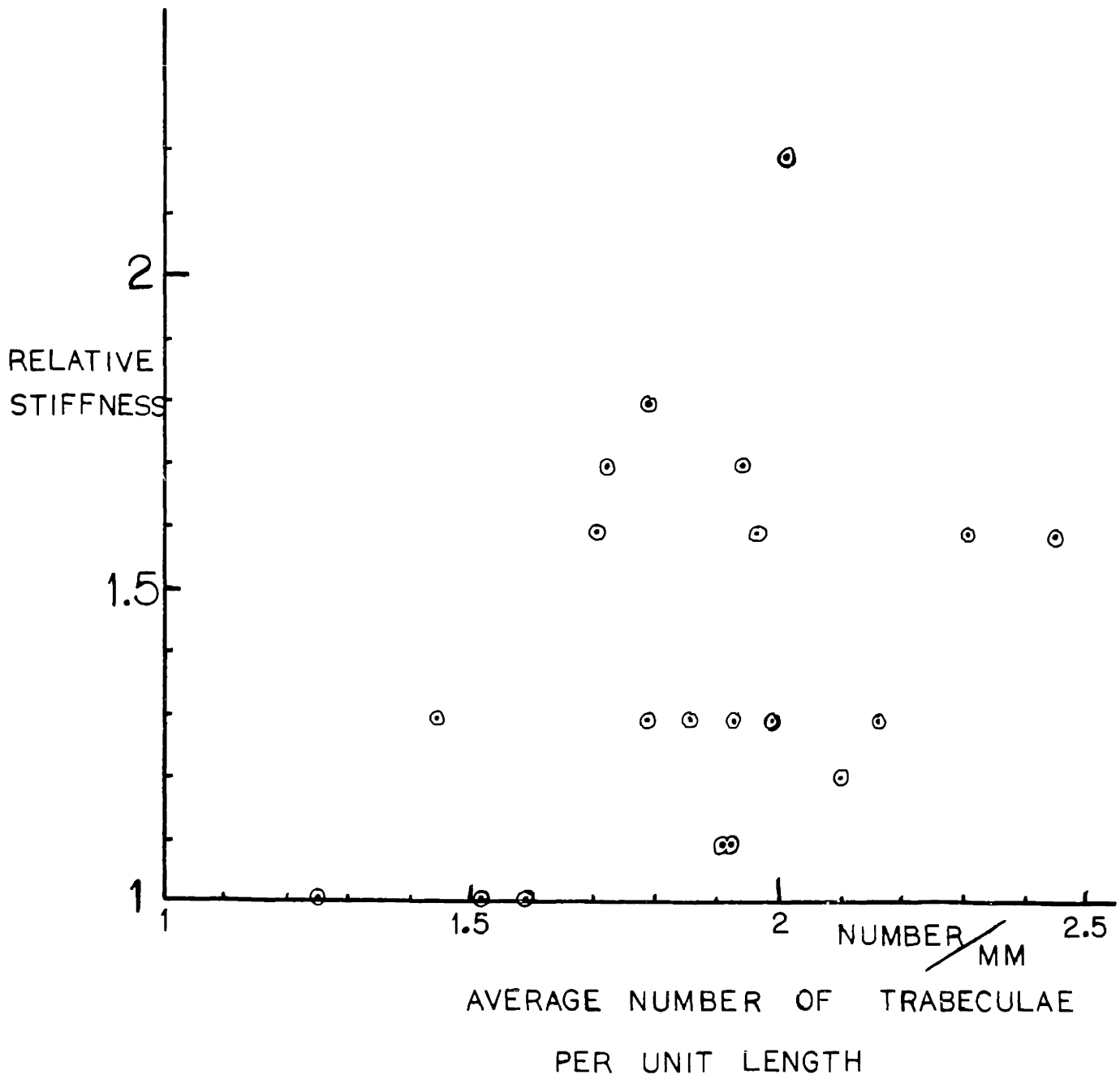
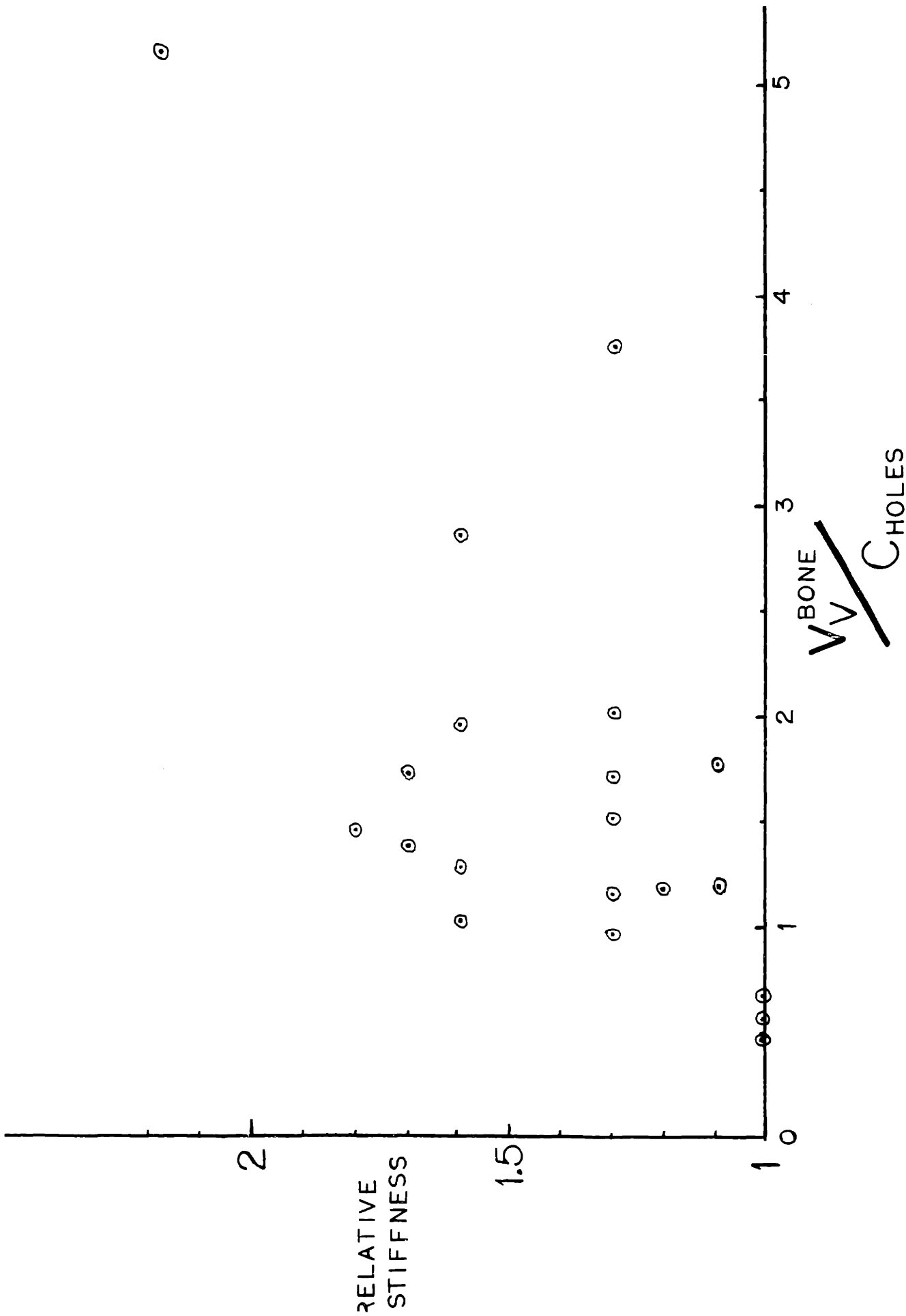


Figure 37: Relative stiffness versus average number of trabeculae per unit length for human trabecular bone.

**Figure 38: Relative stiffness versus $V_{\text{Bone/C}}$ holes
for human trabecular bone.**



by about a factor of two. This, incidentally, correlates well with the observation in Section III that the modulus as a function of frequency varies by a factor of 2 around the average value (see Figure 16).

There is spread in the data for R.S. versus trabecular thickness (t_T), trabeculae per unit length (T_L), and volume fraction bone (V_V^{Bone}). There seems to be a direct proportionality, nevertheless, between R.S. and these quantities. There is less spread in the data for R.S. versus contiguity of holes (C_H), which is an inverse relationship. If R.S. is plotted as a function of V_V^{Bone}/C_H , as in Figure 38, the scatter is even less. This suggests that the V_V and C_H are more important parameters of the microstructure than t_T or T_L .

The microstructures of the twenty samples can be classified as either uniform or non-uniform. The uniform samples had regular arrangements of trabeculae and uniform thickness of trabeculae (See Figure 39A). The non-uniform ones had regions with massive areas of bone, where apparently bone growth had been accelerated locally (See Figure 39B). If the R.S. versus C_H is plotted for the uniform samples, (See Figure 40), much of the scatter in the R.S. versus C_H in Figure 35 is eliminated. Similarly, if the R.S. versus V_V is plotted for the non-uniform samples (Figure 41), a considerable amount of the scatter in Figure 34 is eliminated.

The correlation of R.S. with C_H for the uniform samples suggests a simple explanation for the mechanical behavior of these samples of trabecular bone:

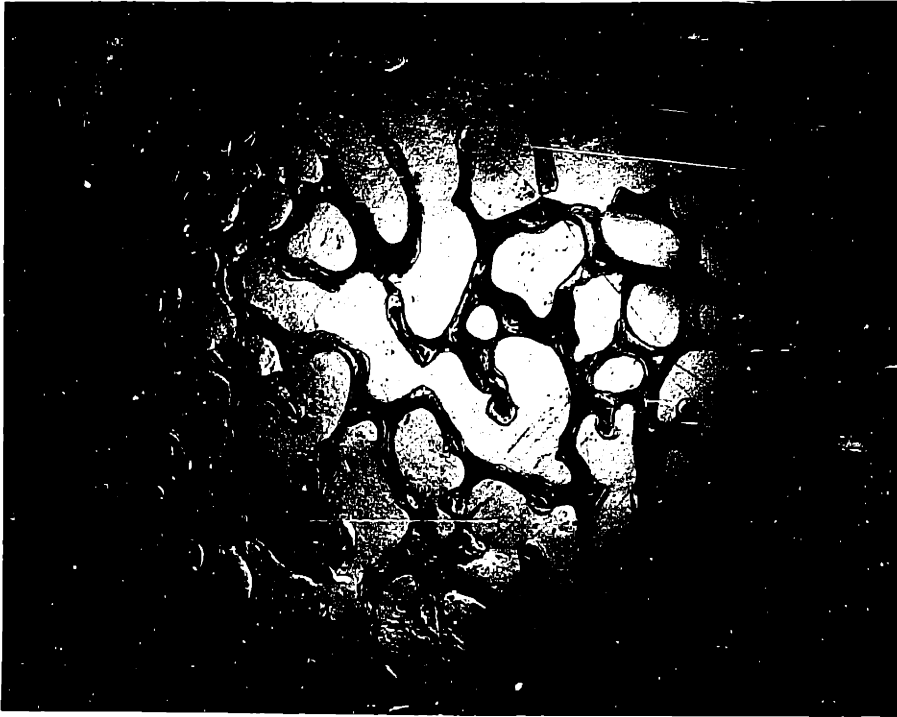


Figure 39A: Human trabecular bone showing uniform microstructure. Transverse section. 20X

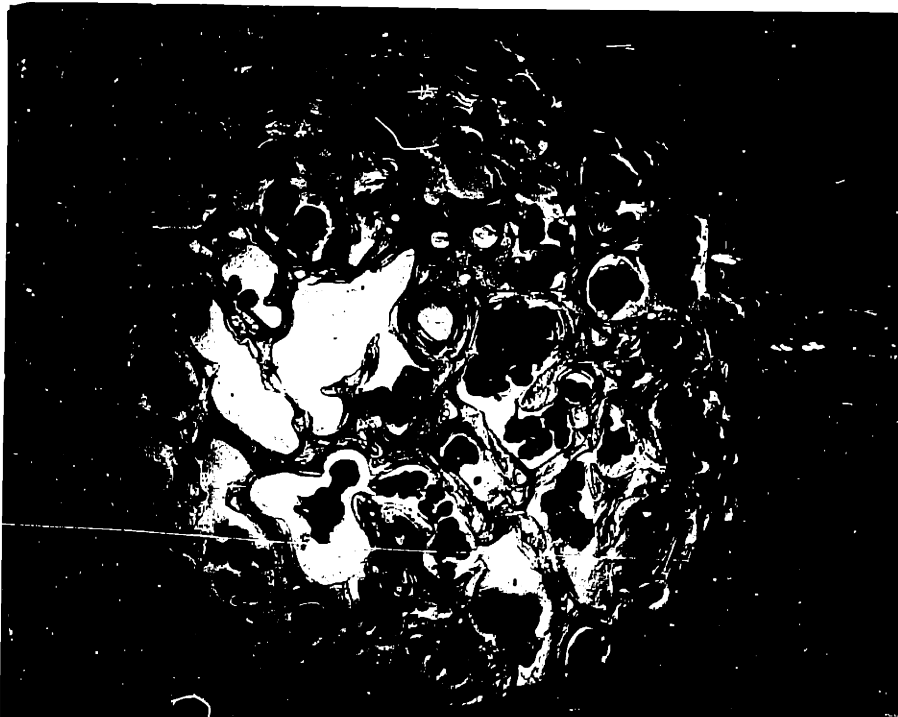
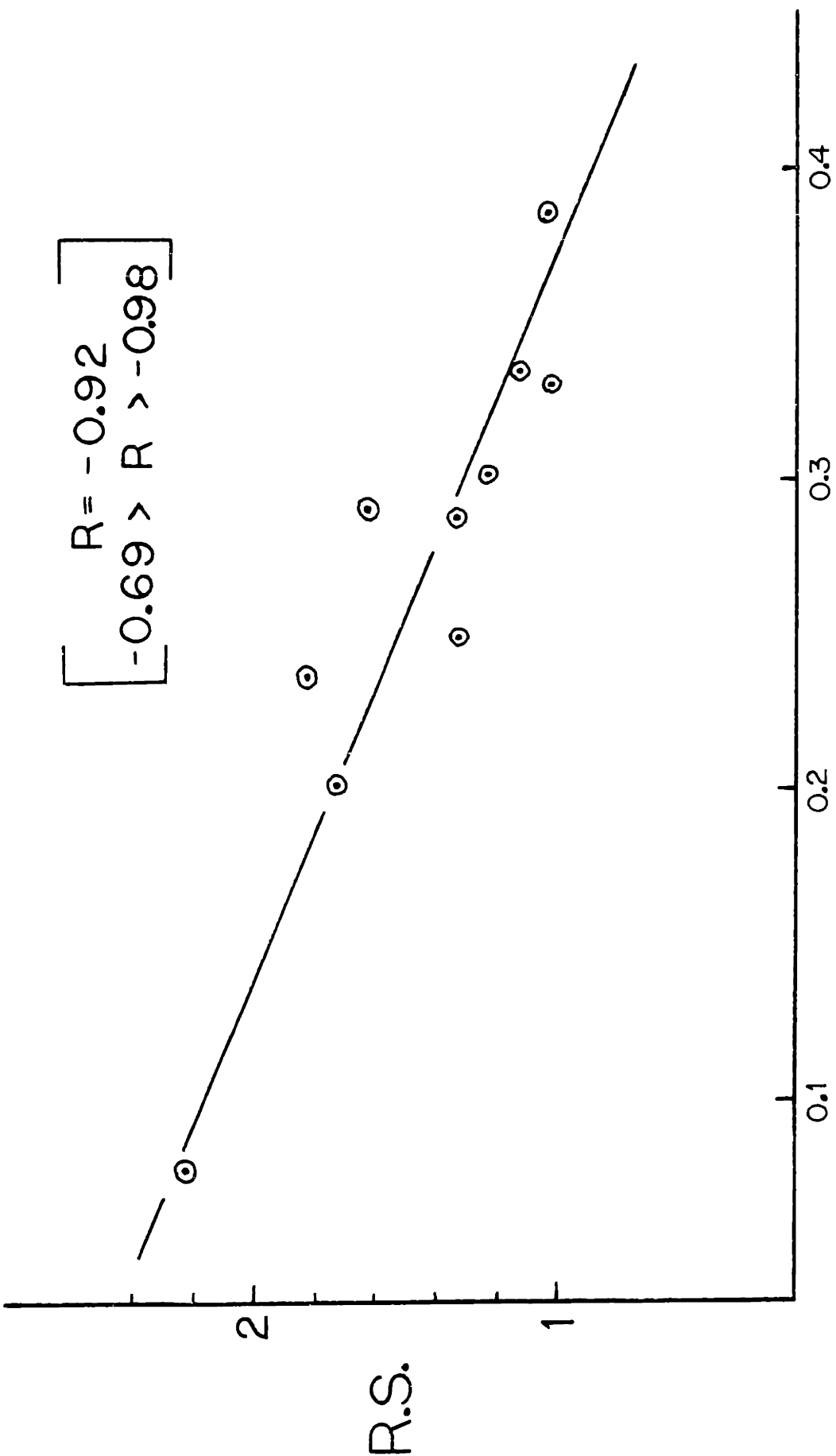


Figure 39B: Human trabecular bone showing non-uniform microstructure. Transverse section. Notice the patches of dense bone, much thicker than normal trabeculae. 20X

Figure 103: human trabecular bone showing non-uniform micropore structure. Transverse section. Notice the presence of closed pores (small circles) and the presence of open pores (small triangles). 20X

Figure 40: Relative stiffness versus contiguity of holes for human trabecular bone with uniform microstructure. Much of the scatter in Figure 35 is eliminated. The line is a least-square regression. The correlation coefficient R and the 95% confidence limits for R are indicated.

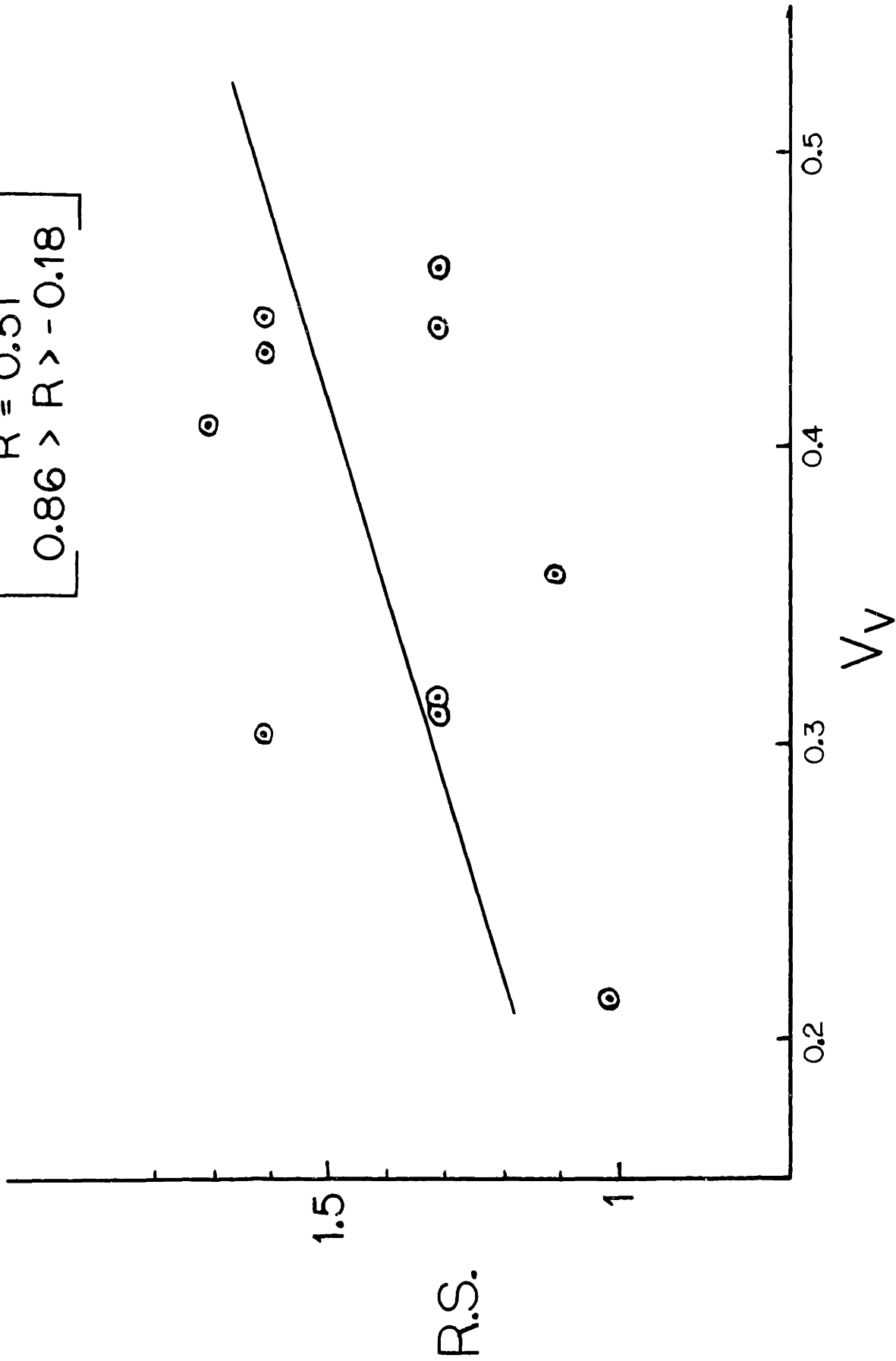


C_H

$R.S.$

Figure 41: Relative stiffness versus volume fraction bone for human trabecular bone with non-uniform microstructure. Much of the scatter in Figure 34 is eliminated. The line is a least-square regression. The correlation coefficient R and the 95% confidence limits for R are indicated.

$$R = 0.51$$
$$0.86 > R > -0.18$$



THE OBSERVED ELASTIC PROPERTIES OF TRABECULAR BONE ARE DUE TO THE FLEXING OF THE SHEETS OF BONE THAT FORM THE TRABECULAE.

When the contiguity of the holes decreases, the trabeculae are kept from bending and buckling under the applied compressive load in the same manner that a floor can be kept from sagging by the placement of a beam under the floor. This is illustrated in Figure 42, for the cases of high C_H and low C_H . These diagrams show that, all things being equal except C_H , the deflection Δl_1 (high C_H) is greater than the deflection Δl_2 (low C_H). Since the applied force is the same in both cases, the resulting moduli are as follows:

$$E_1 = \frac{F/A}{\Delta l_1/l_1} = \frac{Fl_1}{A\Delta l_1} \quad l_1 = l_2, \Delta l_1 > \Delta l_2$$

$$E_2 = \frac{F/A}{\Delta l_2/l_2} = \frac{Fl_2}{A\Delta l_2}$$

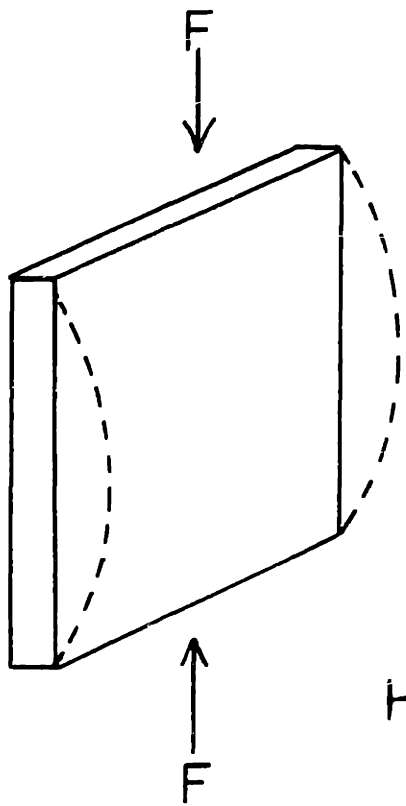
Thus the conclusion is that:

$$E_2 > E_1$$

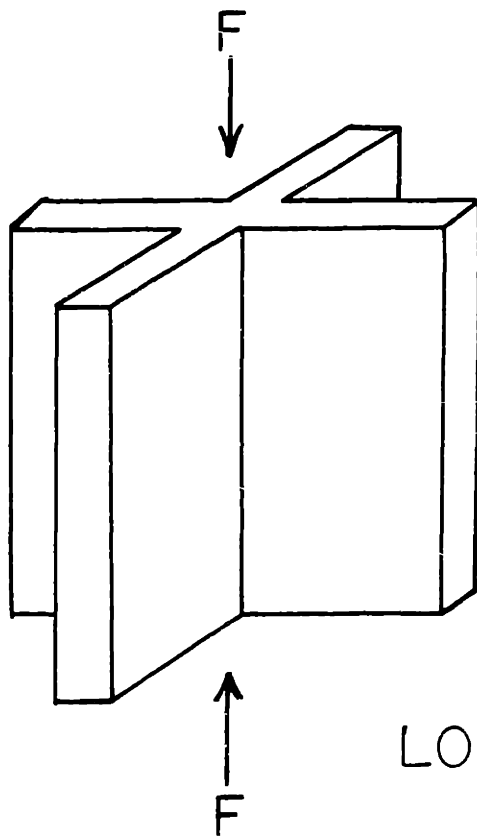
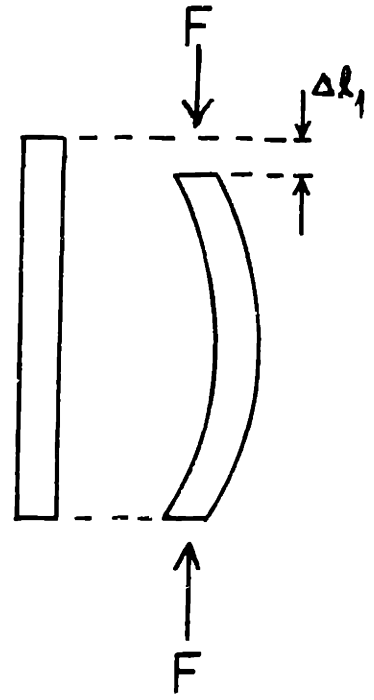
The area A is taken to be the same in both cases, and is the area of the cross-sectional area of the rectangular solid containing the low C_H structure. This is analogous to the cross-sectional area of a cylindrical sample of trabecular bone, and bears no relationship to the actual area (or volume) of bone in the sample.

Figure 43 shows two idealized trabecular microstructures, viewed in a plane normal to the applied compressive stress. The first structure shows two test lines at right angles, one having a C_H of 0 and the other a C_H of 1, giving an average C_H of 0.5. The second structure shows two test lines each with a C_H of 0 for an average C_H of 0. Thus, as the value of C_H goes from 0 to 0.5, the trabecular microstructures go from a complete network to a

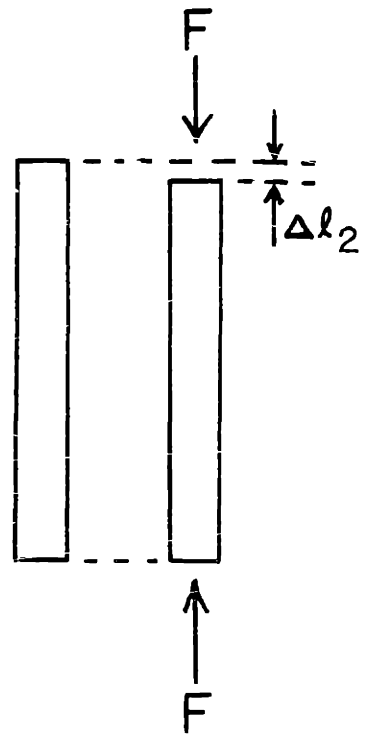
Figure 42: Schematic showing that the modulus of the uniform group of samples is controlled by a plate bending type of deformation.



HIGH C_H



LOW C_H



$$\Delta l_1 > \Delta l_2$$

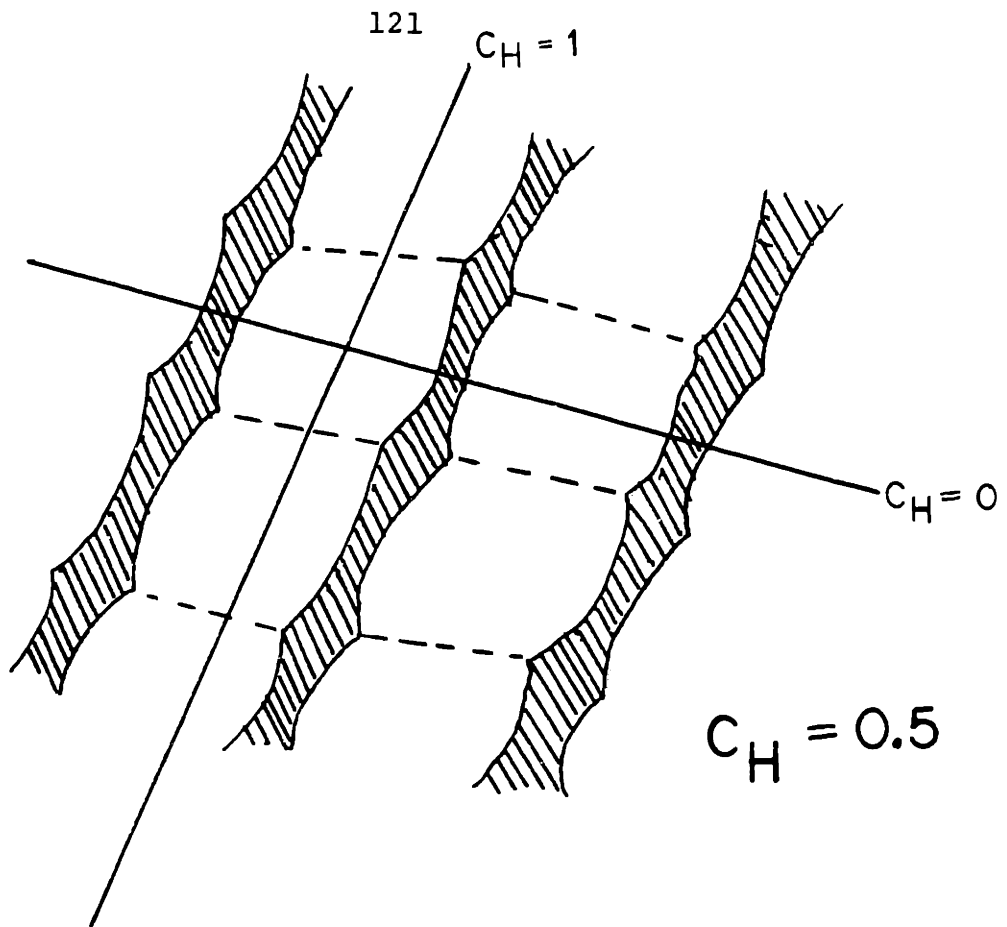
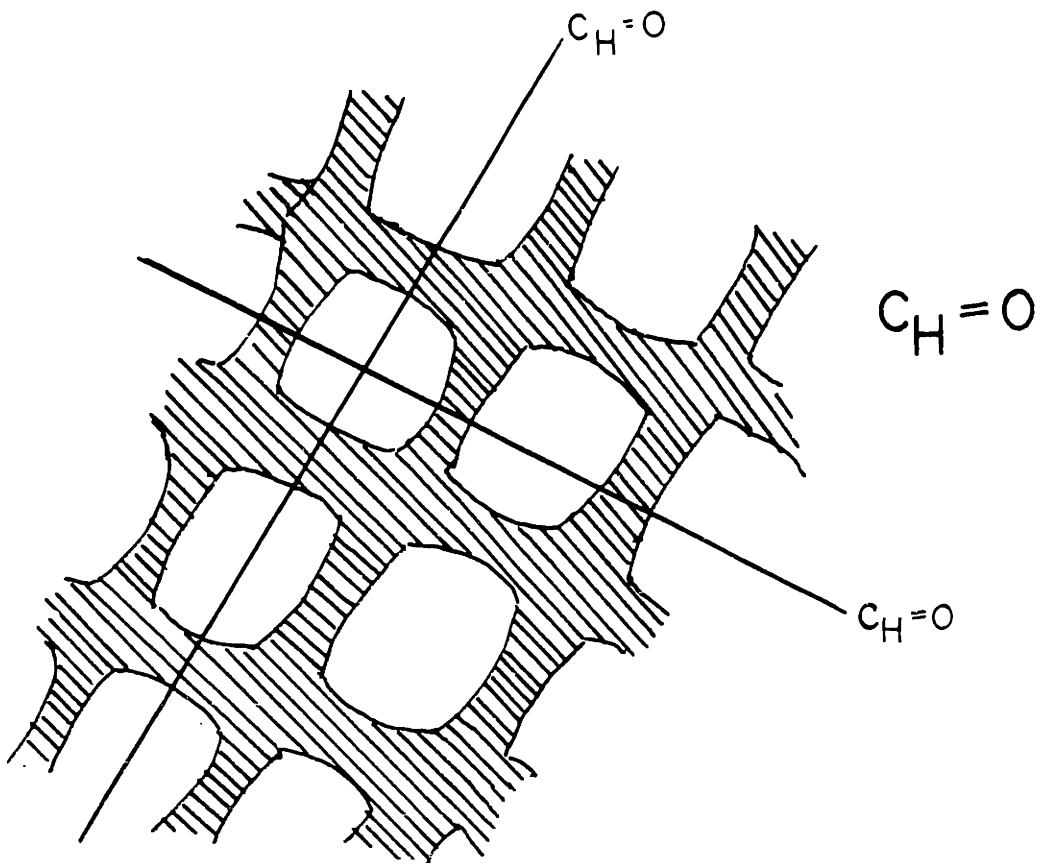


Figure 43: Idealized microstructures exhibiting contiguities of 0.5 and 0. Transverse sections analogous to photomicrographs shown elsewhere.



system of parallel sheets of bone. The latter is capable of a buckling deformation while the former is not. Figures 44A and 44B show actual microstructures of two human samples, the former having a C_H of 0.3 and the latter a C_H of 0.1.

The correlation of R.S. with V_V^{Bone} for the non-uniform group of specimens indicates that the buckling is not as important as for the first group. The buckling seems to be prevented by the large, mechanically stable patches of bone. The mechanical behavior can be depicted as in Figure 45 for the second group, with no buckling effects. The effective area is A in both cases and is the cross-sectional area of the rectangular solid containing either of the two structures. All things being equal except V_V , the deflection Δl_1 , is greater than Δl_2 . Therefore, from the reasoning above, the modulus of the low V_V structure is lower than that of the high V_V structure.

The samples selected as being uniform did not have equal V_V . The variation in V_V in these samples was about the same as for the whole group of twenty samples. However, V_V was unimportant in influencing the R.S. in the uniform samples. An analogous situation occurred for C_H in the non-uniform samples. C_H varied over a wide range, but had no effect on the R.S.

Conclusions

1. The relative stiffness apparatus enables one to measure the relative stiffness of two geometrically identical specimens by obtaining the ratio of the stress levels produced in the apparatus for each sample.



Figure 44A: Human trabecular bone with a C_H of 0.3. Transverse section. 20X

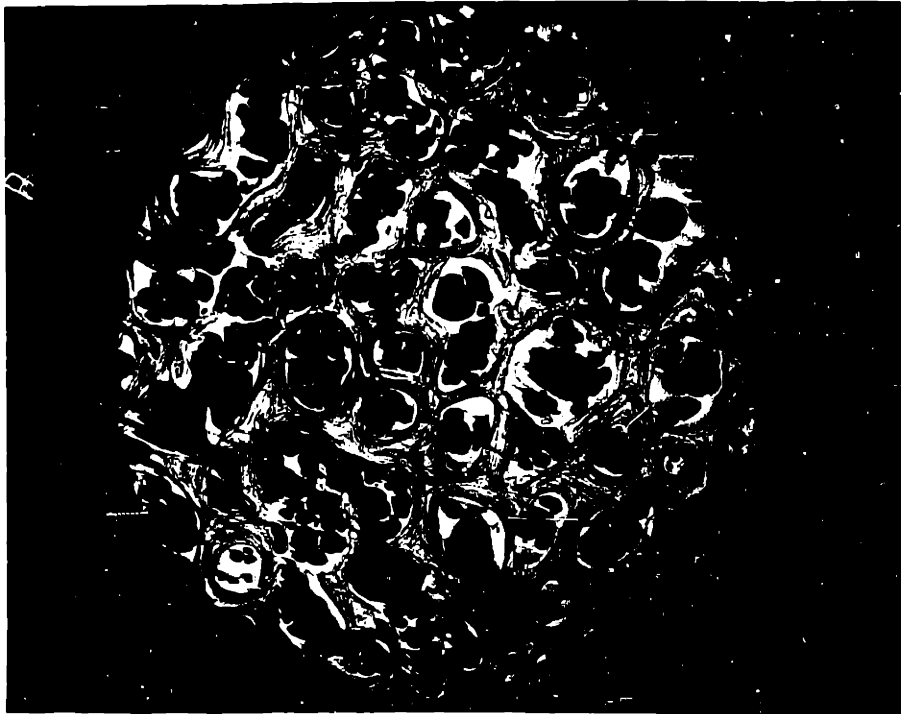
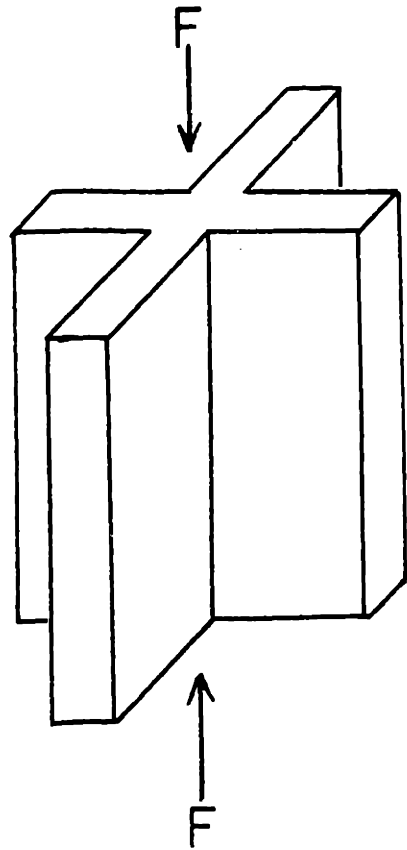


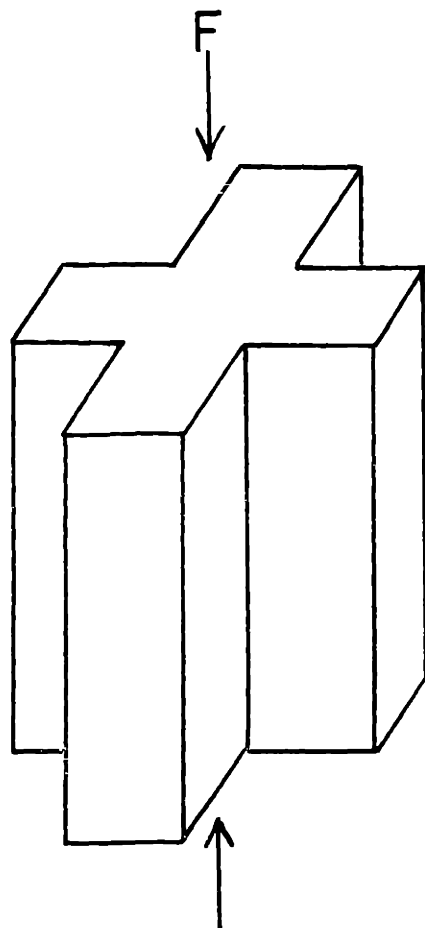
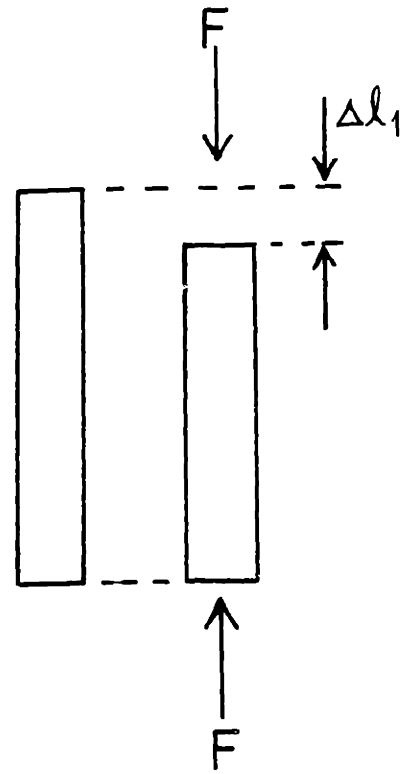
Figure 44B: Human trabecular bone with a C_H of 0.1. Transverse section. 20X



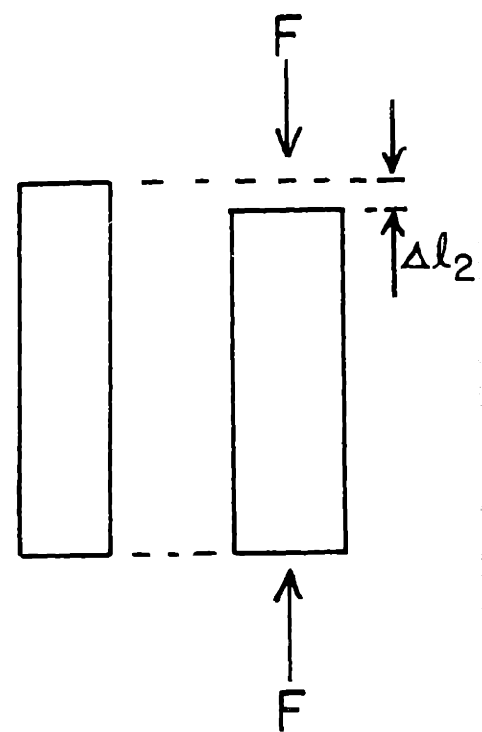
Figure 45: Schematic showing that the modulus of the non-uniform group of samples is controlled by a plate compression mode of deformation.



LOW v_v



HIGH v_v



$$\Delta l_1 > \Delta l_2$$

2. The rabbits run on the impaction apparatus show significant subchondral bone stiffening at day 20.
3. The sections of trabecular bone from the rabbits show increasing stiffness with increasing amounts of bone in the weight-bearing area. This bone reaction is due to Wolff's Law, and is probably due to callus reaction to microfracture and normal osteoblastic-osteoclastic⁷⁹ remodelling.
4. Sections of trabecular bone taken from the weight-bearing area of the medial femoral condyle of humans show the following structure-property relationships:
 - A. If the microstructure is uniform, the relative stiffness is inversely proportional to the contiguity of the holes in the structure.
 - B. If the microstructure is non-uniform (contains patches of dense, thick trabeculae) the relative stiffness is directly proportional to volume fraction bone.
5. The elastic behavior of trabecular bone can be characterized as follows:
 - A. If the sample has a uniform trabecular microstructure, the elasticity is controlled by the bending of the sheets of bone that comprise the trabeculae. In the limit $C_H = 0$, the elasticity is controlled by the bulk compression of the bone.
 - B. If the sample has non-uniform microstructure, the elasticity is controlled just by the compression of the bone with no significant buckling behavior.

V. STRUCTURAL MODEL FOR TRABECULAR BONE

Introduction

Previous Work

The only work done on a structural model for trabecular bone is that by McElhaney, Alem and Roberts.⁸⁰ This model is used only to explain the observed variations of modulus and strength as a function of the density, and is applied only to the cancellous bone in the cranium and the vertebrae. This work explains that much of the standard deviation observed for properties is due to variations in internal arrangement of the trabeculae. The model does not account for these structural effects, and it is semi-empirical. The data show roughly a linear relationship between modulus and volume fraction bone. In developing this model, the assumption was made that all bone has the same physical properties in the small. In other words, bone of different types has the same microscopic properties but varying macroscopic structure and resulting properties.

Structure and Mechanical Function of Trabecular Bone

It is generally accepted that the structure of trabecular bone consists of a system of sheets of bone.⁸¹ Indeed, the photomicrographs presented in this thesis show cross-sections of trabecular bone to consist of interconnected sheets, a conclusion based on the observation that their cross-sections of intersection with the planes of polish are of the type to be expected when a sheet is sectioned. In the vertebral bodies, trabecular bone is shown to have rodlike and sheetlike morphologies under observation by scanning electron microscopy.⁸² The SEM also reveals that the

open spaces present in the trabecular bone are interconnected.

There has been much work done concerning the relationship of structure to function for trabecular bone. The very word "trabecula" gives an indication of the functional role of trabecular bone in the body: the Latin translation is "little beam."⁸³ This definition suggests that the trabeculae act as small supporting members in the bones.

It is generally asserted that the solidity of the skeletal elements is obtained with a minimum of building material.⁸⁴ Trabecular bone is typically present in the ends of the long bones. The stresses in most skeletal elements are determined by the loads exerted at the ends of these bones, i.e. at the joints. Indeed, the joints serve as the weight-bearing areas of the skeleton and also as the points of muscle attachment. The resultants of the body-weight loads and muscle forces usually diverge from the bone axis so as to stress the bone in bending. The function of trabecular bone is to support and direct the loads and forces through the ends of the long bones to the shaft. It is found through photoelastic studies that the trabeculae in the long bones of humans are arranged in the direction of the normal stress trajectories and therefore they serve an important supporting and stress-directing function.

The structure of the human knee joint is shown in Figure 46. The femoral condyles rest on the tibial plateaus and serve to transmit the body weight to the lower leg. The condyles are roughly cylindrical structures, and consist of a thick layer of cartilage, a thin layer of cortical bone referred to as the

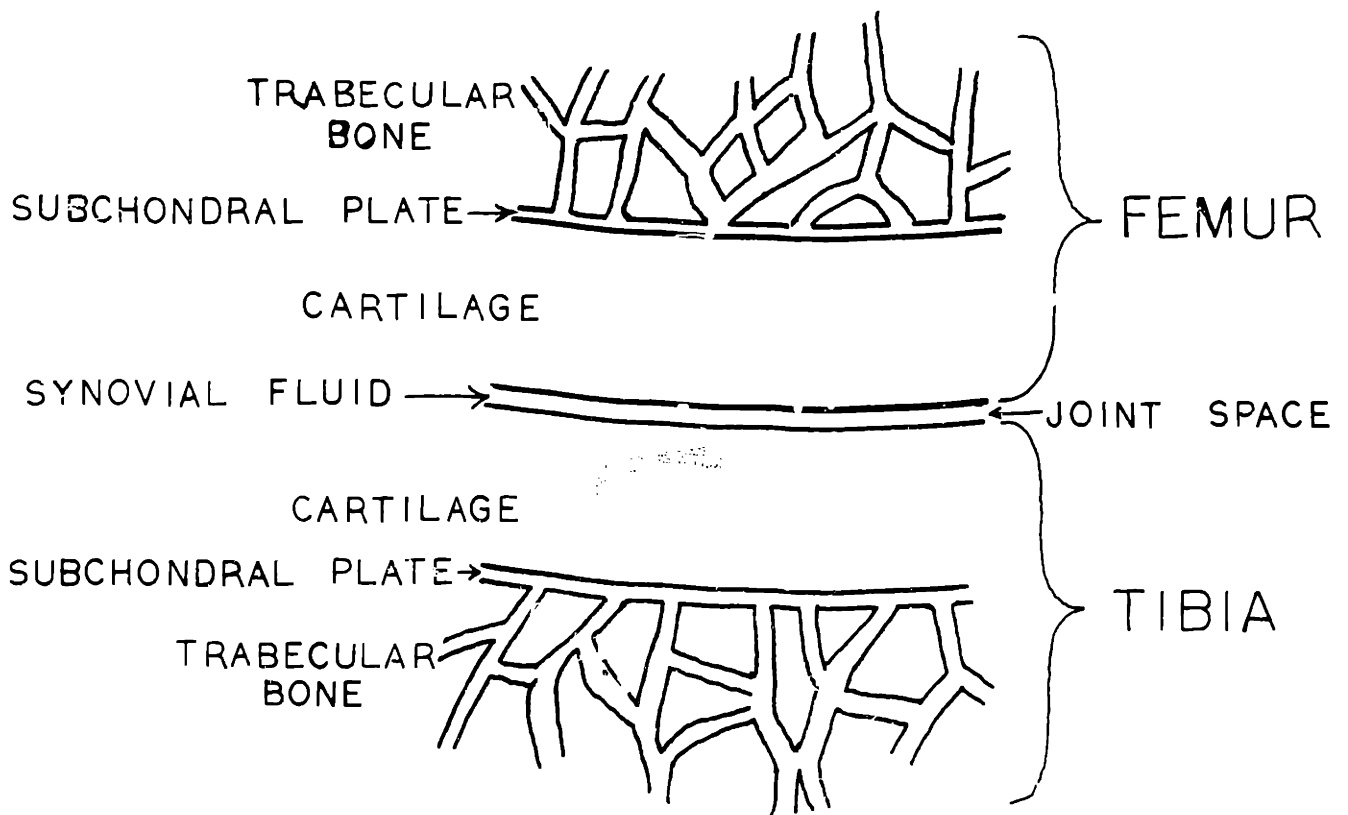


Figure 46: Schematic of human knee joint. The cartilage is very thick compared to a trabecular thickness. The subchondral plate is roughly the same thickness as a trabecula.

subchondral plate, and the region of trabecular bone immediately underneath the plate. The amount of trabecular bone present is large compared to the amount of cartilage and the thickness of the subchondral plate. The region between the cartilage of the condyles and plateaus is filled with synovial fluid, which serves two functions: nourishment of the cartilage⁸⁶ and lubrication.⁸⁷ The synovial fluid serves no mechanical function other than lubrication.⁸⁸

A mathematical model for the elastic properties of condylar structures⁸⁹ has shown that, under static conditions, the role of the trabecular bone in the condyle is important in load-carrying. In addition, 80 percent of the surface loading is transmitted through the trabecular region. The subchondral plate, furthermore, was found to be loaded with a combination of bending and membrane stresses. The trabecular bone was shown to have maximum shear stresses directly under the load in roughly a circular region. Finally, from the differences in properties between cortical and trabecular bone, it was concluded that the stresses in the trabecular region are large compared to those in the cortical bone of the shaft of the femur.

Computer Technique

The use of the computer to solve bio-mechanical problems is not new. Probably the most recent use is a program for the analysis of stresses in long bones.⁹⁰ This allows calculation of stresses and strains through the use of standard stress-strain relations and the stress function ϕ ,^{91,92} for a bone consisting of

any cross-sectional shape and variation of cross-section with length.

The use of finite-element techniques⁹³ has led to a greater understanding of mechanical behavior of composites.^{94,95} It is also applicable to a number of other systems and lends itself especially well to the analysis of very complex structures. The structural system is considered as an assemblage of idealized elastic elements joined together at discrete nodes. Using the direct stiffness concept, which allows adding together at each node the stiffness coefficients of adjacent elements, a stiffness matrix for the structural system is obtained. This matrix relates the external forces acting on the nodes to the displacements of the nodes:

$$\{F\} = [K]\{\delta\} \quad (1)$$

An inversion of the stiffness matrix $[K]$ allows calculation of the influence matrix, which gives the nodal displacements $\{\delta\}$ as functions of the external loads acting on the structural system:

$$\{\delta\} = [K]^{-1}\{F\} \quad (2)$$

This is solved for the nodal displacements $\{\delta\}$; and once the nodal displacements are known, the solution is specified. Using the same strain pattern that was assumed in derivation of the stiffness matrix, one can derive the matrix of stress coefficients giving the stress in a particular element as a function of the nodal displacements:

$$\{\sigma_n\} = [S_n]\{\delta_n\} \quad (3)$$

A continuum, therefore, can be represented as an assemblage of elastic elements joined at nodes as above, and the equations for internal displacements and stresses can be derived using the matrix techniques outlined. The finite-element method is in fact a solution that minimizes the total potential energy of the system.⁹⁶

The system used in the present study is ICES STRUDL II⁹⁷ developed at the MIT Civil Engineering Systems Laboratory. This system allows the calculation of a stiffness analysis on a structure that is specified geometrically in conventional three-space. The stiffness analysis is a linear, elastic, static, small displacement analysis applying the finite-element method in an efficient algorithm. It requires the specification of element properties in acceptable form and treats the nodal joint displacements as unknowns. The analytic procedure provides stresses and strains at the centroid of each element, and displacements and reactions at the joints.

The plate bending and stretching element (PBST)⁹⁸ is a six degree of freedom (six nodal unknowns), flat, triangular element which considers both the in-plane and plate bending forces. The gross results available for this element are displacements, strains, stresses, and moments. The element formulation uses the following displacement expansions: two for orthogonal stretching in-plane, two for in-plane rotation, and two for bending displacements out-of-plane.

Small-Deflection Theory of Flat Plates

The solution of the structure involves the small-deflection theory of flat plates.⁹⁹ This assumes that the thickness h of the plate is small compared with its length and breadth. In the generalized theory of elasticity, there are six independent components of stress necessary to define the state of stress of a body and three displacement components to define its position in space. Therefore a total of nine functions of x , y , and z are necessary for solution of the elasticity problem, as shown in Figure 47A. The small-deflection theory (plane stress) allows the neglect of three stress components as being insignificant σ_z , τ_{xz} , and τ_{zy} , since the plates are thin compared to their length and breadth. The remaining stresses vary over the thickness of the plate. In order to avoid dealing with these distributed stresses, one may represent them by their resultant forces and moment couples. The stress resultants N_{xx} , N_{yy} , and N_{xy} , and the moment couples M_{xx} , M_{yy} , and M_{xy} are given as follows:

$$N_{xx} = \int_{-h/2}^{h/2} \sigma_x dz \quad (4)$$

$$N_{yy} = \int_{-h/2}^{h/2} \sigma_y dz \quad (5)$$

$$N_{xy} = \int_{-h/2}^{h/2} \tau_{xy} dz \quad (6)$$

$$M_{xx} = \int_{-h/2}^{h/2} \sigma_x z dz \quad (7)$$

$$M_{yy} = \int_{-h/2}^{h/2} \sigma_y z dz \quad (8)$$

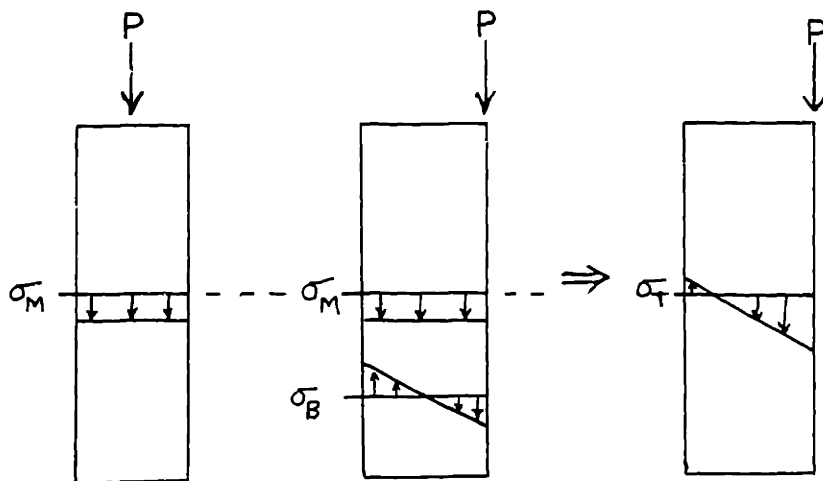
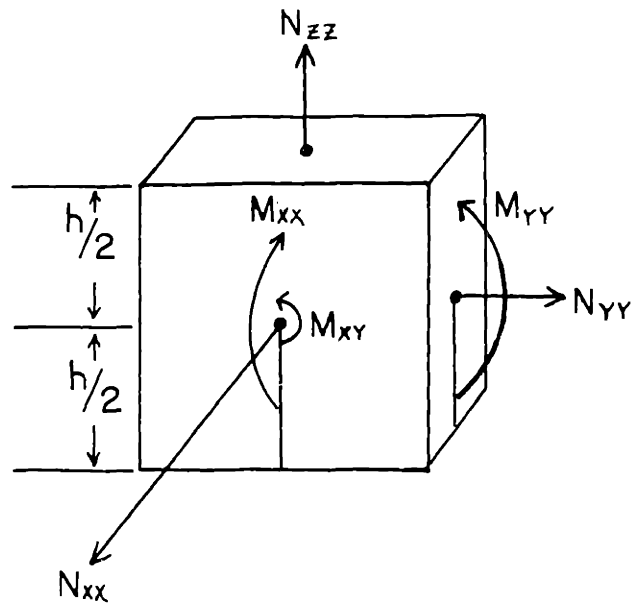
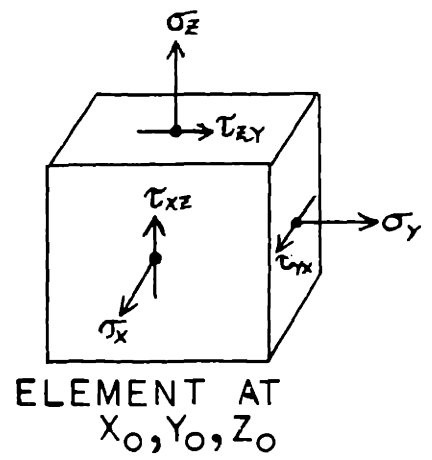
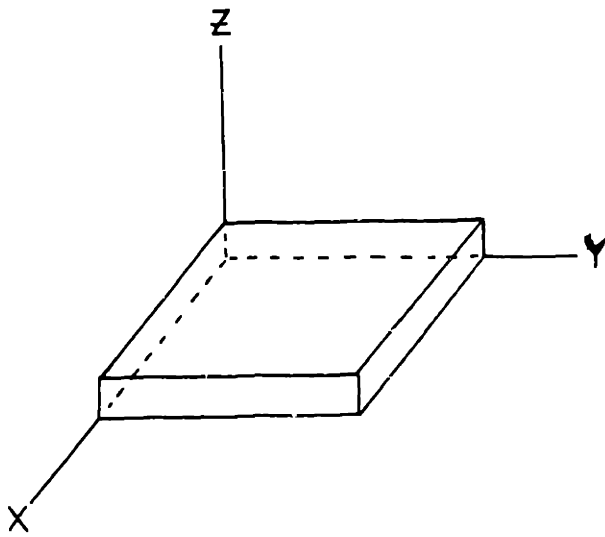
$$M_{xy} = \int_{-h/2}^{h/2} \tau_{xy} z dz \quad (9)$$

The stress resultants and moment couples are given in force per unit length (lbs/in) and moment per unit length (in . lbs/in) respectively. The displacements in the x , y , and z directions are given by u_0 , v_0 , and w_0 respectively. The results of the STRUDL II Analyses are given in the form of stress resultants,

Figure 47A: Non-zero stress components for an infinitesimal element of a sheet in plane stress.

Figure 47B: Stress resultants N and moment couples M of the type calculated by STRUDL II.

Figure 47C: A state of stress in a thin plate resolved into a bending component σ_B and a membrane stress σ_m .



moment couples, and displacements. Strains are presented in a calculation from the displacements. Reactions at the supports are given as forces and moments. In addition, the angular rotations in radians for each joint are given as three components ϕ_x, ϕ_y, ϕ_z for rotations about the x, y, and z axes, respectively.

The problem for thin plates thus separates into two solutions: the membrane problem involving N_{xx}, N_{yy}, N_{xy} and the membrane displacements u_0, v_0, w_0 ; and the transverse bending problem involving the moment couples M_{xx}, M_{yy}, M_{xy} . These are illustrated in Figure 47B. The general solution to the problem is then represented by superposition of these two solutions,¹⁰⁰ as in Figure 47C for a sheet loaded excentrically by a point load of P.

From equations (4), (5), and (6), the membrane stresses are approximately given as follows:

$$\sigma_x \cong N_{xx}/h \quad (10)$$

$$\sigma_y \cong N_{yy}/h \quad (11)$$

$$\tau_{xy} \cong N_{xy}/h \quad (12)$$

The loads for each member are just the stress resultants multiplied by the breadth of the plane:

$$P_x = N_{xx} \cdot b \quad (13)$$

$$P_y = N_{yy} \cdot b \quad (14)$$

The stresses associated with the transverse bending of the plate are given by the following expressions:¹⁰¹

$$\sigma_x = \frac{12z}{h^3} M_{xx} \quad (15)$$

$$\sigma_y = \frac{12z}{h^3} M_{yy} \quad (16)$$

$$\tau_{xy} = -\frac{12z}{h^3} M_{xy} \quad (17)$$

The maximum values of σ_b and τ_b , these bending stresses, are at values of $z = \pm h/2$, which is at the surface of the plate.

Effect of Stress Concentrators

The stress distribution in a thin plate is altered by the presence of a hole of any type. For an elliptical hole (Figure 48A) with semi-axis a (semi-axis in x-direction) and b (semi-axis in y-direction), and stresses σ_θ on the contour of the hole are given by:¹⁰²

$$\sigma_\theta = \sigma \frac{\sin^2 \theta + 2k \sin^2 \theta - k^2 \cos^2 \theta}{\sin^2 \theta + k^2 \cos^2 \theta} \quad (18)$$

where σ is the tensile or compressive membrane stress and $k = \frac{b}{a}$. $\theta = 0$ corresponds to the axis of application of σ .

The bending moments in a thin plate are similarly altered by the presence of an elliptical hole (Figure 48B). The moment M_θ along the contour of such a hole is given by:¹⁰³

$$M_\theta = M \left[1 + \frac{2(1+\nu)(1-m)}{3+\nu} \cdot \frac{m - \cos 2\theta}{m^2 - 2m \cos 2\theta + 1} \right] \quad (19)$$

Figure 48A: Coordinates for calculation of stress concentration due to an elliptical hole in a thin sheet from equation 18.

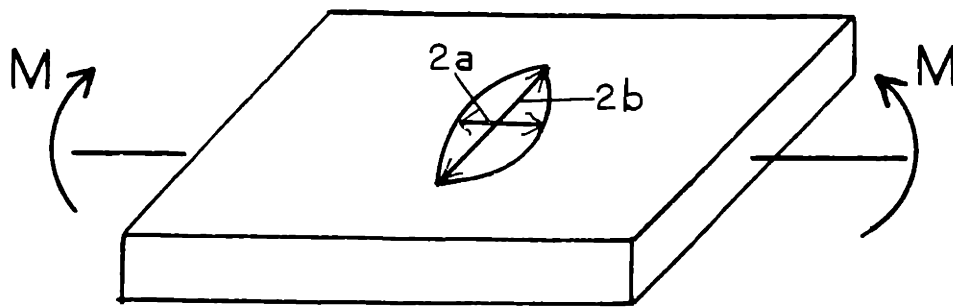
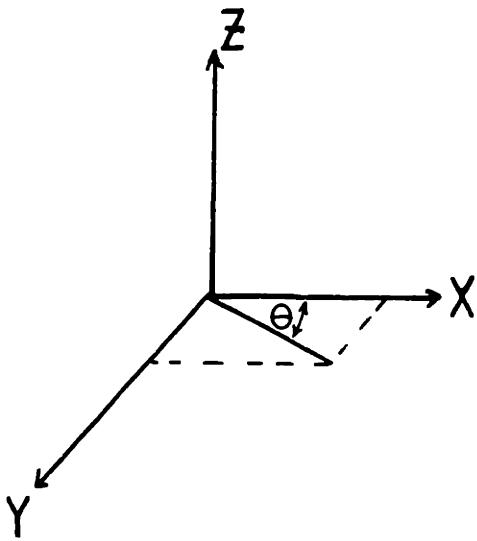
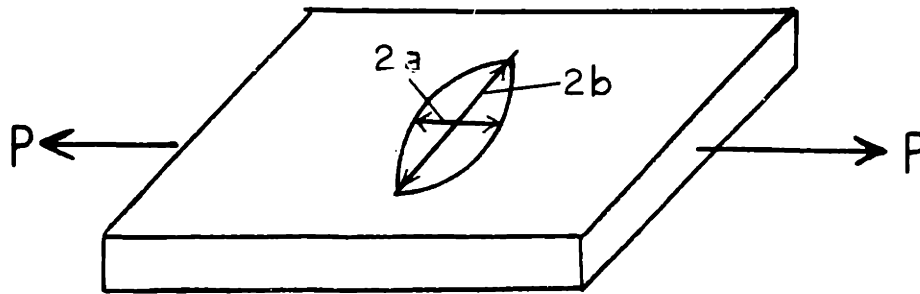


Figure 48B: Coordinates for calculation of moment concentration due to an elliptical hole in a thin sheet from equation 19.

where ν is Poisson's ratio and $m = \frac{a-b}{a+b}$ (notice that $\frac{1-m}{1+m} = K$).

It is well-known that the stress concentrations around these holes can lead to failure if the fracture strength of the material around the hole is exceeded. The material develops a small unstable fracture and then tears apart.

Griffith Fracture

Whether or not the local fracture leads to complete failure is answered by the Griffith theory of fracture.¹⁰⁴ According to the theory, a local crack will propagate and produce failure if an incremental increase in its length does not change the net energy of the system, that is, the tradeoff between surface energy created when the crack opens up and the elastic energy change when the material strains locally. The critical stress necessary for failure due to a crack of length c is given by:

$$\sigma = \left(\frac{2\gamma E}{\pi c} \right)^{1/2} \quad (20)$$

where E is the modulus and γ is the surface energy of the crack surface. It is assumed, of course, that the fracture strength of the material is exceeded at the edge of the crack.

Buckling

Another method of failure is buckling.¹⁰⁵ This can occur in compression of thin plates loaded uniaxially. The criterion for buckling is basically as follows: "When slightly disturbed from an equilibrium configuration, does a system tend to return to its equilibrium position or does it tend to depart even further?"¹⁰⁶ The critical uniaxial compressive load for buckling of a plate

with both ends clamped is given by:¹⁰⁷

$$P = \frac{4\pi^2 EI}{l^2} \quad (21)$$

Where E is the modulus of elasticity, I the moment of inertia of a cross-section and l the length of the plate. The value of I for a plate is:¹⁰⁸

$$I = \frac{bh^3}{12} \quad (22)$$

where b is the breadth of the plate and h the thickness. Substituting,

$$P = \frac{\pi^2 E b h^3}{3l^2} \quad (23)$$

This is the maximum load that a plate can support in a stable configuration.

It should be pointed out that buckling failure occurs under compressive loads. Stress concentration failure may occur under either tensile or compressive conditions. The critical area for failure around a stress concentrator may change position θ for two identical plates with identical holes, one loaded in tension, the other in compression, as shown by equations (18) and (19), depending on the particular geometry of the stress concentrator.

Mechanical Properties of Trabecular Bone

The accepted value for the modulus of cortical bone is 2×10^6 psi (see Section IV). The strength properties¹⁰⁹⁻¹¹² for cortical bone are approximately 20,000 psi in compression and 18,000 psi in tension. Poisson's ratio for cortical bone is very close to 0.3.¹¹³ The compressive strength of cancellous

bone is 500 - 1000 psi depending on where in the femur the bone is taken.¹¹⁴

Experimental Procedure

A structural model for trabecular bone was developed that, it is hoped, best incorporates the salient structural features of the real material and exhibits the same mechanical behavior, yet is soluble through the use of finite-element techniques. In developing this model, effort was made to have a structure very similar to the trabecular bone in the human knee.

Similar to the model for cancellous bone developed by McElhaney, Alem, and Roberts,¹¹⁵ the assumption is made that the trabeculae individually have roughly the same mechanical properties as cortical bone, that is, a modulus of 2×10^6 psi and compressive and tensile strengths of 20,000 and 18,000 psi respectively, and Poisson's ratio of 0.3.

It was decided to model a small section of trabecular bone just beneath the cartilage in the distal end of the femur. The model simulates the structure of the subchondral plate and the trabeculae immediately beneath the plate. A photograph of the model is shown in Figure 49A. It is instructive to compare this with a photograph of the transverse section through the human medial condyle given in Figure 49B. From studies of longitudinal sections similar to that in Figure 49B, it is evident that trabeculae oriented perpendicular to the subchondral plate are the exception rather than the rule. Most of them are inclined at some angle to the vertical. The model contains 5 vertically-oriented

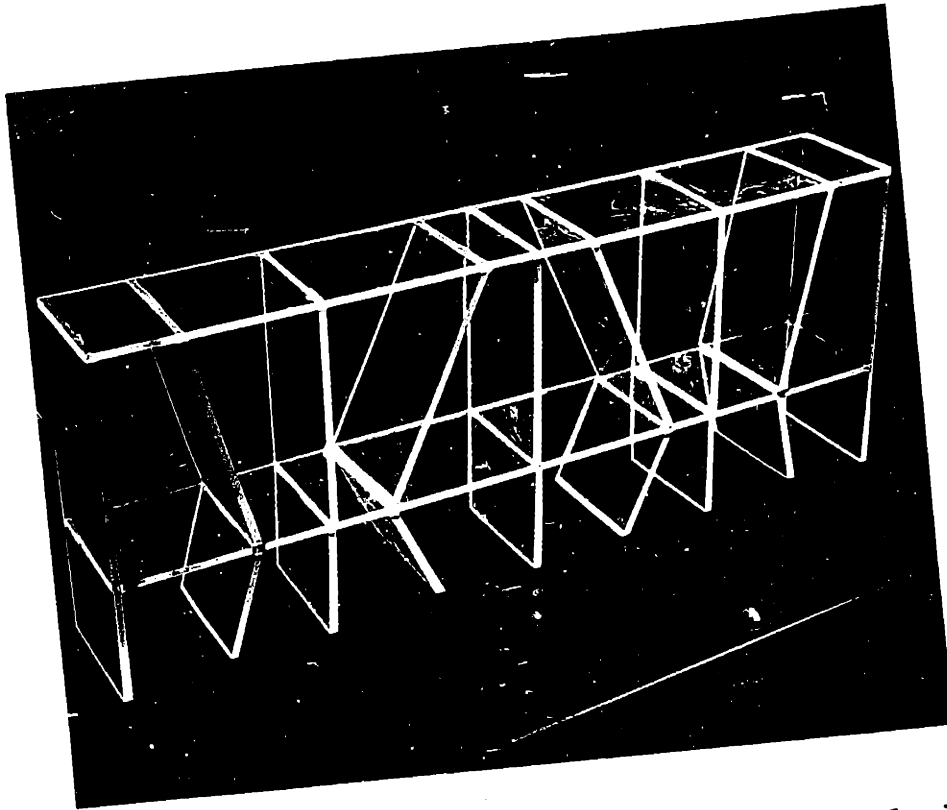


Figure 49A: Model for trabecular bone. The subchondral plate is the plane at top. 1/5X



Figure 49B: Transverse thin section, H & E stained, through human knee showing cartilage at top right, the subchondral plate, and supporting trabeculae. Compare this with the idealized model above. 50X

Handwritten text, possibly a list or notes, with several lines of illegible characters and some numbers.

Handwritten text, possibly a list or notes, with several lines of illegible characters and some numbers.

trabeculae to add structural stability and 4 inclined trabeculae for investigation of the behavior of these elements. The vertical trabeculae act as stiffer supports because of lower internal bending moments (the computer output verifies this). To reduce the effective stiffness of the model to that of real trabecular bone, it was necessary to have a slightly smaller V_V^{Bone} (larger trabecular spacing and thinner trabeculae) in the model as compared to the real bone (see Table 3). It was reasoned that the mechanical behavior of the model should then be very similar to that of the real bone.

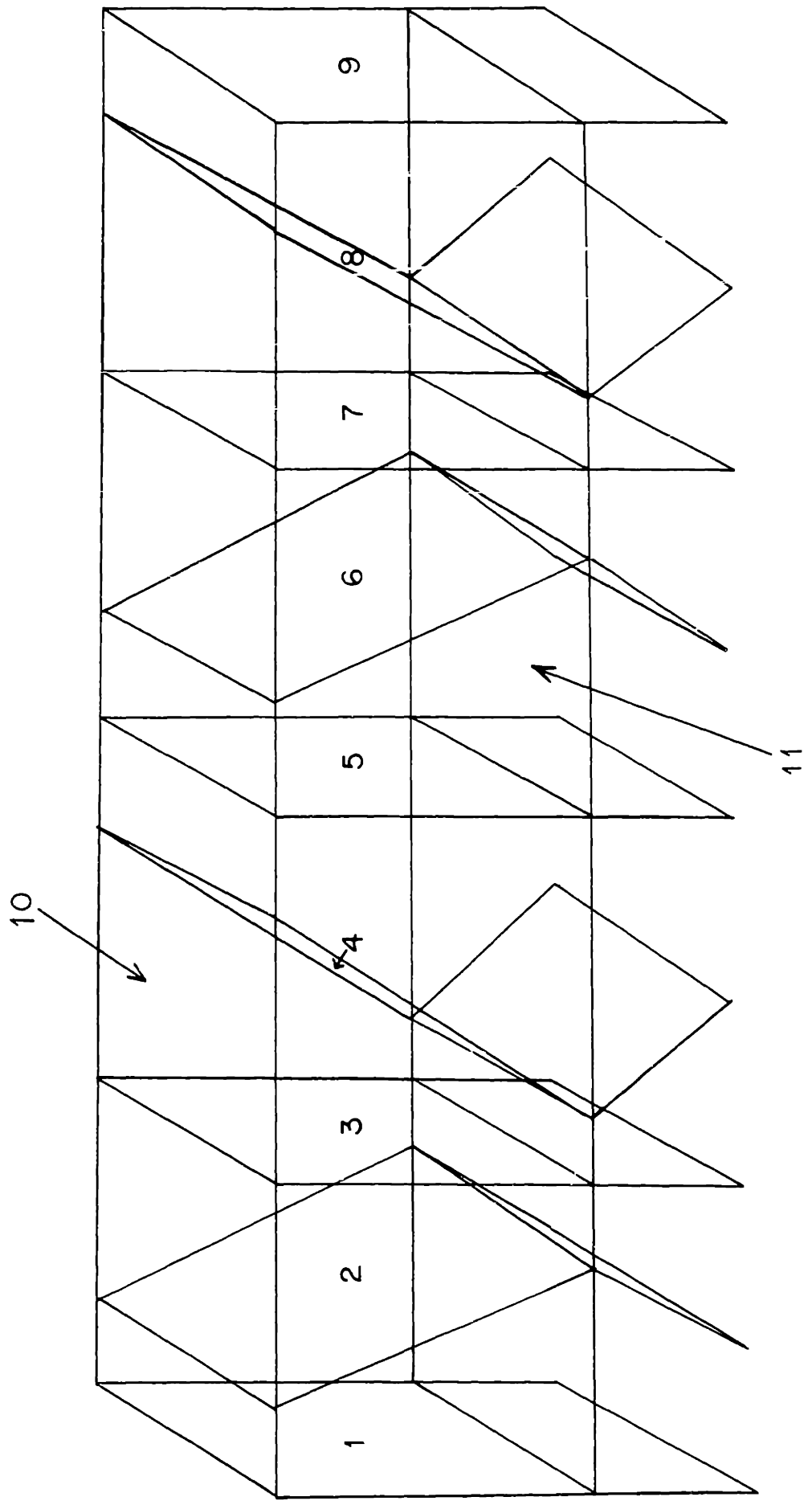
The model is illustrated schematically in Figure 50. The plane labelled 10 is the subchondral plate. Planes 1 through 9 are the supporting trabeculae, and plane 11 is a plane added to simulate the lateral stabilizing trabeculae observed in longitudinal sections of trabecular bone. In scanning many thin sections of trabecular bone, it was decided to use a length of 0.1 inch for the distance between the subchondral plate and the lateral trabeculae, since this was about the scaled spacing between lateral trabeculae in the human knee. The area of the subchondral plate, plane 10, is 0.4 X 0.06 inches. To approximate the effect of inclined trabeculae, planes 2 and 8 are inclined at an angle of 24° from the vertical, and planes 4 and 6 at an angle of 37° . Angles of this size have been observed in thin longitudinal sections. These inclined planes were included to investigate the response of inclined trabeculae to applied stress. The portion of the model below plane 11 is a mirror image of the structure above plane 11, but is only one half of that structure. The ends

TABLE 3

COMPARISONS BETWEEN MODEL AND HUMAN TRABECULAR BONE

	<u>MODEL</u>	<u>HUMAN</u>
E, psi	10^5	10^5
Thickness of Trabeculae; inches	0.003	0.003 - 0.0079
Trabeculae/inch	22.5	31.6 - 63.5
v_V^{Bone}	0.11	0.2 - 0.47
C_{Holes}	0.5	0.1 - 0.45
Loading	100 psi	100 psi (estimated)
Properties of Con- stituent Material	Same as cortical bone $E = 2 \times 10^6$ psi UCS = 20,000 psi UTS = 18,000 psi $\nu = 0.3$	Unknown. But pro- bably close to that of cortical bone, by assumption.

Figure 50: Schematic of model. Plane 10 is the subchondral plate. Planes 1 - 9 are the supporting trabeculae.



of the supports are fixed in space. The model is thus symmetrical about plane 5.

The trabecular thickness was chosen as 0.003 inches, just about at the lower limit observed for the human patients studied in Section IV (see Figure 36). The average trabeculae per unit length in the model is 23 per inch as opposed to 30 per inch for the human samples examined. The volume fraction bone in the model is 0.11. The lowest volume fraction encountered in the human samples was 0.2.

A transverse section through the model just beneath the subchondral plate reveals that the model has a contiguity ratio C_H of 0.5 (see Section IV). The highest contiguity ratio in the human group was 0.44.

The model was loaded uniformly on the subchondral plate with a stress of 100 psi. This is based on an estimation of a weight-bearing area in the human knee of 2 square inches and a body weight of 200 pounds. It is assumed all the body weight is being carried on one leg, for example, during walking. The thick layer of cartilage in the knee is capable of evenly distributing the load to the subchondral plate,¹¹⁶ so the assumption of even loading of the plate is justified.

The comparisons of the model to the real trabecular bone in the human knee are summarized in Table 3.

To render the model soluble by STRUDL II, each of the planes numbered 1 through 11 had to be broken up into triangular elements. Figures 51A and 51B show how a typical horizontal plane and a typical vertical plane were broken up. The accuracy of

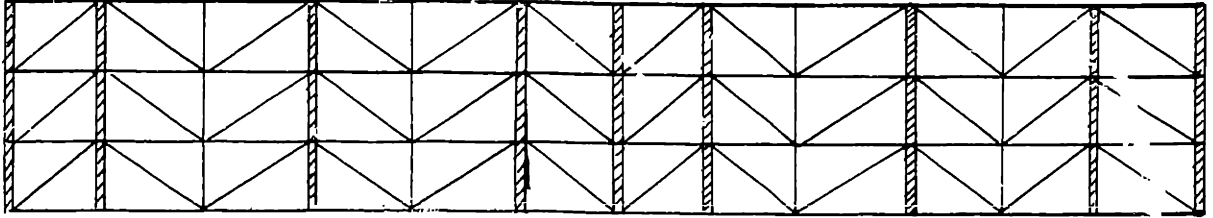


Figure 51A: The subchondral plate, plane 10, as divided into PBST finite elements. The cross-hatched areas are positions of supporting trabeculae (planes 1 - 9) beneath plane 10.

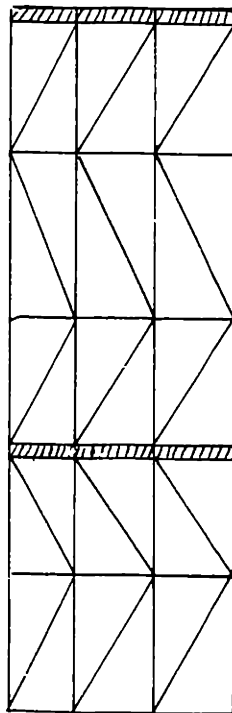


Figure 51B: A vertical trabecula, plane 1, as divided into PBST finite elements. Planes 10 and 11 intersect this plane at the cross-hatched areas.

the solution improves as the number of elements increases, but the practical limitation on number of elements is economy, as the cost to analyze a structure is roughly proportional to (elements).² This model had 244 nodal joints and 414 elements.

All joints were free to move in three-space except the supports, (the bottom ends of planes 1 through 9). The joints at these positions were fixed in space. This was necessary to render the structure statically determinate.

Three analyses were made on the structure. The first was a static stiffness analysis on the intact structure (INTACT). The second (FRACTURE) was run with plane 6 removed to simulate a fracture of a trabecula in order to determine the redistribution of stresses in the structure. The third run (CALLUS) was made with plane 6 back in but with a thickness of 0.005 inches to simulate fracture healing and callus formation.

A program for a very simple structure is given in Appendix C as an example of a typical run.

Results and Discussion

INTACT

The data from the run on INTACT revealed that, in the supporting trabeculae just beneath the subchondral plate, the highest bending moments exist where the trabeculae contact the plate. Indeed, a free-body diagram (see Appendix D) on a trabecula inclined at an angle to the subchondral plate and loaded vertically has bending moments as a function of vertical distance X along the trabecula as follows:

$$M_b = P \tan \alpha \left(\frac{L}{2} - x \right) \quad (24)$$

where P is the vertical load, L the length of the trabecula, and α the angle of inclination of the trabecula from the vertical. This equation shows that a zero bending moment exists at $x = L/2$, and that M is a maximum for $x = 0$ and L . Figure 52 shows a plot of the computer data for the bending moment M_{yy} for plane 6 as a function of vertical distance below the subchondral plate. The maximum bending moment occurs at the subchondral plate. The plot is not symmetrical along the length of plate 6 because of effects of the transverse plate present at the bottom and the inclined support beneath this. These data generally agree with the prediction of equation (24).

Using the computer-generated data, and equations 10 and 15, the average compressive stress (membrane stress) in the plate is 2600 psi. The maximum bending stresses are ± 5230 psi. Therefore, on one surface of the trabecula, a compressive stress of 7830 psi exists, while a tensile stress of 2630 psi exists on the other surface.

Using equations (18) and (19), one calculates that the maximum stress and moment concentrations are at $\theta = \pm 90^\circ$, leading to the following relations:

$$\sigma_\theta = \sigma(1 + 2K) \quad (25)$$

$$\sigma_{b\theta} = \pm \sigma_b(1 + 0.79K) \quad (26)$$

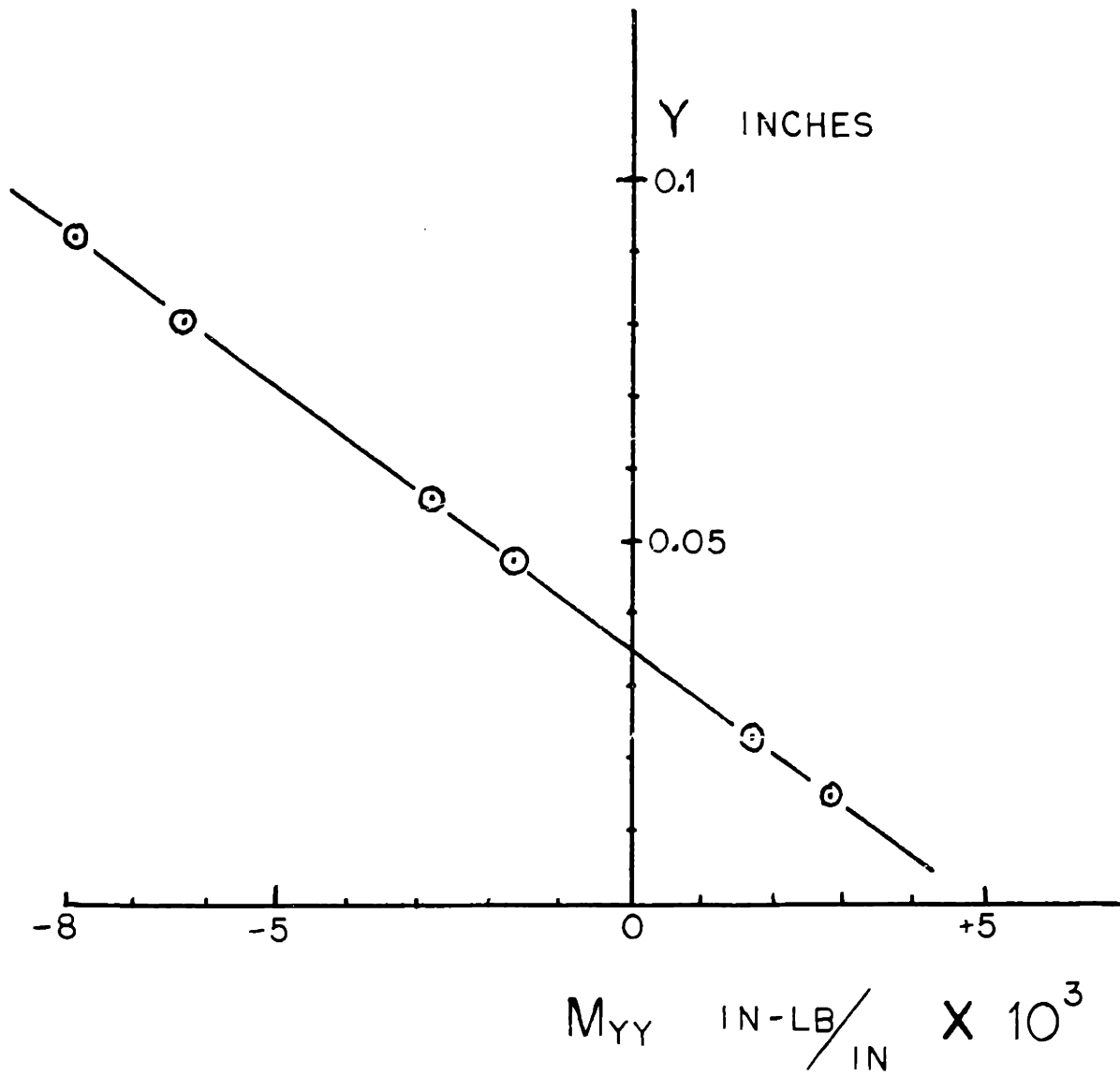


Figure 52: Bending moment M_{yy} along plane 6 as a function of vertical distance y beneath the subchondral plate, plane 10.

For a membrane stress of -2600 psi and $K = 2$, $\sigma_{\theta} = -13,000$ psi. For bending stresses of 5230 psi and $K = 2$, $\sigma_{\theta} = \pm 13,500$ psi. Therefore on one surface of the trabecula, there exists a tensile stress of 500 psi, while on the other surface, a compressive stress of 26,500 exists, which exceeds the compressive strength of the bone. Local fracture would therefore be expected to occur at the end of the major axis of the elliptical hole on the compressive side of the trabecula (the positive - Z side of the plane in Figure 53).

The structure of trabecular bone is known to consist of sheets with holes in them.¹¹⁷ The holes provide interconnecting passageways for marrow and blood vessels. Therefore, the presence of stress concentrators as above is to be the rule rather than the exception. Local fracture would therefore be expected in the real trabecular bone. Whether these local fractures widen to cause a break in a typical trabecula is open to question. The Griffith criterion for fracture could be invoked if the surface energy of the bone-fluid interfaces were known (see Section VI). There is some reason to believe that, whether trabecular microfracture occurs by a Griffith mode, or by fatigue, it does occur in vivo. (See typical examples of trabecular microfracture in Figures 54A and 54B.) Callus reaction to the fractures indicates that the fractures occurred in vivo and are not artifacts.

FRACTURE and CALLUS

Since some type of trabecular fracture is to be expected, in unfavorably oriented trabeculae, the FRACTURE model was run to show the redistribution of stresses and displacements occurring

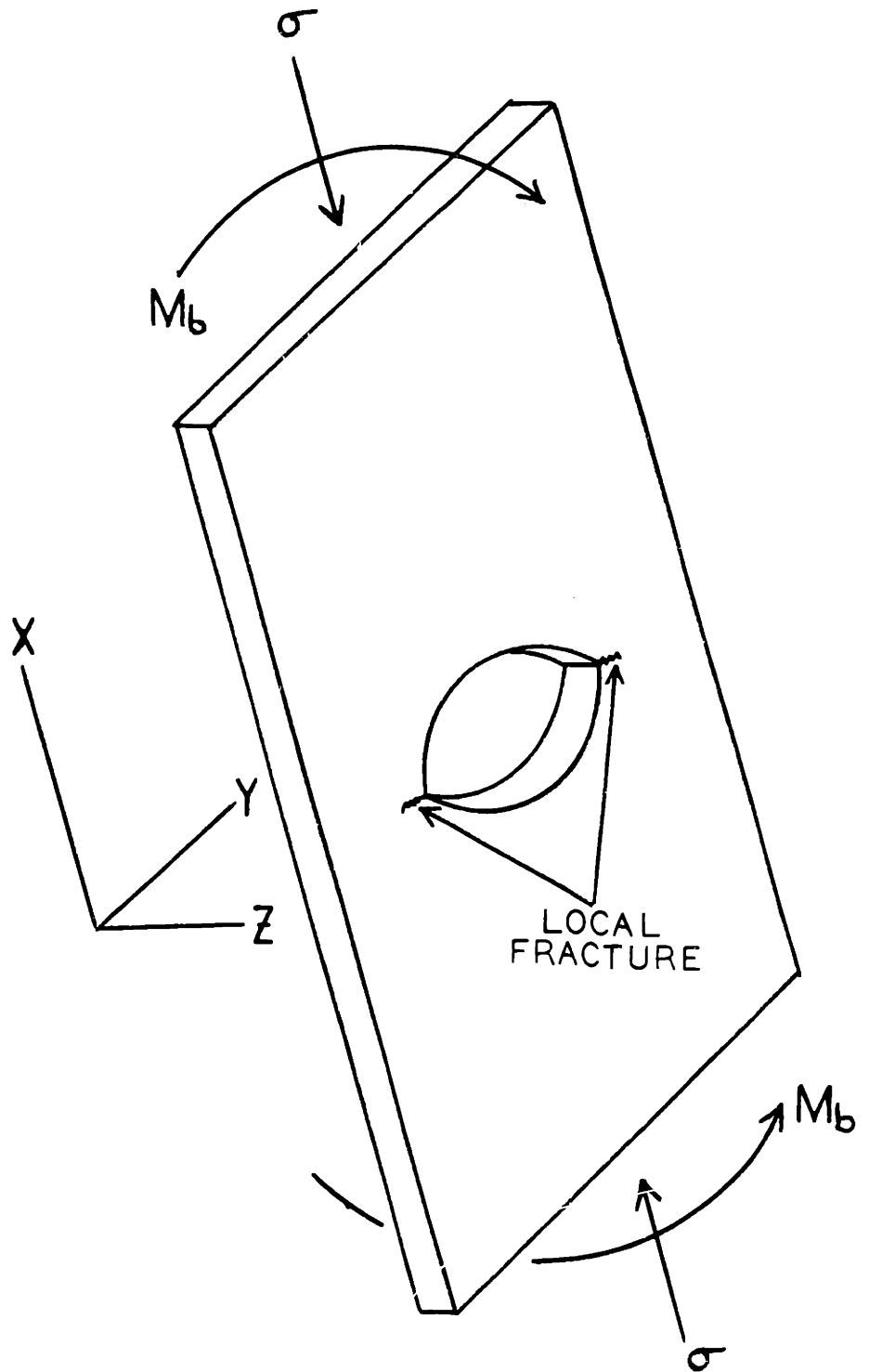


Figure 53: Position of local fracture around stress concentrator in an inclined trabecula.



Figure 54A: Trabecular microfracture in human bone. Slight callus reaction evident. 180X



Figure 54B: Trabecular microfracture in rabbit bone. Advanced callus formation is evident. 260X



after fracture of a selected trabecula, in this case, plane 6, which is the one in which the stresses are the highest.

Thickening of the trabeculae (probably following fracture) in rabbits and humans of up to 50% has been observed in the bone studies (see Figure 55). Therefore, the CALLUS model was used to study the redistribution of stresses after a thickening of a trabecula from 0.003 to 0.005 inches. A comparison of the data for the three runs should give an indication of the redistribution of stresses occurring after fracture and subsequent healing.

Figure 56 gives the vertical displacements for positions along plane 10 (the subchondral plate) for the three runs. Since the ability of a structure to act as a shock-absorber (see Section VI) is dependent on the deflections the structure undergoes, it is evident that the shock-absorbing properties vary locally across the subchondral plate. Shock-absorption is less above vertical supporting trabeculae, and greater where the plane can flex freely.

Figure 57 shows the local modulus on plane 10 for each of the three models. The modulus was calculated by using only the vertical displacements, v_0 . The local strain at the positions indicated is given by:

$$\epsilon = \frac{v_0}{l} \quad (27)$$

where l is the total height of the model, in this case 0.15 inches. The local modulus is given by dividing the stress, 100 psi, which is imposed on the subchondral plate, by the local strain.



Figure 55: Thickening of trabeculae in rabbit tibia. 97X

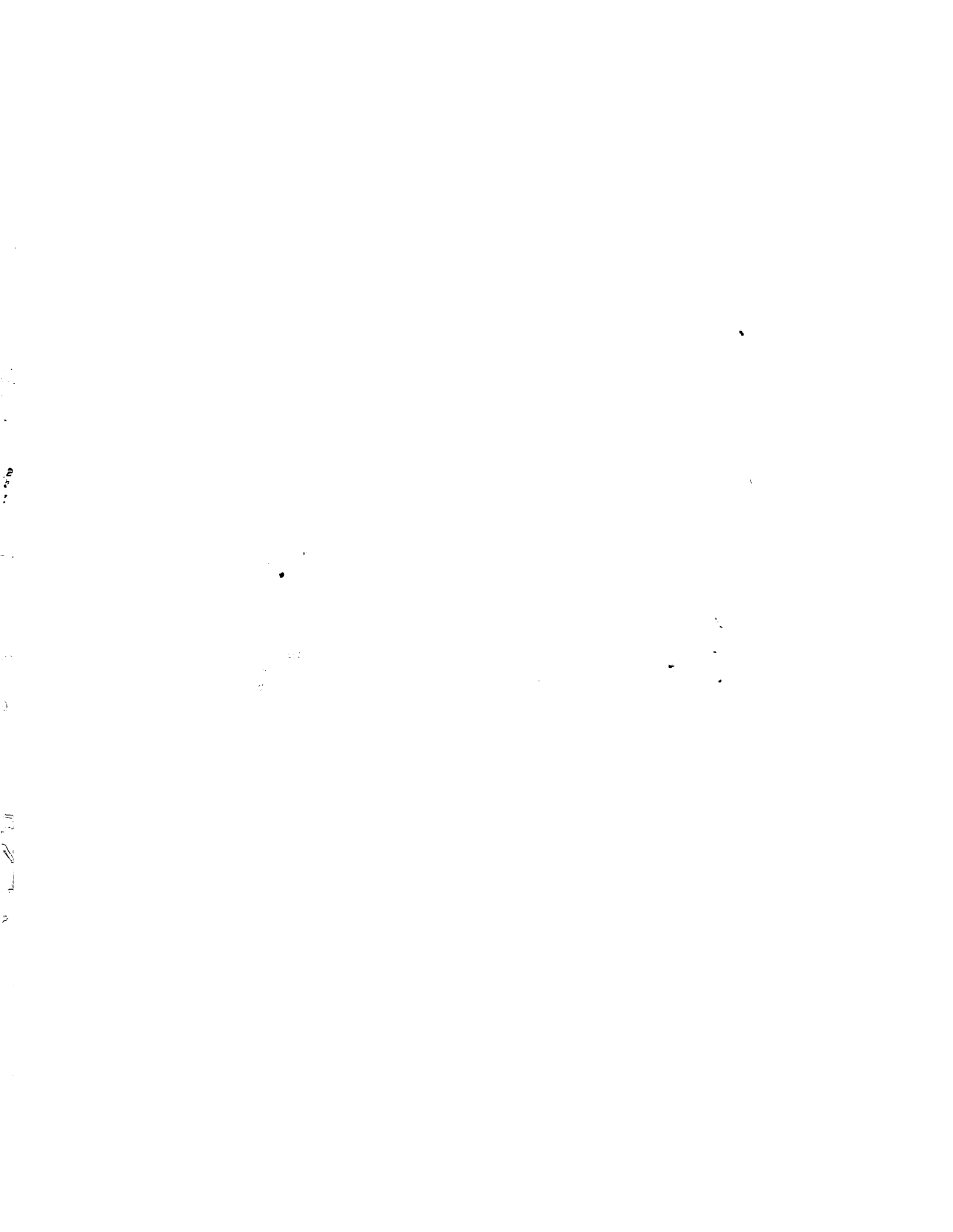
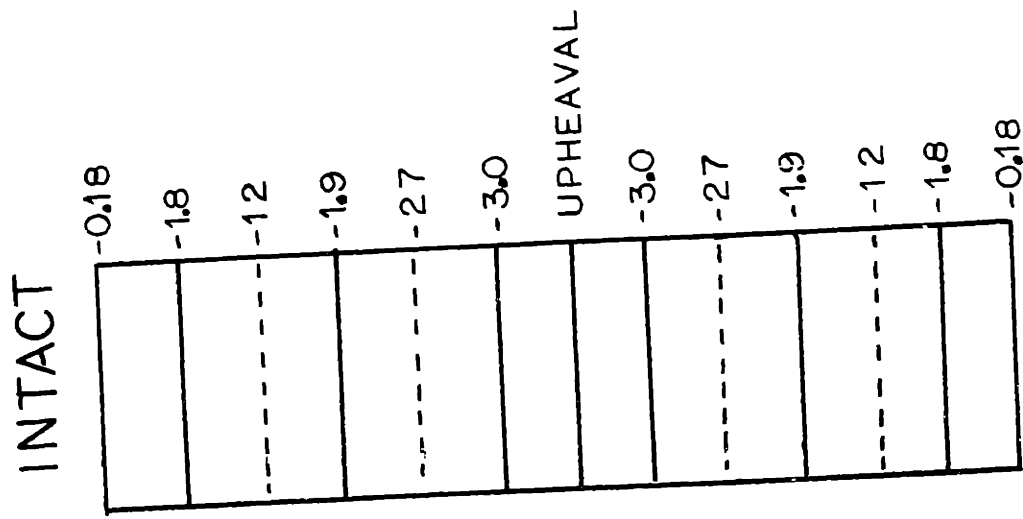
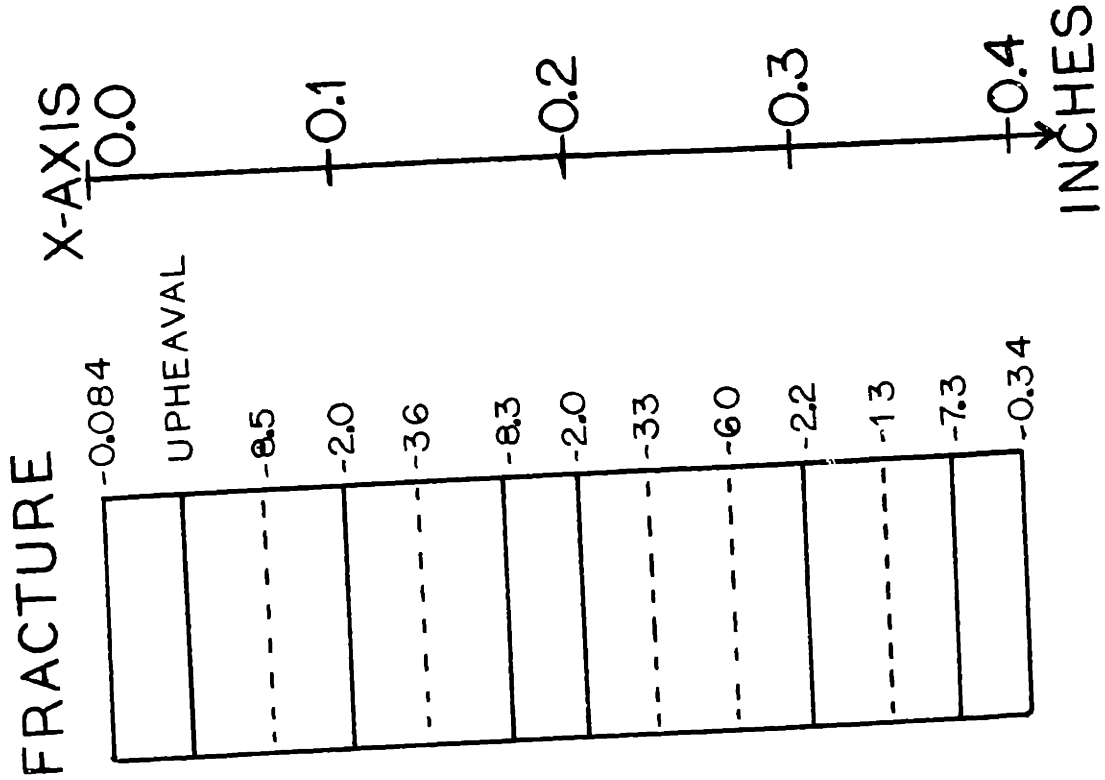
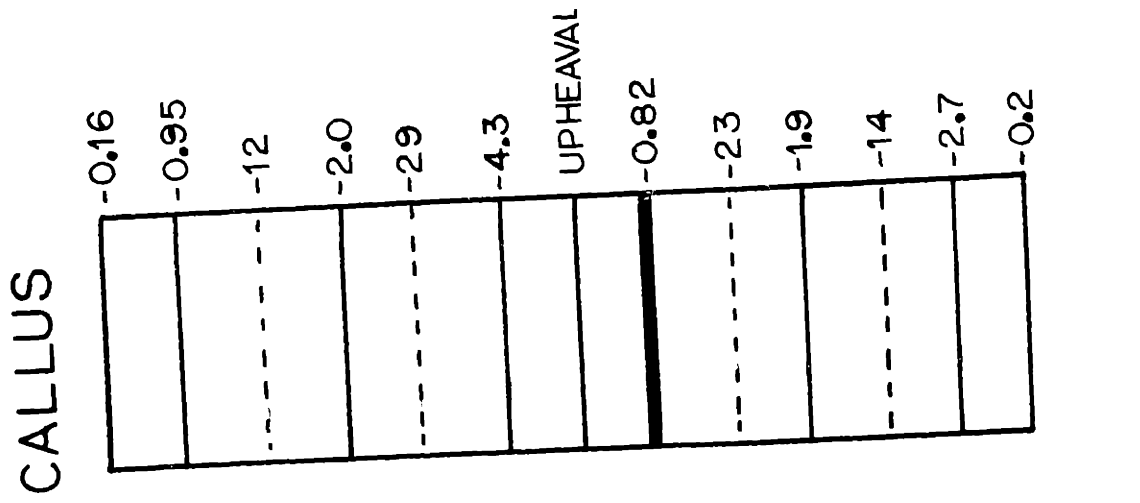


Figure 56: Local deflections of the subchondral plate, viewed normal to plane 10, for the three models. In three instances, upheavals occurred, indicating that the shock-absorbing properties of the model vary considerably on a local basis across the subchondral plate.



X-AXIS

0.0

0.1

0.2

0.3

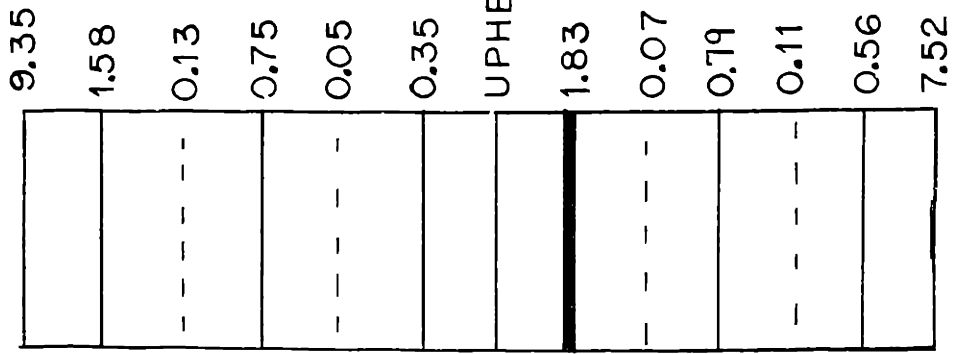
0.4

INCHES

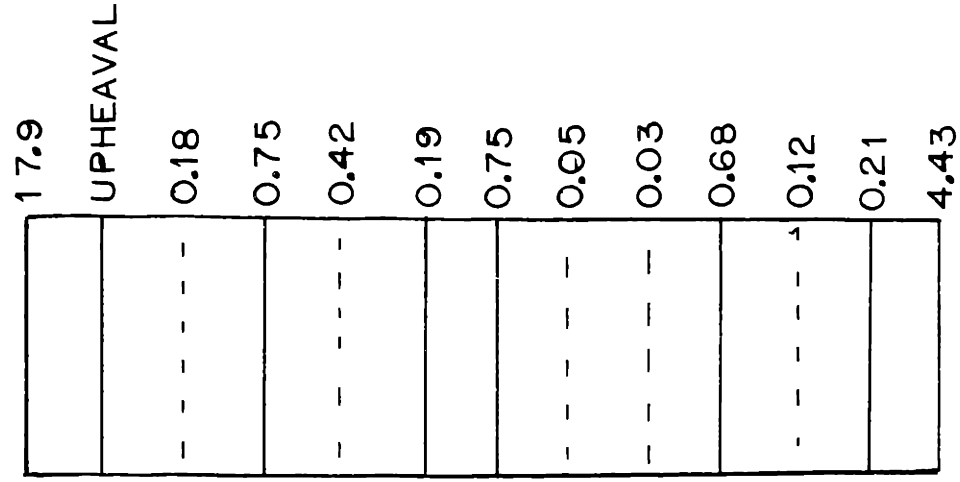
DEFLECTIONS IN X 10⁴

Figure 57: Local modulus across the subchondral plate as calculated from the data in Figure 56.

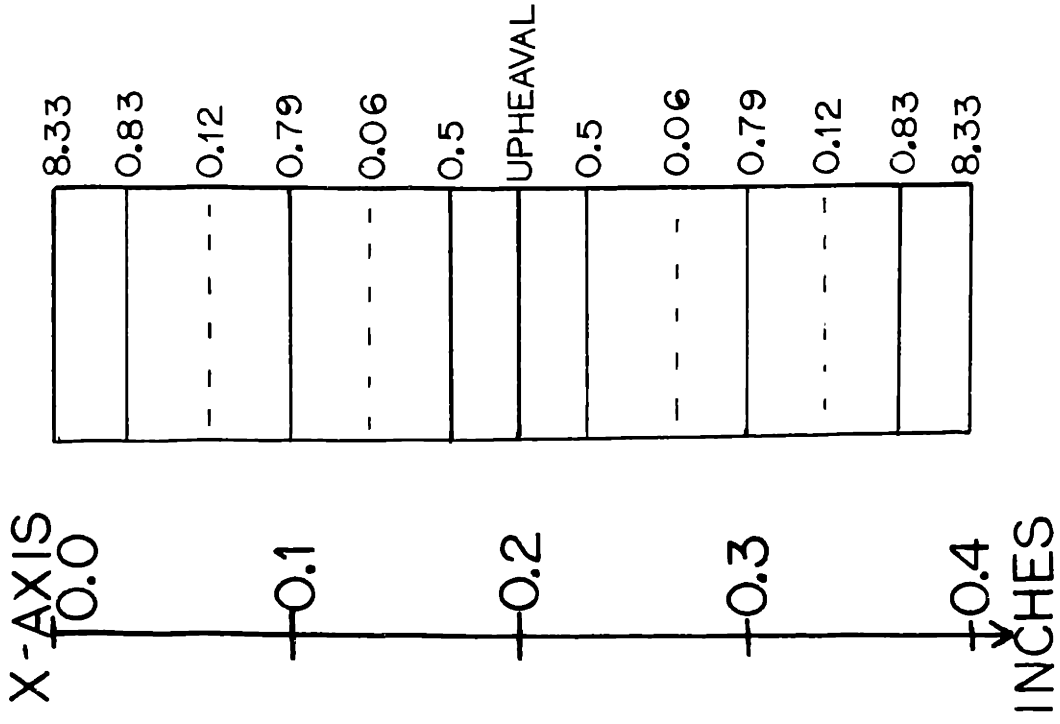
CALLUS



FRACTURE



INTACT



E X 10⁻⁵ PSI

Modulus Changes

The comparison of the local modulus at the same positions for the INTACT, FRACTURE, and CALLUS models is indicative of the effects of trabecular microfracture and subsequent callus formation on the local mechanical properties of the bone immediately adjacent to the knee. Notice that, due to the geometric configurations and resulting bending moments, the deflections were positive in 3 positions. Even though a compressive load was applied evenly on the subchondral plate, the compressive load leads to local upheavals of bone in these positions.

In the INTACT model, the modulus (neglecting the values at the ends of the model due to edge effects) varies from about 10^4 to 10^5 psi. The positive deflection in the center would probably increase the effective modulus of the whole structure to about 10^5 psi. The modulus measurements in Section III were made under conditions of uniform applied strain to the trabecular bone. This is the method employed in measuring modulus of most materials. In the model, the local moduli are calculated from conditions of constant surface loading. The moduli determined in this manner should have more physiological significance than machine-moduli. In vivo, the stresses are uniform through the weight-bearing area and the bone responds locally to the uniform stress. Some areas of the bone are stiffer than others, but the cartilage tends to compress into the less stiff areas and away from the stiffer ones. Most of the local moduli are close to 10^5 psi, the value measured experimentally for trabecular bone in Section III.

In the FRACTURE model, the local modulus in the area above the fractured trabecula is roughly a factor of 10 lower than the same area in INTACT. The local moduli away from the fracture are affected, due to changes in the deflection of the subchondral plate. Some of these areas become stiffer than in INTACT.

After the callus has formed, the region of callus formation is roughly four times as stiff as the same area in INTACT. The areas immediately adjacent to the callus are roughly the same mechanically as in INTACT, but significantly stiffer than in FRACTURE.

Stresses in Trabeculae

Tables 4, 5, and 6 summarize the stress resultants and moment couples in the areas of interest in the three models. Positive stress resultants are tensile. The convention for the moments is shown in the figure accompanying each table. The stress situation is seen to be worse in the subchondral plate than in the trabeculae. The moments are higher, and the stresses are more often tensile than compressive, due to the sagging of the subchondral plate, in the data for INTACT. For example, point 9 in Table 4 has tensile membrane stresses of 730 psi and bending stresses of $\pm 8,700$ psi. In the presence of a circular stress concentrator, $K = 1$, the tensile stresses become 2190 psi and the bending stresses are $\pm 15,600$ psi. Therefore, on the tensile side of the subchondral plate, a tensile stress of 17,790 psi exists. This is very close to the tensile strength of the bone. It should be emphasized that the stress concentrator in this case is a very mild one, a circular hole.

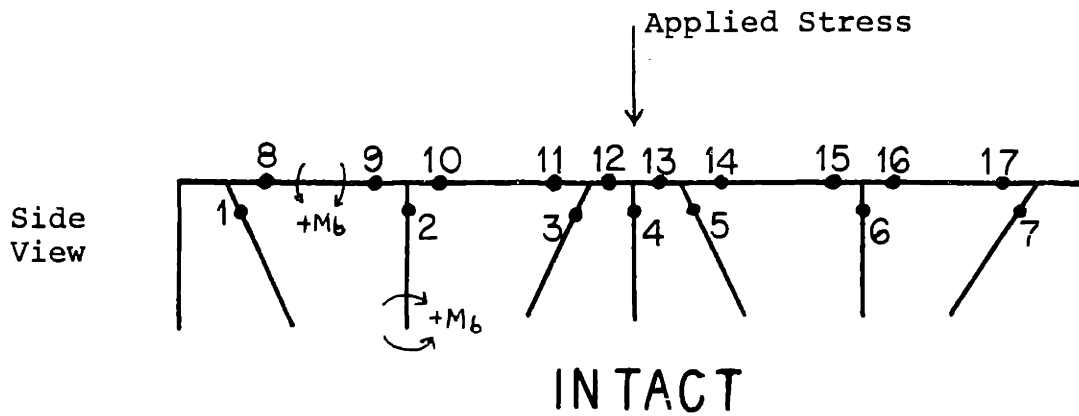
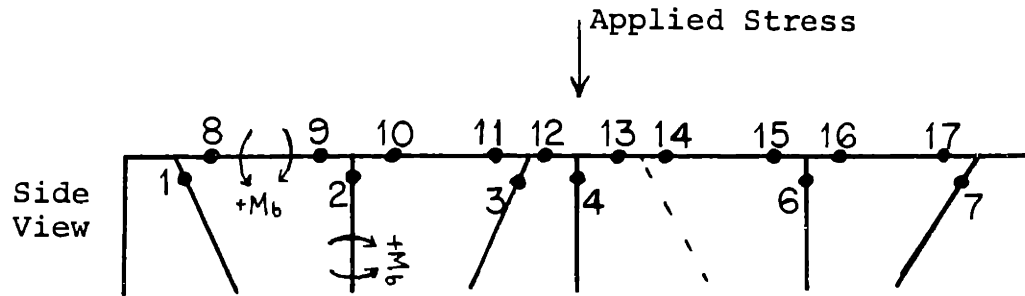


TABLE 4: STRESS AND MOMENTS FOR INTACT MODEL

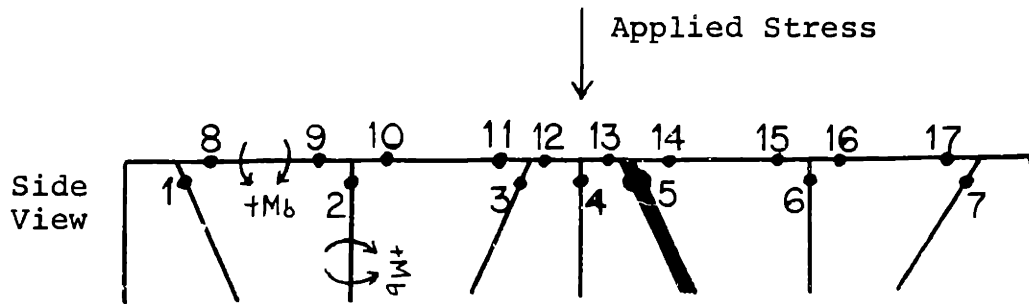
POINT	ELEMENT NUMBER	STRESS RESULTANT (lb/inch)	MOMENT COUPLE (in lb/in)
1	33	-6.1	-4.7×10^{-3}
2	63	-8.5	-3.6×10^{-3}
3	93	-7.8	7.8×10^{-3}
4	123	1.4	1.3×10^{-6}
5	153	-7.8	-7.8×10^{-3}
6	183	-8.5	3.6×10^{-3}
7	213	-6.1	4.7×10^{-3}
8	279	2.2	-6.0×10^{-4}
9	286	2.2	1.3×10^{-2}
10	291	2.1	7.7×10^{-3}
11	298	2.2	-4.8×10^{-4}
12	303	-1.7	1.8×10^{-2}
13	310	-1.7	1.8×10^{-2}
14	315	2.2	-4.8×10^{-4}
15	322	2.1	7.7×10^{-3}
16	327	2.2	1.3×10^{-2}
17	334	2.2	-6.0×10^{-4}



FRACTURE

TABLE 5: STRESS AND MOMENTS FOR FRACTURE MODEL

POINT	ELEMENT NUMBER	STRESS RESULTANT (lb/inch)	MOMENT COUPLE (in lb/in)
1	33	-6.6	-1.3×10^{-3}
2	63	-8.7	-4.4×10^{-3}
3	93	-2.5	1.5×10^{-2}
4	123	-8.6	-7.4×10^{-3}
5 (deleted)			
6	183	-9.8	1.2×10^{-2}
7	213	-5.0	7.5×10^{-3}
8	279	2.5	1.3×10^{-3}
9	286	2.5	1.5×10^{-2}
10	291	2.4	7.8×10^{-3}
11	298	2.5	-7.1×10^{-3}
12	303	1.3	2.8×10^{-2}
13	310	1.2	1.9×10^{-2}
14	315	1.4	-3.2×10^{-2}
15	322	1.3	1.8×10^{-2}
16	327	1.6	2.2×10^{-2}
17	334	1.6	-5.0×10^{-3}



CALLUS

TABLE 6: STRESSES AND MOMENTS FOR CALLUS MODEL

POINT	ELEMENT NUMBER	STRESS RESULTANT (lb/inch)	MOMENT COUPLE (in lb/in)
1	33	-6.2	-4.0×10^{-3}
2	63	-8.5	-3.6×10^{-3}
3	93	-7.5	8.8×10^{-3}
4	123	8.7	1.4×10^{-3}
5	153	-7.4	-1.9×10^{-2}
6	183	-8.4	2.9×10^{-3}
7	213	-6.1	5.5×10^{-3}
8	279	2.3	-2.3×10^{-4}
9	286	2.2	1.3×10^{-2}
10	291	2.2	7.7×10^{-3}
11	298	2.2	-1.3×10^{-3}
12	303	-1.5	1.7×10^{-2}
13	310	1.4	1.4×10^{-2}
14	315	2.1	3.6×10^{-3}
15	322	2.1	7.2×10^{-3}
16	327	2.1	1.2×10^{-2}
17	334	2.1	-9.0×10^{-4}

In FRACTURE, the stress problems are even worse. The redistribution of stresses and moments leads to increased probability of additional localized fracture both in the trabeculae and in the subchondral plate, as indicated by the changes in stresses and moments for points 9 and 14.

In CALLUS, things seem to have returned to close to those values in INTACT, even in the thickened trabecula. The increased moment gives a maximum outer-fiber stress of 4550 psi, based on a calculation involving a plate thickness of 0.005 inch. The compressive stress is 2460 psi, leading to compression on one side of the plate by a stress of 7010 psi and a tensile stress on the other side of 2090 psi. These calculated stresses are similar to those of the original trabecula. During the callus formation, the defect that originally led to the fracture would probably have filled up so that fracture would probably not reoccur.

Buckling Calculations

Using equation (18) for the critical buckling load, one calculates a buckling load of 0.356 pounds for the idealized plate. The stress of 100 psi on the subchondral plate is distributed evenly over an area of 0.06 inch by 0.4 inch. The total load on the structure is 2.4 pounds. Since there are 9 supporting trabeculae, each must support roughly 0.267 pounds. This is below the critical buckling load for an individual trabecula. However, each trabecula does not support the same load, as shown by the membrane stress resultants in Tables 4 through 6. The highest load supported is that at point 4 in INTACT. The effective load at this point is 0.51 pounds. The minimum load in any element in

this trabecula is 0.45 pounds. Thus, buckling of such a trabecula is to be considered. Any trabecula with a stress resultant greater than 6.0 lb/in compression is a candidate for buckling. The bending moments in the trabecula are such that (see Figure 52) the trabecula is deformed into a S. This tends to cause a mode of buckling different from that predicted by eq. (21). The fixity factor (coefficient of $\frac{\pi^2 EI}{l^2}$) in equation (21) varies typically from 1/4 to a maximum of 4 for different configurations of the plates.¹¹⁸ The calculations in this section for a fixity factor of 4 can thus be regarded as an upper limit for the critical load for any geometry encountered.

Other Considerations

Additional types of stress concentrators present in trabecular bone could be of importance. The canaliculi, lacunae, and the lamellar structures (Section II) are all present in the sheets of bone. The canaliculi and lacunae are so small and localized, in that they do not extend all the way through the sheet of bone, that they would probably be of less importance. Lamellae that end inside the structure could cause obvious problems at their points of termination, depending on the mechanical properties of the interfaces between the lamellae. These interfaces, however, could provide effective barriers to crack propagation, whether they were fatigue or Griffith type.

It must be remembered that the model was only loaded with a stress roughly equivalent to static body weight. It is to be expected that, during walking or running, the peak stresses developed will be several times this value.¹¹⁹ Therefore, the

results presented in this section must be interpreted as minimum calculations. If the stress on the subchondral plate is increased by a factor of four, buckling of some trabeculae would be expected. Furthermore, the stresses would be such that the ultimate strength would be exceeded in the outer-fibers of the trabeculae even without the presence of stress concentrators. This has great implication as far as fatigue life considerations are concerned (see Section VI). The possibility of buckling and fracture suggested for the static loading will become a probability during abnormal conditions of high stresses. The static stress of 100 psi applied to the model is well below the compressive strength of 500 - 1000 psi observed for cancellous bone as a whole. The possibility of collapse of trabeculae due to overall stresses in excess of 500 psi should be mentioned.

Conclusions

1. A model for trabecular bone has been developed that is good for exhibiting elastic properties under conditions of static body-weight loading. The elastic modulus of the model compares very well with measured modulus of 10^5 psi for trabecular bone.
2. Some areas of the trabecular bone in the weight-bearing area of the distal human femur are expected to show local variations of up to an order of magnitude in elastic modulus. In some places, upheavals in the subchondral plate are to be expected.
3. The membrane and bending stresses in the trabeculae are such that, in the presence of mild stress concentrators, such as

the holes in the trabeculae that allow intercommunication of the marrow spaces, the tensile and compressive strengths of the constituent material is exceeded. Fatigue fractures and Griffith-type fractures are thus a possibility.

4. Calculations of critical buckling load show that buckling is to be expected in some of the trabeculae.
5. The bending moments and buckling behavior support the hypothesis in Section IV that in certain types of trabecular bone (uniform trabecular bone, a description that the model fits) the elastic behavior is controlled by the buckling and bending of the sheets of bone that comprise the structure.
6. The role of the subchondral plate as a stress-transmitting and supporting structure is demonstrated. The moments and stresses in the subchondral plate are such that mild stress concentrators, such as circular holes (lacunae, canaliculi), are all that is necessary for local fracture initiation. Under abnormal stresses, no stress concentrators would be needed for local fracture.

VI. SPECULATIONS ON THE ETIOLOGY OF OSTEO-ARTHRITIS

Introduction

Osteoarthritis

Degenerative arthritis, osteoarthritis or arthrosis, is a disease of the joint that involves changes in the structure and properties of the cartilage and the underlying bone. Bony spurs often develop, as well as bone thickening (sclerosis) and cysts in zones of pressure. Total disintegration of the joint often results after years of suffering and misery. The joints most often affected by osteoarthritis are those that bear weight (hip, spine, knee) and the joints subjected to unrelenting muscle action and muscle compression (finger joints).¹²⁰

The degree of degeneration in a joint can be revealed by studying the chemical makeup of the cartilage in the weight-bearing area of the joint.¹²¹ One of the first detectable changes in the joint at the onset of osteoarthritis is loss of mucopolysaccharides (MPS) from the cartilage. Longitudinal sections stained with safranin red-0 and counterstained with methyl green show clearly and geographically the distribution of MPS in the cartilage. Normal cartilage (Group 0) exhibits MPS rather uniformly in the cartilage all the way to the surface. Early arthritic joints (Group I) show slight MPS loss from the surface. Moderately advanced arthritic joints (Group II) show moderate MPS loss and occasional cloning of the cartilage cells. Advanced arthritic joints (Group III) exhibit marked MPS loss associated with cartilage thinning, fibrillation, and frequent chondrocyte cloning.¹²²

The only work relating trabecular bone mechanical property changes to osteoarthritis¹²³ suggested that the stiffness of Group I is significantly higher than either Groups 0 or II. An additional conclusion that was dismissed as statistically insignificant was that the stiffness of Group III bone is higher than Groups 0 and II, but not as high as Group I. These measurements have been criticized because of the mode of deformation of the bone employed: dropping a weight on the bone plug to be measured.

The most recent hypothesis¹²⁴ for the etiology of osteoarthritis suggests that joints wear out by repetitive impulse loading. The coefficient of friction of the cartilage is so low that rubbing is not a possible mechanism for wear. The mechanism proposed for the process is that increased impulsive loading leads to Wolff's Law (see Section IV) stiffening of the trabecular bone underlying the cartilage. It is suggested that this remodeling occurs through the mechanism of microfracture. Since the components in the joint can be thought of as elastic elements in series, an increase in stiffness of one element implies higher peak forces in other elements. Thus, the stiffening of the trabecular bone causes the cartilage to receive more mechanical punishment and leads to cartilage degeneration. A similar proposal has been made by Frost¹²⁵, in a discussion of the effect of changes in the elasticity of the subchondral region on the function of the joint as a bearing.

Function of Trabecular Bone

This theory suggests the importance of trabecular bone as a

shock-absorber. This role is very likely, since trabecular bone is present in areas where such a function is important: the skull, vertebral bodies, condylar structures in the knee, and in the femoral head. The shock-absorbing abilities of trabecular bone were demonstrated as early as 1827 by simple experiments¹²⁶ involving the momentum transfer by collision of ivory balls. The momentum was seen to be almost completely absorbed if a trabecular bone ball was substituted for an ivory one. Articular cartilage has been shown not to absorb peak forces, but to transmit them to the soft tissues and bone.^{127,128} This in combination with the observation that the amount of trabecular bone present in the bones is much larger than the amount of cartilage shows that the trabecular bone functions as a shock-absorber in the joint, sparing the cartilage from mechanical punishment.

A treatment of the purely-elastic shock-absorber shows that the important criteria for shock-absorption are prescribed stiffness and capability of experiencing a specified maximum deflection.¹²⁹ The helical spring is widely used as a shock-absorber because of its capability of experiencing a relatively large deflection while limiting the stress to a safe magnitude. The deflection seems to be the most important criterion for shock-absorption. Damping, on the other hand, serves to dissipate energy from a vibrating structure.¹³⁰

It is evident that the shock-absorbing characteristics of the human joint can be broken into two parts: (1) The elastic part corresponding to the trabecular bone, which serves to limit peak stresses, and (2) the damping part provided by the soft

periarticular tissues, which serve as regions of energy dissipation in close proximity to the joint.

Usually the trabecular bone acts as an elastic shock-absorber. However, if the gross compressive strength (500 - 1000 psi) of the trabecular bone is exceeded by a peak force, massive collapse will occur. In this case, to spare the cartilage and long bones, the impact energy is absorbed by fracture. Collapse would only occur in the weight-bearing region, and would probably not extend very deeply into the subchondral region, because of the functioning of the joint as a variable surface bearing. The weight-bearing area would simply increase due to trabecular collapse until the load is supported.¹³¹

Fracture in Bone

There have been some recent experiments done by Swanson, Day and Freeman¹³² to investigate the pathogenesis of the bony spur formation in osteoarthritis. The first step in the formation of these osteophytes is the vascularisation of the normally avascular cartilage,¹³³ the blood vessels entering either through the synovial membrane or the subchondral plate. The experiments were designed to examine the possibility that vessels enter the cartilage through mechanically-induced defects in the subchondral plate such as microfractures, around the margins of the articular surface of the femoral head. The results are relevant to the present work not because of their applicability to fracture at the periphery of the cartilage surface, but because of the possibility of fracture in the weight-bearing area,

which the authors do not discuss. They also calculated the fatigue life of cortical bone subjected to zero minimum stress (as opposed to zero mean stress) of roughly 10^3 cycles at a maximum stress of 11,700 psi to 10^7 cycles at a maximum stress of 8,750 psi (Figure 58). The measured stresses at the margin of the articular cartilage were such that, considering the natural turnover rate of bone, fatigue fracture would not occur.

It is difficult to understand why Swanson, Day, and Freeman made no reference to the work on fatigue fractures by Blickenstaff and Morris.¹³⁴ The general characteristics of fatigue fractures observed by them clinically are as follows:

- (1) Generally, involvement of the shaft of a long bone.
- (2) Onset without violence.
- (3) Frequently, association with prolonged muscle effort.
- (4) Except occasionally in a metatarsal or rib, absence of any audible snap or of any suspicion by the patient that fracture has occurred.
- (5) Usually, pain as the outstanding symptom.
- (6) Liberal formation of callus and its subsequent development into mature bone.
- (7) Presence of variable degrees of accumulated fluid in the tissue spaces.

The suggestion is also made that the affected bone may have some defect in crystalline structure, trabecular orientation, or ground substance.¹³⁵

The effects of stress on bone are well known and may be generally characterized by Wolff's Law (Section IV). Disuse or

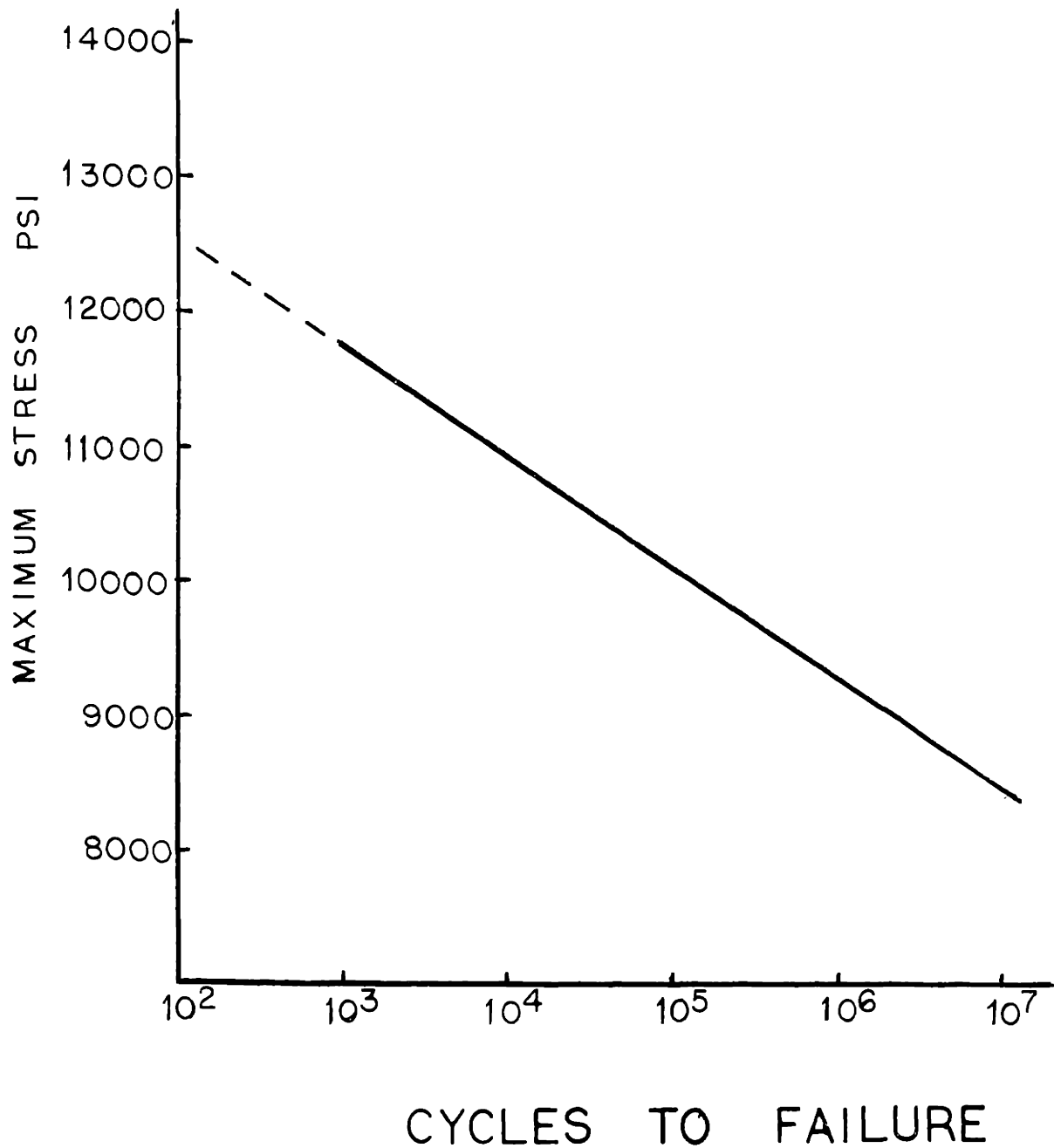


Figure 58: Maximum stress versus cycles to failure for cortical bone. Adapted from Swanson, Freeman, and Day.¹³²

immobilization results in rapid osteoclastic resorption and decreased osteoblastic activity. Overuse, as in the case of fatigue fractures, leads initially to the resorption of bone. This is the so-called "law of Weinmann and Sicher"¹³⁶ which states that "increase of pressure or tension beyond the limits of tolerance leads to the destruction of bone by resorption." Increase in stresses within the tolerance limit leads to apposition of bone and consequent strengthening.

A study¹³⁷ performed on 30 patients with fatigue fractures in the thin posteromedial region of the tibial cortex approximately 10 to 12 cm below the tibial plateau revealed a partial disorganization (unraveling) of the collagen lamellar structure due to stress on the bone and resulting elastic deformation and recoil. These fractures occurred just beyond the last of the internal bracing supplied by the metaphyseal cancellous bone. This area is completely osteonal in adults but consists of circumferential lamellar bone in teenagers. The remodelling from lamellar to osteonal bone occurs between the ages of 18 and 28 years. Because the lesion developed within the lamellar cortex, the suggestion is made that fatigue fracture may represent an acceleration of the normal internal remodelling of circumferential lamellar bone to adult osteonized bone.¹³⁸

In summary, fatigue fracture, as characterized by Blickenstaff, begins with excessive elastic deformation. Subsequent local resorption of bone is followed by callus formation. In these unsupported osteoporotic areas, if the mechanical stress is too great, a gross fracture occurs.

Fatigue fractures have been observed 1 to 2 cm below the articular surface of the medial tibial plateau.¹³⁹ The same types of fractures have been diagnosed in the femoral neck, very close to the margin of the articular cartilage, in patients from 20 years to over 60 years of age.¹⁴⁰ These were gross fractures all the way through the femoral neck.

Measurements of the work of static crack propagation in cortical bone have been made by Piekarski.¹⁴¹ The work of fracture (area under the stress-strain curve) was equated to the surface energy of the crack. This is not an equality. It is known that, when a crack propagates, elastic energy is reduced in the area of the crack, and this contribution goes to surface energy in addition to the work done by the machine. Thus, the true values of the surface energy should be higher than the fracture work as measured by Piekarski. Nevertheless, using Piekarski's data, one calculates typical values of the work for slow propagation of the crack of 60 kg-cm/cm^2 . If the Griffith crack theory (Section V) were applied, a critical crack length of 76.5 mm is necessary for propagation. The Griffith theory therefore does not apply because the critical crack length is impossibly large, and this is confirmation of the microscopic indications that the slowly-propagating fracture is essentially a mechanism of pullout of fibers from the organic matrix and not a Griffith-type brittle fracture mode. This pullout is typical behavior of a fiber-reinforced composite material. For fast catastrophic crack propagation, γ is about 1 kg-cm/cm^2 and C is 1.3 mm. Defects of this size exist in trabecular bone, but not in cortical bone.

Additional observations made by Piekarski were the following:

- (1) The fracture tends to avoid Haversian canals and follows the interlamellar interfaces and cementing lines.
- (2) Blood vessels, canaliculi, and lacunae can act as crack arrestors by blunting the tip of the crack which enters them.
- (3) Non-critical cracks may nucleate at the tips of voids such as canaliculi and lacunae, in addition to the critical crack that is propagating.

Piekarski made no comments as to the behavior of the observed non-critical cracks in a fatigue situation.

Experimental Procedure

The sections of cartilage that were machined from the weight-bearing area of the medial femoral condyles of the twenty patients in Section IV were fixed in neutral buffered formalin. They were decalcified in a solution of 25% buffered formic acid, and longitudinally sectioned. The thin sections were stained with safranin red-0 and counterstained with methyl green and examined for degree of degeneracy (Groups 0, I, II, and III). The relative stiffness data from Section IV was used to see if any correlation existed between stiffness and degree of degeneracy.

The autopsy reports, charts, and case histories of the twenty patients were obtained and the specifics that might relate to arthritis and mechanical behavior of bone (occupation, body weight, age, muscular activity) were noted and recorded systematically.

Metallographic sections of the trabecular bone from the rabbits and humans in Section IV were studied to determine if any

significant microstructural changes could be related to the etiology of arthritis. In particular, areas of resorption, callus formation, microfracture, trabecular thickening, and unusual formations of trabeculae were noted.

Results and Discussion

Mechanical and Structural Changes with Osteoarthritis

Table 7 summarizes the case histories of the twenty patients used in this study. The age and height are for time of death. The weight is the normal weight of the patient prior to death. The causes of death indicated should have no effect on the mechanical properties and structure of the bone in the legs, or on the degree of degeneracy of the joint as given in Table 8. Occupation, age, and body weight are seen to have no effect on the degeneracy of the joint, if the data in Tables 7 and 8 are compared. Of course, the occupation does not generally indicate the level of activity in which a person engages in his leisure time. The level and type of activity should have an effect on the joint degeneracy, but, unfortunately, these data were not available.

If the relative stiffness data for the trabecular bone is plotted for each group of degeneracy (0, I, II, III) as in Figure 59, it is evident that the stiffness of Group I is the highest, Group III next, and Groups 0 and II the lowest. This is the same conclusion as was reached in the original study by Radin, Paul, and Tolkoff.¹⁴² The hypothesis that subchondral bone stiffening occurs in early arthritic joints is supported.

Figure 60 shows the relative stiffness as a function of

TABLE 7

CASE HISTORIES OF PATIENTS IN STUDY

<u>I.D.</u>	<u>CAUSE OF DEATH</u>	<u>AGE</u>	<u>HEIGHT</u>	<u>OCCUPATION</u>	<u>DESCRIPTION</u>	<u>WEIGHT</u>
1	Coronary thrombosis	65	5'9"	Unemployed	Obese	198
2	Cerebral embolism	30	6'2"	Mason	Mildly wasted	135
3	Gastro-intestinal hemorrhage	62	5'6"			139
4	Carcinoma of pancreas	39	5'11"		Thin, 25 yr. illness	128
5	Pneumonia	59	5'9"	Truck driver, maintenance worker		175
7	Marfan's syndrome	20	6'3"		Well, nourished; well, developed	173
9	Sepsis	66	5'7"		Slightly obese; well-developed	196
10	Staph Septicemia	41	5'9"		Well-developed	204
11	Marfan's syndrome	27	6'2"	Student-fine arts	Healthy	172
12	Arteriosclerotic heart disease	57	5'9"		Well-developed; sweaty	190
13	Acute myocardial infarction	45	5'6"	Truck driver	Well-developed	
14	Arteriosclerosis	54	5'7"			167
15	Carcinoma of stomach	44	5'7"	University teacher		

TABLE 7 (continued)

CASE HISTORIES OF PATIENTS IN STUDY

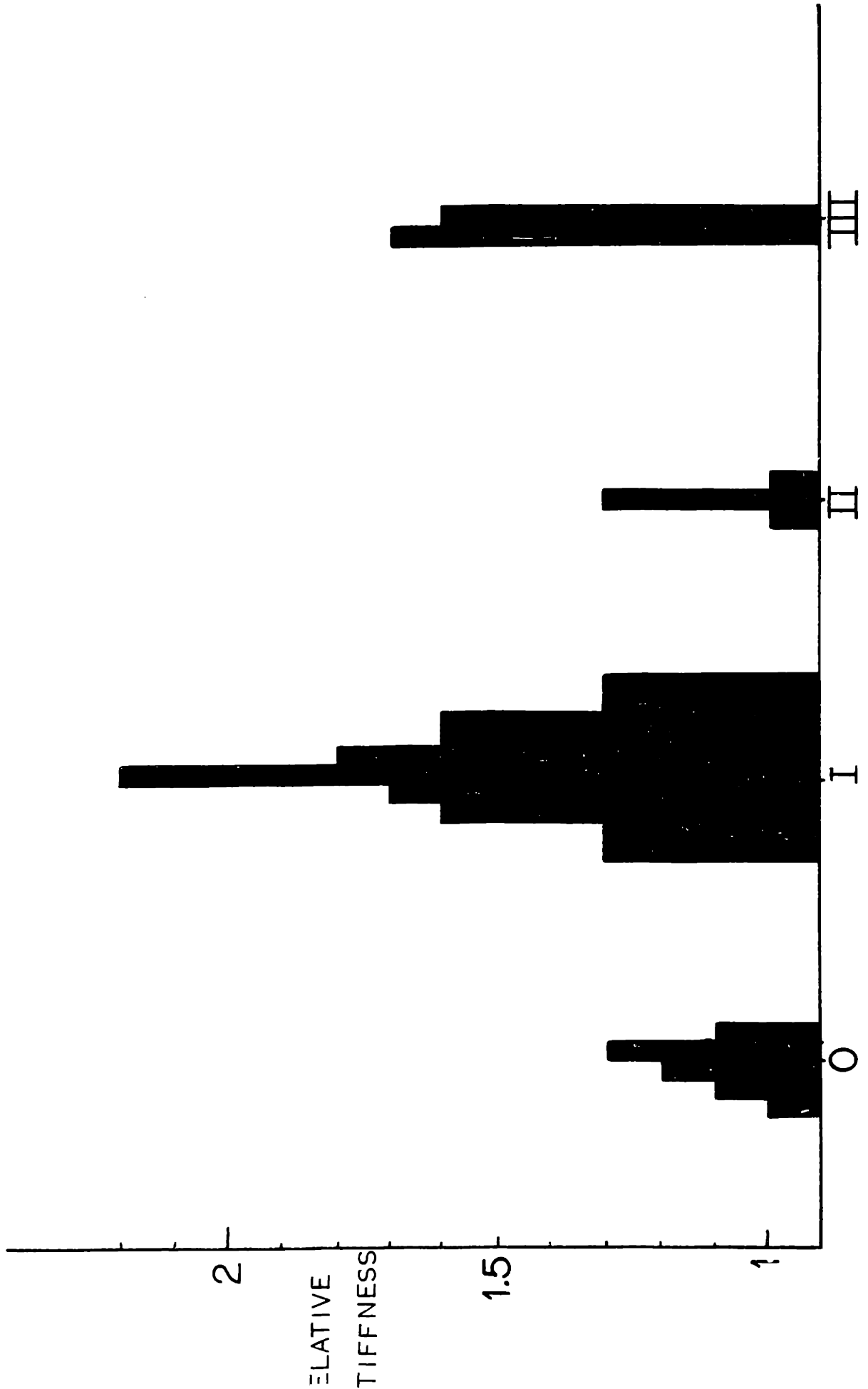
<u>I.D.</u>	<u>CAUSE OF DEATH</u>	<u>AGE</u>	<u>HEIGHT</u>	<u>OCCUPATION</u>	<u>DESCRIPTION</u>	<u>WEIGHT</u>
16	Intracerebral hematoma	44	5'7"	Electronics assembler		179
17	Astrocytoma	53	5'11"	Unemployed machine designer		155
18	Staph pneumonia	43	5'7"	Control engineer	Obese	203
19	Pneumonia	44	6'3"	Business - MBA	Alcoholic	215
20	Acute bacterial endocarditis	53	5'3"	Musician	Thin, chronically ill	150
21	Carcinoma of Esophagus	50	5'7"	Production line worker		145
22	Aortic aneurism	35	6'5"	Laborer, hustler	Well-developed	193

TABLE 8

RELATIVE STIFFNESS, DEGENERACY OF JOINT,
AND MICROSTRUCTURE FOR PATIENTS USED IN STUDY

<u>I.D.</u>	<u>RELATIVE STIFFNESS</u>	<u>GROUP</u>	<u>MICROSTRUCTURE</u> (Uniform or Non-uniform)
1	1.0	II	U
2	1.1	0	N
3	1.3	II	N
4	2.2	I	U
5	1.7	I	U
7	1.2	0	U
9	1.0	0	U
10	1.3	0	U
11	1.6	I	U
12	1.3	I	N
13	1.3	I	U
14	1.8	I	U
15	1.3	I	N
16	1.6	I	N
17	1.7	III	N
18	1.6	I	N
19	1.1	0	U
20	1.3	I	N
21	1.0	II	N
22	1.6	III	N

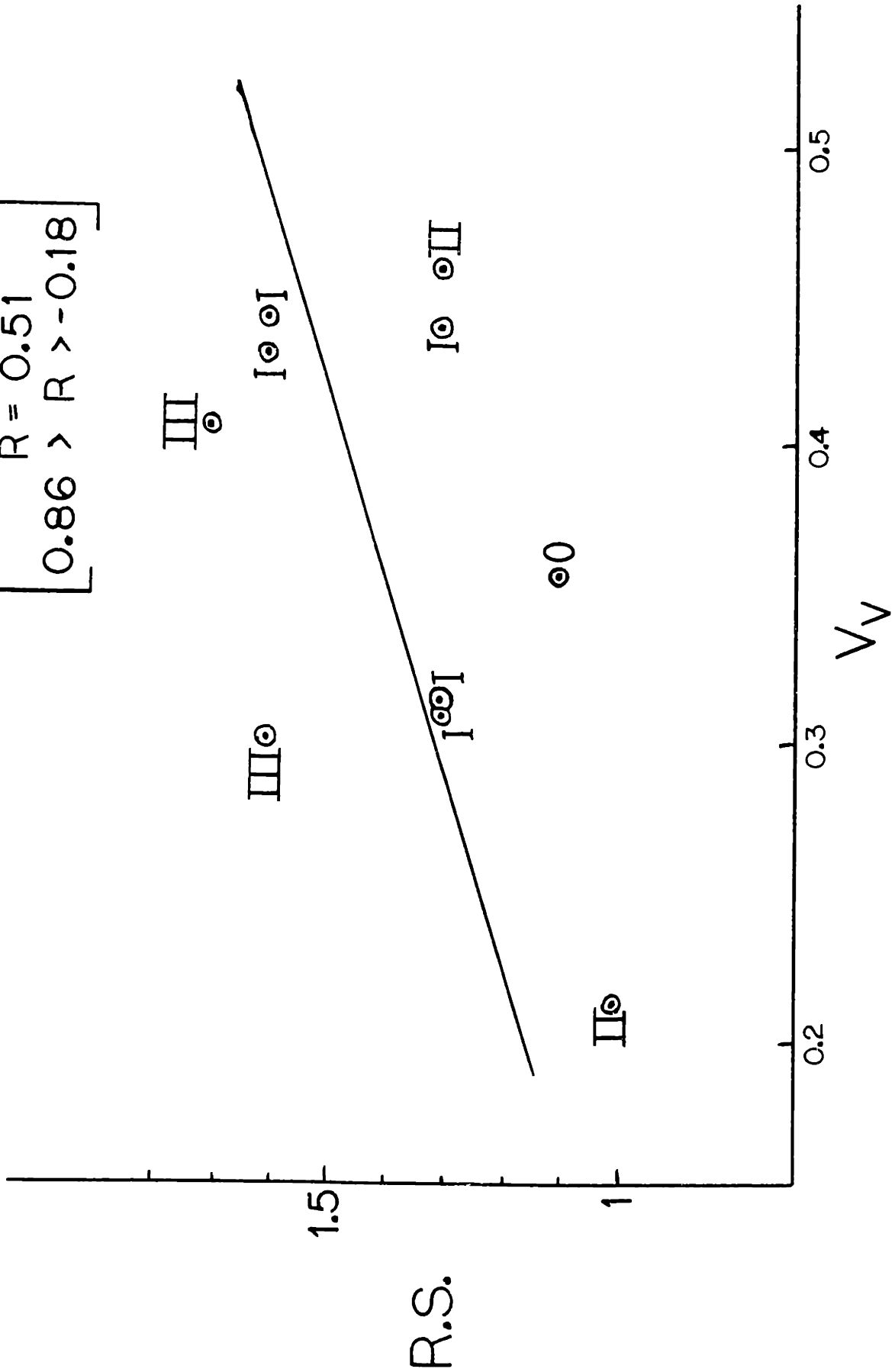
Figure 59: Relative stiffness for each sample grouped according to degree of joint degeneracy. Most of the samples were in Groups 0 and I; only 3 and 2 samples fell into Groups II and III, respectively.



ARTHRTIS GROUP

Figure 60: Relative stiffness versus volume fraction bone for human samples with non-uniform microstructure. Most of these are Groups I, II, and III. The line is a least-square regression. The correlation coefficient R and the 95% confidence limits for R are indicated.

$R = 0.51$
 $[0.86 > R > -0.18]$



volume fraction bone for the set of samples with nonuniform trabecular bone (see Section IV). The degeneracy group is indicated beside each data point. Group III's are stiffest, then Group Group I, and Groups 0 and II lowest. Figure 61 shows the relative stiffness versus contiguity of the holes between the trabeculae for the uniform set of samples. Group I's are highest, Group 0's lowest. Although the correlation of properties to structure is good (as discussed in Section IV), these plots are not very revealing concerning the effect of arthritis. However, there are definitely more 0's and I's in the uniform set and more I, II, III's in the non-uniform set.

If all the points are plotted as relative stiffness versus the ratio V_V/C_H , (Figure 62), the points for the same groups fall closer together than in the plots of R.S. versus other micro-structural quantities. The Group I's with high R.S. are clustered about medium and high values of V_V/C_H ; Group 0's and II's are low on the curve, both in V_V/C_H and R.S. The two points for Group III's are very close together and indicate rather high stiffness and low V_V/C_H . It is easy to draw fields (Figure 63) to indicate regions in the plot where data points for the four groups fall. Such a plot might be useful in predicting the degeneracy of a joint from measurement of R.S., V_V , and C_H . This plot does not imply a relationship between R.S. and V_V/C_H . The data points in Figure 62 show little correlation.

Proposed Etiology for Osteoarthritis

A characterization of bone changes in the development of osteoarthritis is therefore proposed as follows:

Figure 61: Relative stiffness versus contiguity of holes for human samples with uniform microstructure. These are predominately Group 0 and 1. The line is a least-square regression. The correlation coefficient R and the 95% confidence limits for R are indicated.

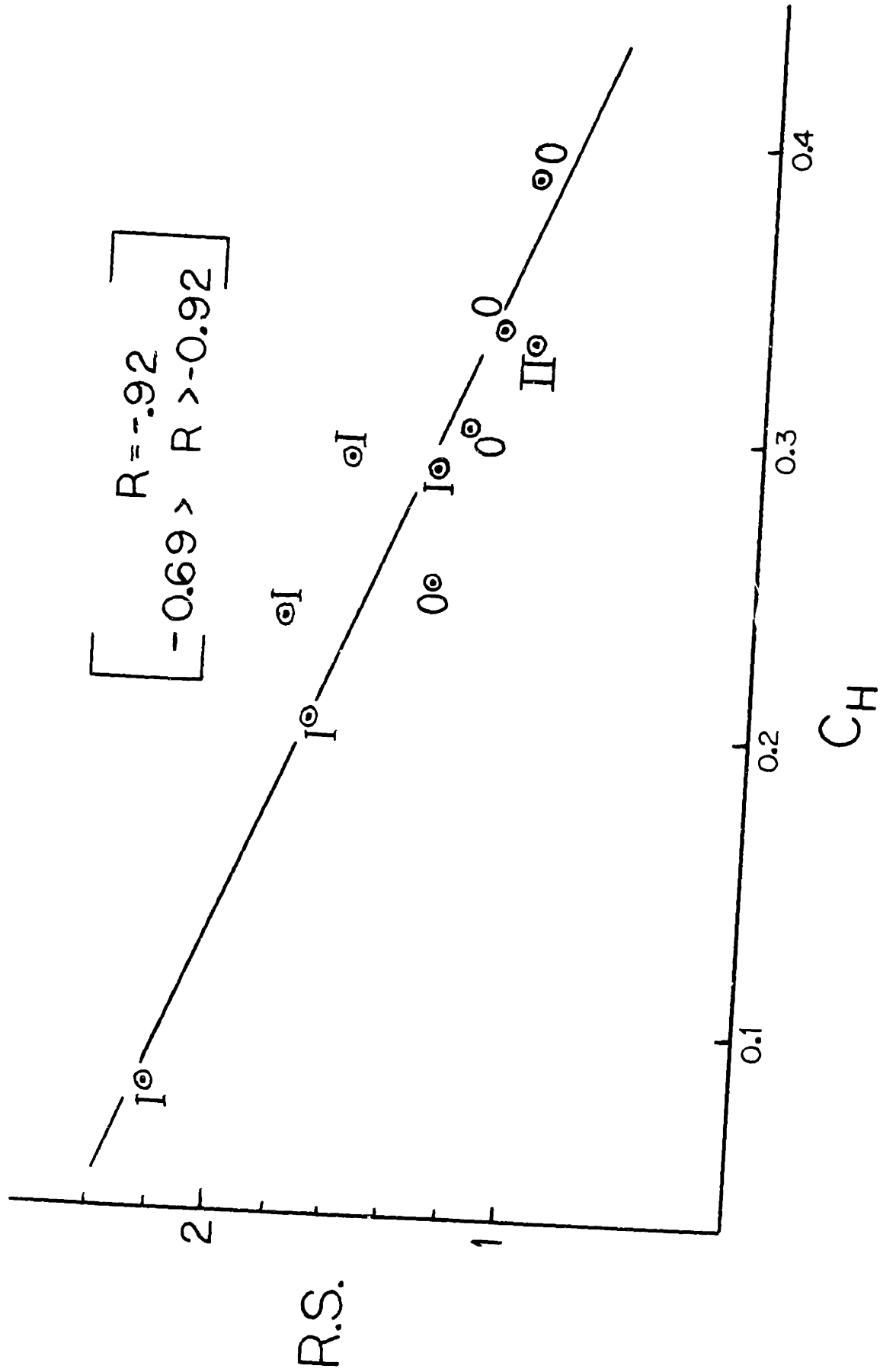
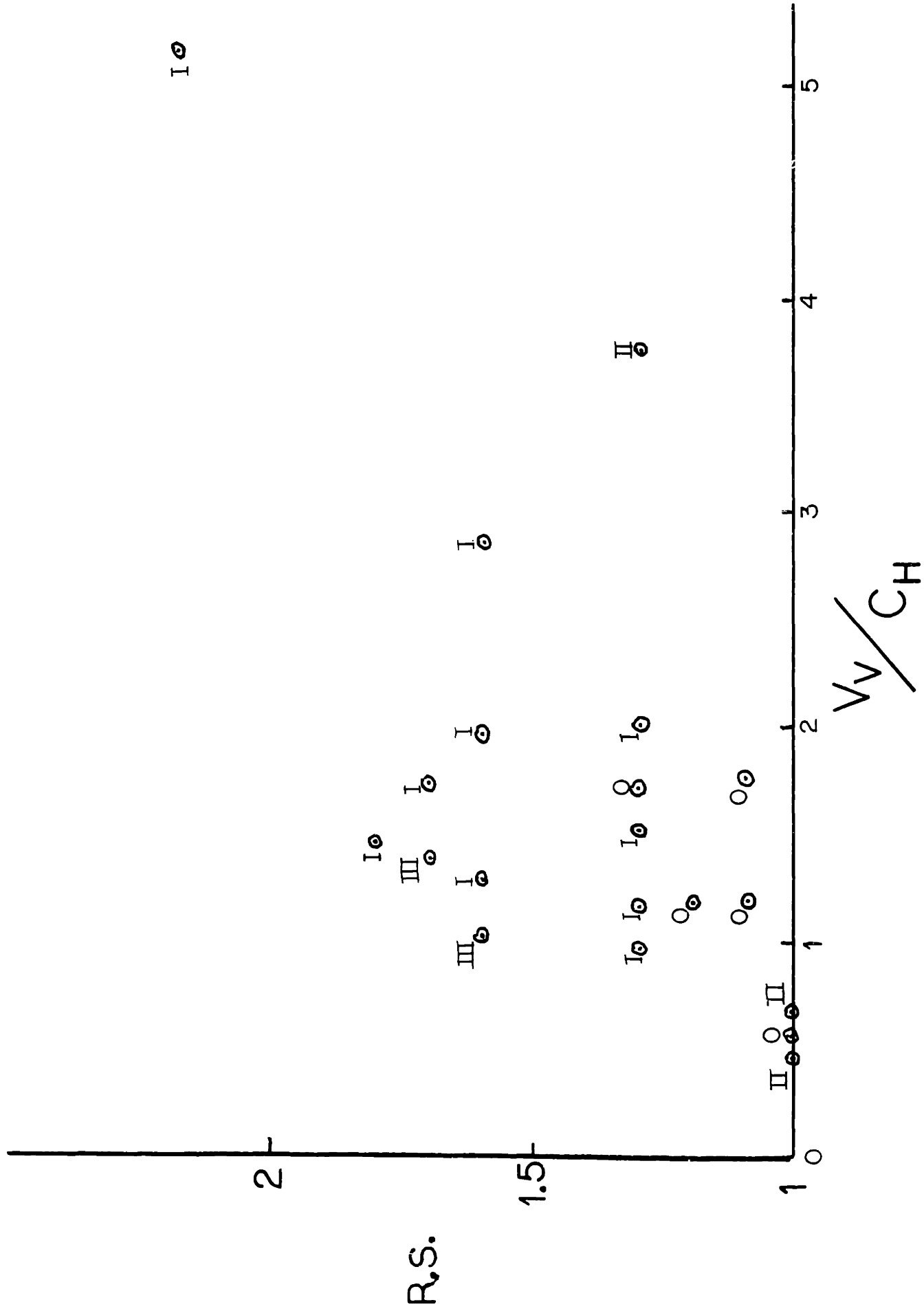


Figure 62: Relative stiffness versus $V_{\text{Bone/Choles}}$ for human trabecular bone. Notice how the points for each group tend to fall close to each other.



I

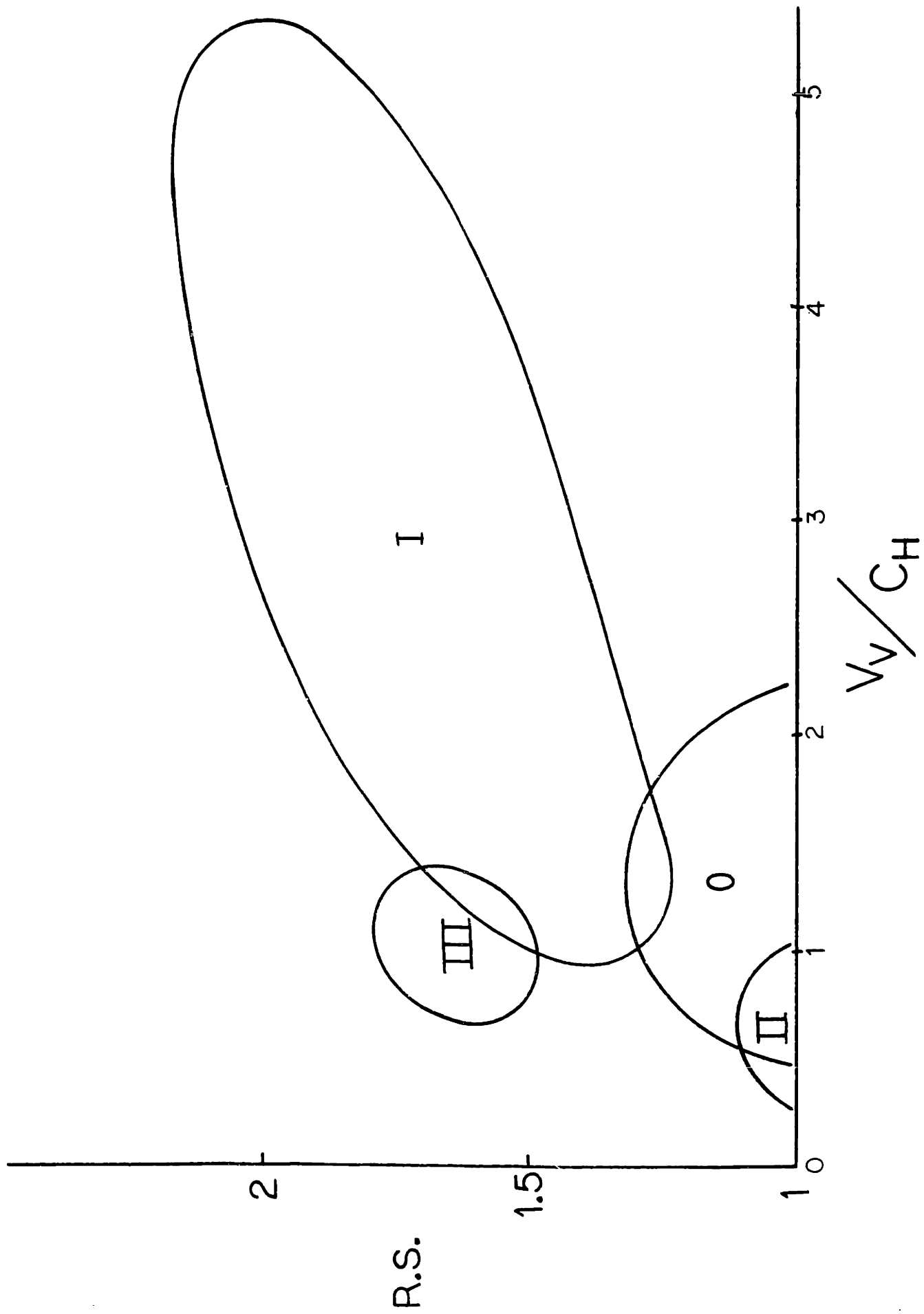
II

II

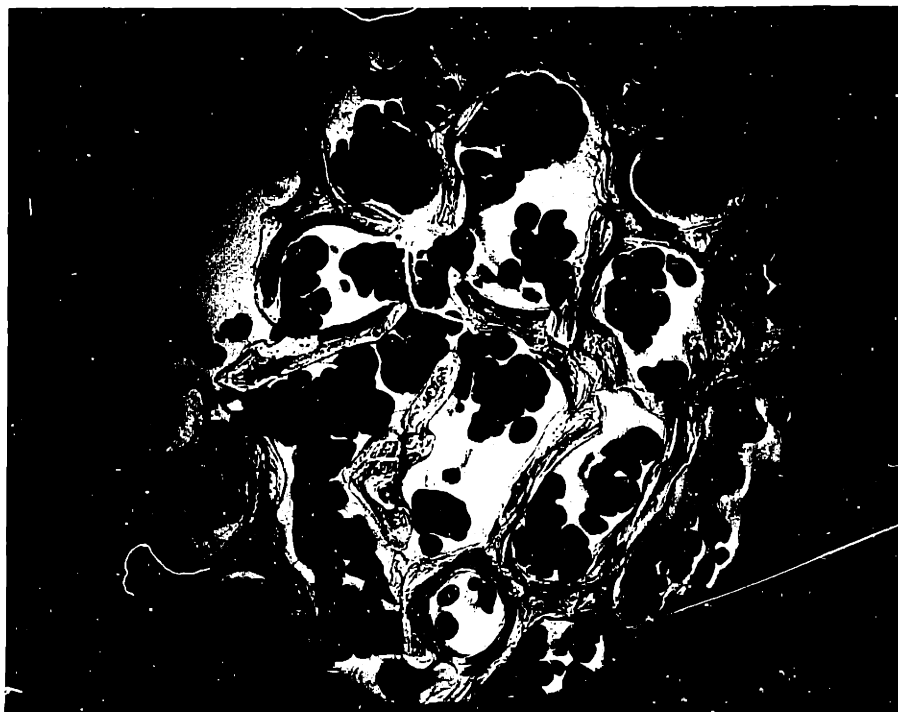
R.S.

V_w/C_H

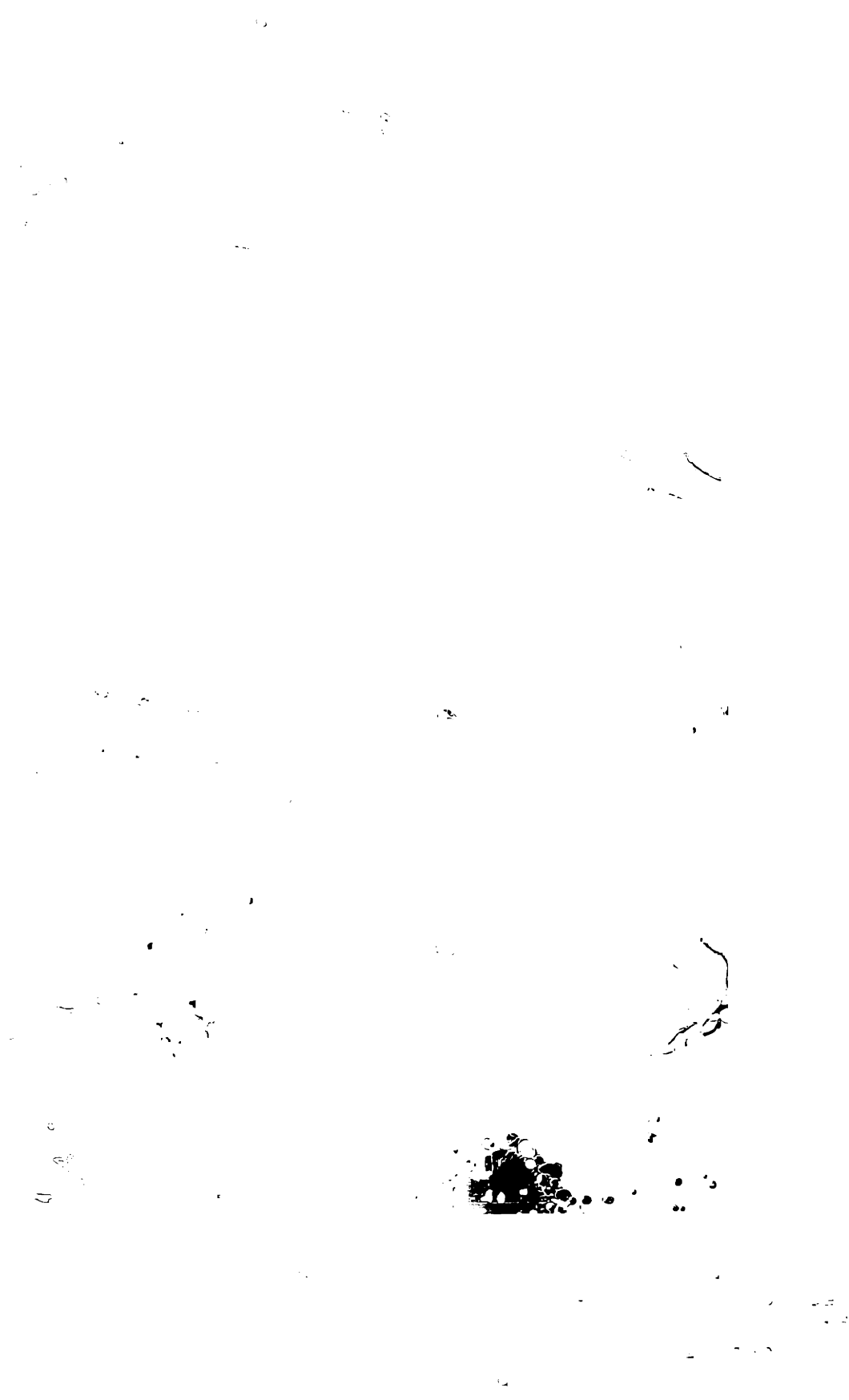
Figure 63: Relative stiffness versus $V_{\text{Bone}}/C_{\text{Holes}}$.
Data from Figure 62 grouped schematically to
to indicate possible arthritic trends.

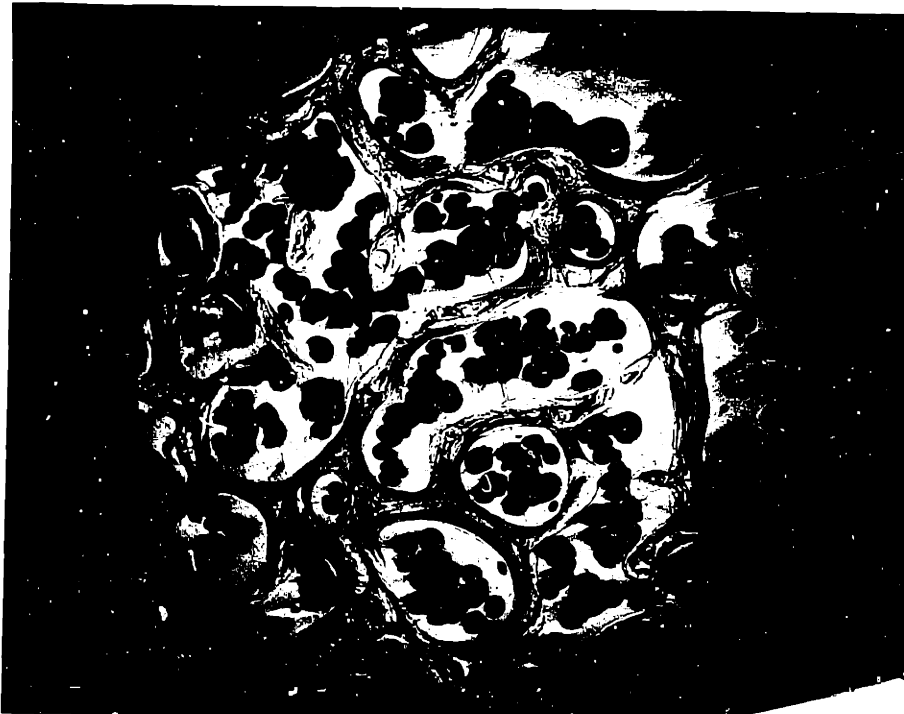
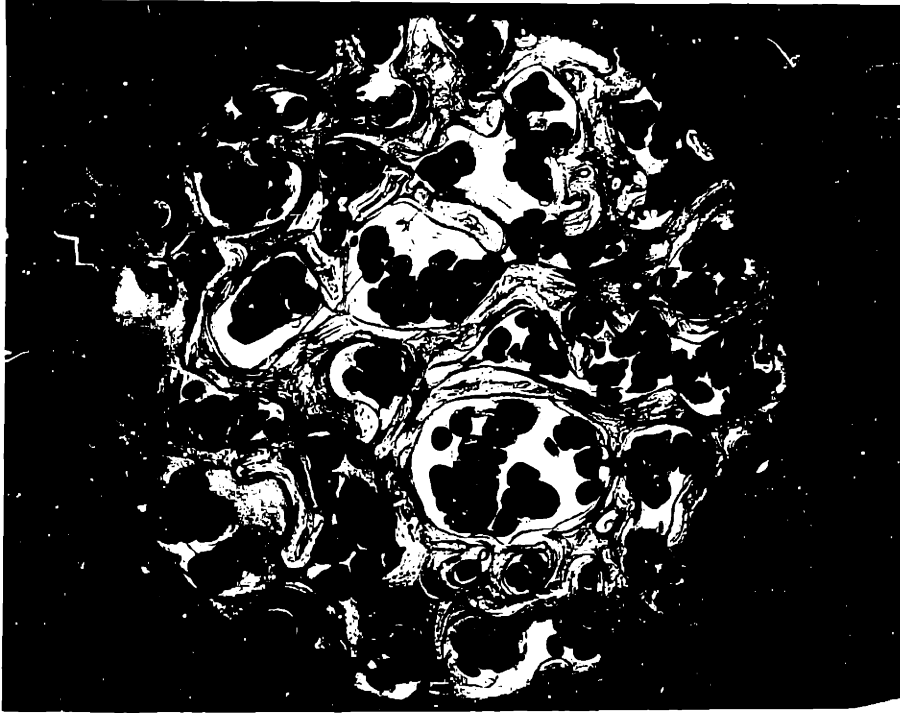


1. Normal and early arthritic joints contain trabecular bone in which the stiffness is controlled by the contiguity of open spaces between trabeculae, C_H .
2. The early arthritic bone (Group I) is significantly stiffer than the normal bone.
3. The change from Group 0 to Group I is effected by the formation of a network of trabeculae which results in lower C_H . This is a natural consequence of Wolff's law: the trabeculae are shown to deform elastically in a bending mode (Section IV, V). Increased impulsive loading within the limit of tolerance, as suggested in the introduction, tends to cause the bone to stiffen to resist this compression. The best way for it to strengthen is to build up supports perpendicular to the sheets of bone that are bending. Thus, the value of C_H decreases and the R.S. goes up. Typical microstructures from four different patients showing osteoid growing perpendicular to the pre-existing trabeculae so as to wall-off the open spaces are given in Figures 64A through 65B.
4. The transition from Group I to II occurs with the microstructure changing into non-uniformity, with large patches of dense bone growing in the structure (Figure 66). These persist into Group III. Resorption is noted in many places in the trabeculae (Figures 67A,B). The stiffness decreases are due to resorption and lowered V_V in Group II.



Figures 64A,B: Typical microstructures of Group 0 and Group I bone respectively. Transverse sections. Notice that the C_H is lower for Group I than 0. Osteoid is seen to be growing so as to stabilize the trabeculae against buckling deformation. 28X





Figures 65A,B: Typical microstructures of Group I bone. Transverse sections. Notice the osteoid growth. From two different patients. 28X



... of bone ...
osteoid ground.



The patch of G.
...ing in
...ion.

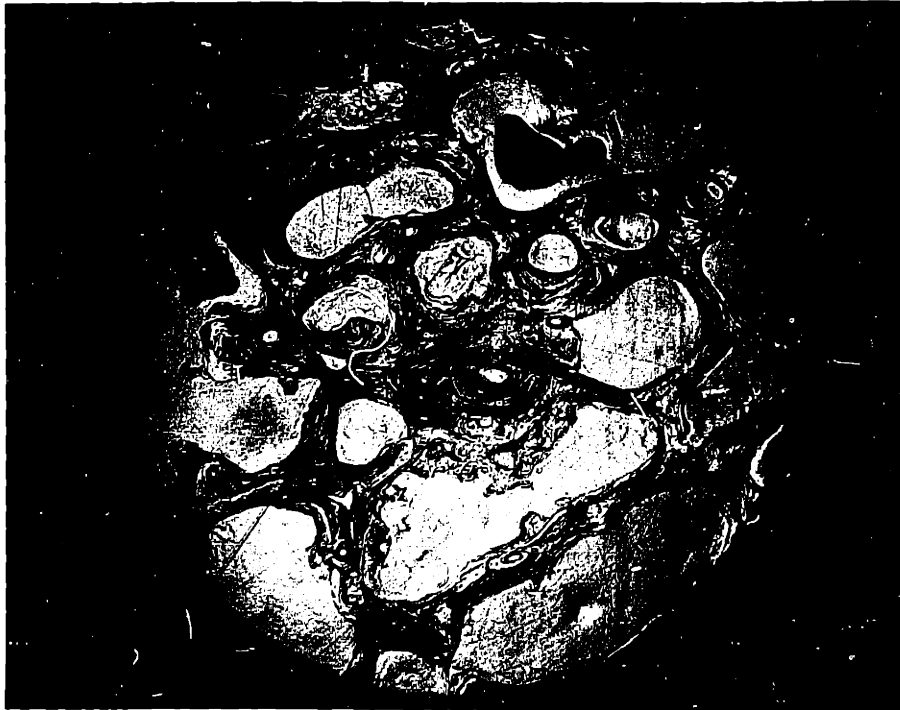
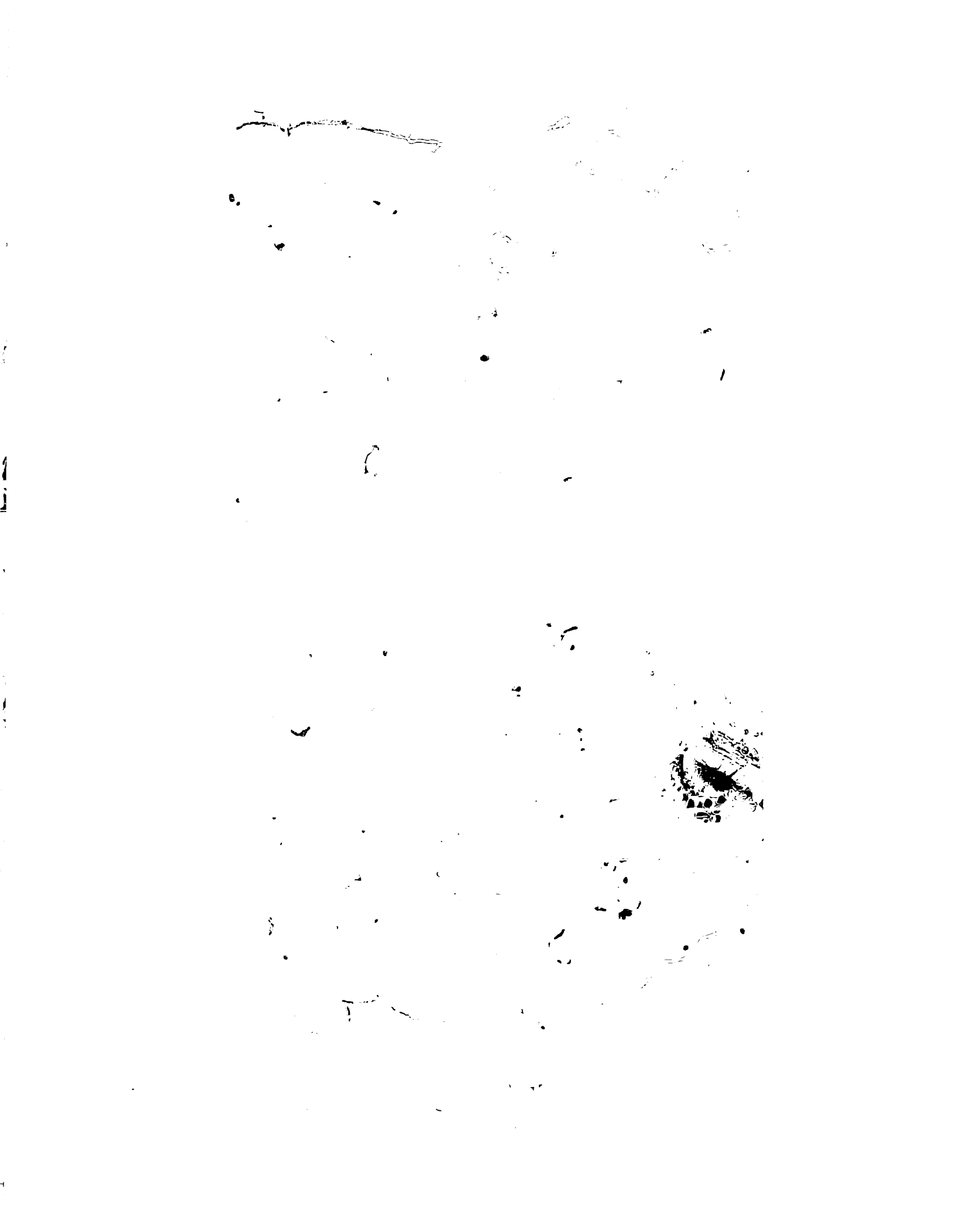


Figure 66: Large patch of dense bone in a sample presumably undergoing transition from Group I to II. Transverse section. 28X



Figures 67A,B: Resorption areas in Group II bone. Transverse section. Resorption appears as scalloped out areas in the trabeculae. 110X



5. Group III bone seems to be necrotic, with regions of osteoid forming and regions of resorption (Figure 68). The new bone growth accounts for the slight increase in stiffness of the Group III's. Although the microstructure is classified as non-uniform, the structure nevertheless resembles in many ways the transition from Group 0 to Group I. There are probably V_V and C_H dependence in this group, as evidenced by the closeness of the two points in Figure 62 for the plot of R.S. versus V_V/C_H . These points were brought significantly closer than they were either in R.S. vs. C_H or R.S. vs. V_V .

Feedback Mechanism for Initial Degeneration

The postulate of a feedback mechanism for the degeneration of the joint is made on the basis of the above five observations. The cartilage probably begins slight MPS loss due to repeated impulse loading. As shown in the model in Section V, the trabecular bone is often very stiff locally, and may even upheave under compressive stresses. The formation of the dense patches of bone in Figure 66 are regions of high stiffness. If the impulsive loading of the joint is continued, the cartilage just above this region naturally receives more punishment and compression than cartilage just adjacent to this area, because of the local variation in shock-absorbing properties. Therefore, the MPS loss is accelerated locally, and a lesion develops. (This has been observed in thin longitudinal sections of cartilage.) This merely aggravates the problem, because, as the cartilage



Figure 68: Typical Group III bone. Transverse section. Notice the resorption areas and osteoid growth. The general appearance of the older bone is different from that in Group 0, I, and II bone, indicating that it is probably necrotic. 19X



I bone. Transverse section showing resorption areas and the appearance of the trabeculae that in Group I it is profuse.

degenerates, the Wolff's law reaction of the bone accelerates. The cartilage degenerates locally at the same time as the bone stiffens locally. This happens in the transition from Group I to Group II. Thus, the initial process leading to joint degeneration is a coupling of local changes in the cartilage and in the subchondral bone immediately underneath. This initial local destruction of the arches of collagen in the cartilage paves the way for massive disintegration in later development of the disease.

Subsequent Changes

The mechanical integrity of the joint has been impaired by the above process. The stresses change, and pain in the joint is noted. This probably leads to reduced physical activity of the patient, and resulting resorption of bone due to disuse. During this period of reduced activity, the bone continues to change and the cartilage degeneration continues, even under low applied stresses. A reasonable alternative to this is the possibility that resorption occurs because the changed geometry of the trabecular bone causes changes in stresses beneath the subchondral plate and the law of Weinmann and Sicher is invoked. If the patient indulges in normal activity, fracture in the cancellous region may occur due to the resorption and reduced mechanical integrity of the joint. Disruption of vascularity results, with bone death, and subsequent osteoclastic-osteoblastic remodelling. Trueta has discussed these possibilities.¹⁴³

Bone death is indeed observed in Group III, and therefore, normal remodelling accounts for the changes in this stage of osteoarthritis, when the Group III bone begins its resorption and

apposition. The sequence of mechanical and structural changes in the bone and cartilage are self-consistent and a very natural process of remodelling, the response of the joint to its initial mechanical disruption. The proposed etiology is summarized in Table 9.

Remodelling

Exactly how does this remodelling occur? In all probability, the normal osteoclastic-osteoblastic remodelling accounts for a part of it. However, certain trabeculae in rabbits and humans have been seen to fracture and remodel, as in Figures 69 - 72. As discussed in Section V, if a trabecula is oriented unfavorably under an applied stress, it will break. If the ends of the fracture do not meet, the trabecula will be under no stress, and resorption occurs to remove the trabecula. If the ends do meet so as to stress the trabecula, normal healing and callus formation begins, and the new trabecula thickens and grows in a slightly different orientation so as to best resist the applied stress. Thus, a mechanism of remodelling based on microfracture is appropriate, similar to the remodelling from lamellar to osteonal bone in the tibial cortex, by fatigue fracture. As the calculations on the idealized model show, the initial fracture of one trabecula can lead to overload of adjacent trabeculae. The law of Weinmann and Sicher says that these overloaded trabeculae will undergo resorption. It is possible that the areas of local fracture, i.e. incipient fatigue fractures, will undergo resorption rather than callus formation, leading to increased stresses in the smaller

TABLE 9

PROPOSED ETIOLOGY FOR OSTEOARTHRITIS

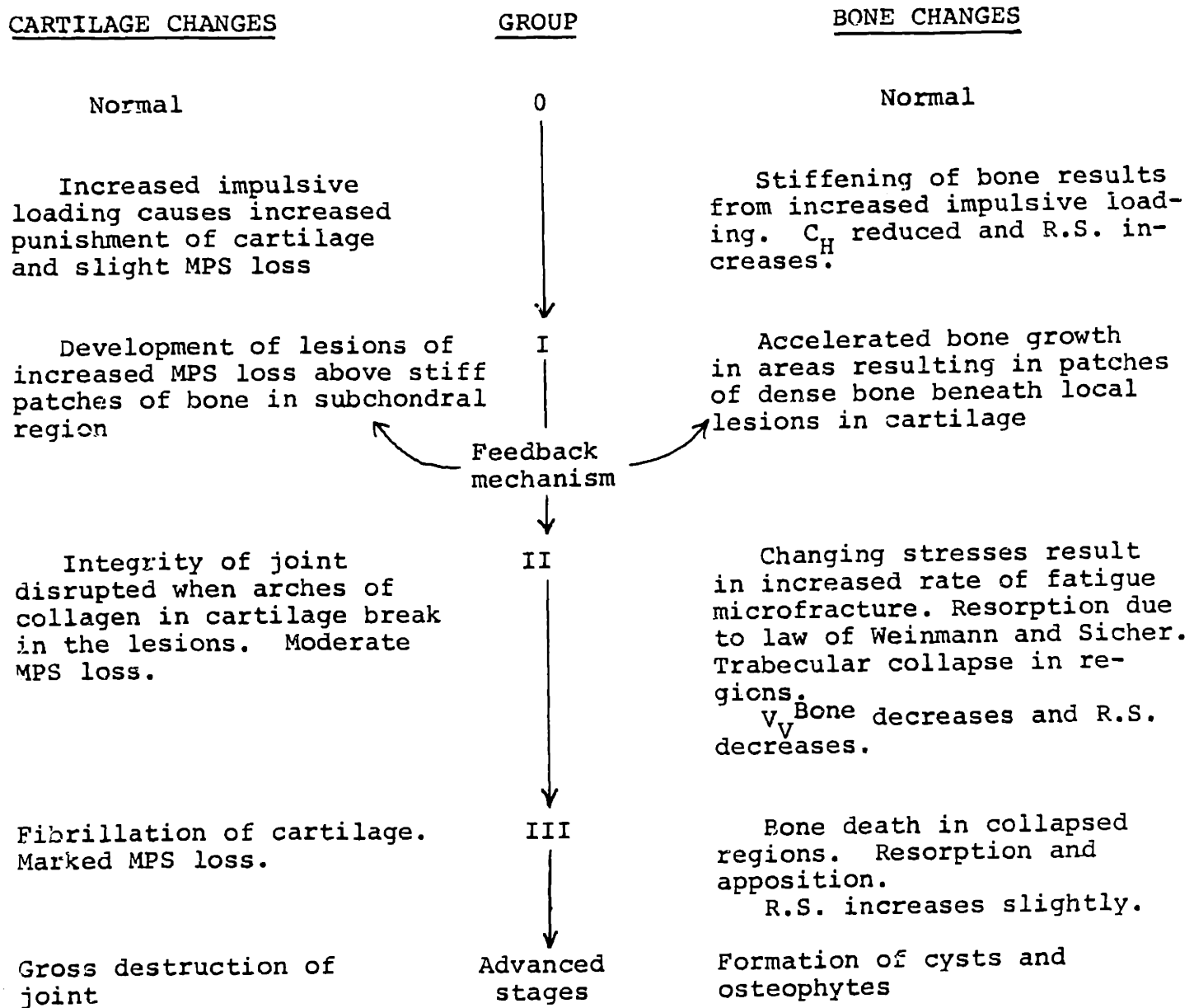
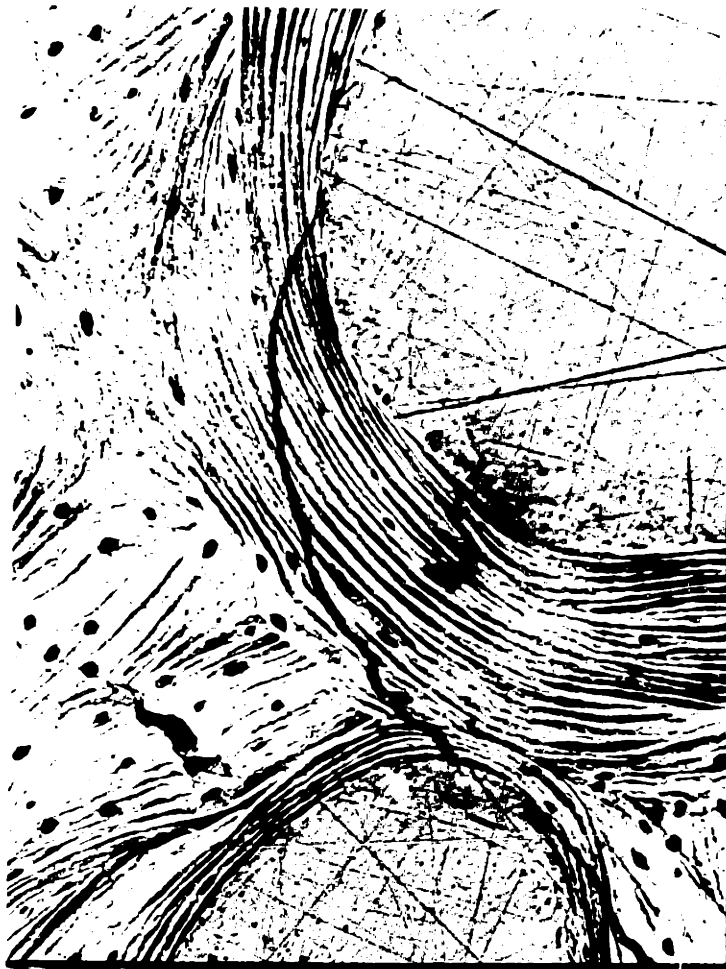


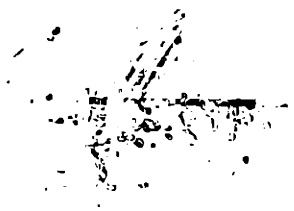
Figure 69: Fractured trabecula showing no callus formation. 240X

Figure 70: Site of probable fracture with extensive callus formation evident. 120X

Figure 71: Site of probable fracture after significant remodelling has occurred. Notice how patches of lamellar bone have been rearranged. 240X

Figure 72: Site of probable fracture after extensive remodelling. 120X





42011/11

11/11/11

amount of bone that is left.

Fracture of Trabeculae

How does the trabecula fracture? The possibilities as discussed in Section V and the introduction to this section include buckling, Griffith-type fracture, and fatigue. Buckling was shown to be a distinct possibility. Indeed, static compression tests on individual trabeculae¹⁴⁴ in which there were no macroscopic holes reveal that buckling occurs before the fracture point is reached. Thus, buckling contributes to the bending stresses necessary for fracture. Suffice it to be said that some trabeculae will fracture in a buckling mode, depending on the value of C_H . This probably a less important mode of fracture in intact trabecular bone.

Piekarski's work concerning Griffith fracture in bone showed that the stress concentrator necessary for slow-propagation is too large to be considered for cortical bone. This is also true for cancellous bone. However, in catastrophic propagation, the critical crack length is shown to be roughly 1.3 mm. This is often the size of the open spaces between the trabeculae and also the size of some holes observed in the sheets of bone that comprise the trabeculae. Thus, catastrophic crack formation is also a distinct possibility in trabecular bone.

Fatigue fracture, however, is most important. "A fatigue fracture always starts as a small crack which, under repeated applications of the stress, grows in size."¹⁴⁵ The results of Section V show that local yielding and fracture is to be expected around elliptical and circular defects in trabeculae. These stress-

concentrators exist in large numbers in normal bone. The Piekarski work rules out the possibility of a Griffith-mode of fracture for these concentrators. Therefore, fatigue considerations become important. The work of Morris and Blickenstaff has shown clinically that macroscopic fatigue-type fractures are exhibited in different regions of the body, notably the femoral neck and 1 to 2 cm below the articular surface of the tibial plateaus. These observations strongly suggest that the macroscopic fracture is preceded by microscopic fatigue fractures in the trabecular bone just beneath the plateaus. The cortex fractures in fatigue because the important supporting and shock-absorbing functions of the trabecular bone in the tibia are disrupted.

The stresses present in the trabeculae and the subchondral plate (Section V) are very similar to the stress levels reported in the fatigue tests on cortical bone by Swanson and Freeman. Thus, the fatigue behavior of trabecular bone should be similar to that for cortical bone. If anything, the fatigue life should be shorter for trabecular bone because higher stresses are developed during abnormal physical activity. It is expected therefore, that the trabeculae fatigue fracture before the cortex fractures.

From the computer model, stresses higher than 11,700 psi (fatigue life of 10^3 cycles) were observed in the presence of stress concentrators at static loads. Assuming a conservative increase of a factor of 2 in stress during walking, the stresses in trabeculae in the absence of stress concentrators exceed 11,700 psi. It should be emphasized that these calculated cyclic

stresses are for zero minimum stress. Extrapolating the data of Swanson and Freeman as shown in Figure 58, the expected fatigue life of a trabecula is less than 10^3 cycles. 10^6 cycles represent a year's walking, during which time incipient fatigue fractures would undoubtedly heal. Assuming a walking rate of 1/second, it would take roughly a twenty-minute walk to exceed the fatigue life of some of the trabeculae. Fatigue fracture during normal activity in selected areas of trabecular bone is therefore postulated.

Defects strikingly similar to fatigue cracks have been observed in human bone (Figure 73). Frost¹⁴⁰ has also observed fatigue-type fracture in human bone.

Remodelling in Normal Bone

It is suggested, in addition, that fatigue fracture occurs in trabecular bone in normal use, and that this is a normal mechanism of remodelling in the bone, as discussed above. A low level of constant fatigue fractures is physiologically tolerable, due to the constant turnover of bone. Many of the structural changes observed in the development of osteoarthritis could be related to an accelerated rate of fatigue fracture. The remodelling effects of fatigue fracture in the cortex of the tibia have already been shown by Johnson as discussed in the introduction. The work of Swanson and Freeman concerning fatigue fractures in subchondral bone suggests that fractures do not occur at the periphery of the cartilage. This author feels that if they had measured the stresses under the load, that fatigue fracture in the weight-bearing area is to be expected.



Figure 73: Possible fatigue cracks in human trabecular bone.
220X



Further Implications

The preceding discussion depends very heavily on the nature of trabecular bone acting as an elastic shock-absorber. The impulsive nature of the type of loading causing injury to the cartilage has been demonstrated in Apf. The frequencies in the force wave in the bone are in the same range with higher-frequency Fourier components. Apf showed that trabecular bone behaves purely elastically at certain frequencies. Thus for most of the components of the wave in the leg, the bone behaves elastically. The components of the wave that are at the resonant frequencies will not be damped out, due to considerable energy dissipation at resonance. The resonant behavior of trabecular bone is a way of supplying damping in an otherwise purely elastic medium. Extremely sharp force peaks would necessarily be absorbed by the trabecular bone, thus sparing the cartilage from injury.

Since the resonances are controlled by the structure of the trabeculae, it is expected that changes in the structure will change the resonance spectrum. The osteoarthritis proposed in this thesis involves a wiping out of lamellar bone and growth of calcified lamellar bone that later fully calcifies into lamellar bone. It is suggested that detailed studies of the resonance spectrum of trabecular bone from normal and osteoarthritic bones be made. Changes related to the degeneracy. Recent work has shown that the resonant frequency of long bones changes with age and with active diseases. This is more than likely due to

changes in the trabecular bone present in the ends of these long bones, as discussed in Section V.

Conclusions

1. Osteoarthritis occurs as a result of concurrent changes in bone and cartilage. The bone changes follow this sequence: increased stiffness in early development of the disease followed by decreased stiffness in later stages.
2. The lesion on the cartilage begins because of a local increase in stiffness in the underlying subchondral region. These areas have been observed in patients with known degenerative joints, and are shown to consist of dense patches of bone in an otherwise normal-appearing trabecular region.
3. Griffith-fracture is a possibility in trabecular bone, as well as fracture caused by a buckling mode of deformation.
4. The most probable mode of fracture in trabecular bone is fatigue. It is suggested that fatigue fracture plays a role in the development of structural changes observed in the course of osteoarthritis, by mediating remodelling in addition to the normal osteoclastic-osteoblastic type.¹⁴⁸
5. A normal joint is expected to exhibit microfractures. Similar to fatigue fracture remodelling in the tibial cortex of normal bone, remodelling in the trabecular region due to microfracture is probable, even in the absence of osteoarthritis.

VII. GENERAL CONCLUSIONS

1. Trabecular bone behaves purely elastically in the low audio range except at sharp resonant frequencies, under conditions of low strain-rate, low stress, and low strain.
2. Young's modulus of trabecular bone may depend on C_{Holes} or $v_{\text{v}}^{\text{Bone}}$, according to the type of microstructure.
3. The shock-absorbing properties of the bone in the knee are expected to show great local variation across the weight-bearing area.
4. Fatigue fracture in trabecular bone is important.
5. The structure and properties of trabecular bone are intimately related to osteoarthritis.

VIII. SUGGESTIONS FOR FUTURE WORK

1. Use a frequency analyzer in experiments similar to that in Appendix A. This would provide detailed information as to the frequencies present in force waves in the human skeleton and across the joints.
2. Measure the static (Instron) modulus and fracture behavior of samples of trabecular bone. See how the small-strain modulus compares with the dynamic data in Section III.
3. Set up and analyze computer models for structures with varying C_H and V_V , to determine analytically the dependences of modulus on these quantities.
4. Increase the batch of samples studied in Sections IV and VI, especially for Groups II and III. It would be interesting to see how the data for a new set of human specimens fit into the theories developed in this thesis.
5. Design and build a viscoelastometer of the type described by Ferry¹⁴⁹ and Fitzgerald.¹⁵⁰ This would be more versatile and easier to operate than the viscoelastometer used for this thesis.
6. Perform a critical experiment to determine if the resonances discussed in Section III are controlled by the lamellar spacing in the trabecular bone. A possible experiment would be to measure the resonance spectrum for several samples with widely varying lamellar spacing. This could be done for samples from different animals such as elephants, horses, etc. It would be interesting to characterize the resonance spectrum for both the cortical and trabecular bone from these animals.

7. Do a controlled study of the changes in the resonance spectrum for trabecular bone from Group 0, I, II, and III joints to see if the spectrum depends on the degree of degeneracy.
8. Run a set of rabbits on the impacting apparatus at varying dynamic loads to investigate the law of Weinmann and Sicher.
9. Run a set of rabbits until the joints totally deteriorate to investigate the formation of osteophytes in arthritic joints. The rabbits could be sacrificed at various intervals and examined as in Section III for mechanical properties and microstructure. The possibility of fatigue fractures could also be examined in such an experiment.
10. Complete the work already in progress on the mechanical properties of individual trabeculae. An extension of this work would be to examine the fatigue behavior of individual trabeculae in a specially-designed three-point bending apparatus.

IX. APPENDICES

APPENDIX A

RESPONSE OF THE HUMAN FRAME TO PHYSIOLOGICAL MECHANICAL LOADS

Introduction

It has been suggested in the literature that so-called "impulse loading" of the body during daily activity may be important in activating certain changes that bone is known to undergo.¹⁵¹ The hypothesis is that, even though we walk, for instance, at a rate equal to roughly one cycle per second, the actual rise time for the mechanical impulse through the skeleton is significantly higher than this and is in fact in the low audio frequency range. Opponents of this argument state that the shock absorbing properties of articular cartilage and soft tissues would insure that such relatively high frequencies would be severely attenuated.^{152,153} If they were present in the impulse at the heel, they would in all probability not be present in the femur or even in the tibia. Recent work^{154,155} has shown that articular cartilage does not attenuate peak forces. Only the periarticular soft tissues and bone have significant force-attenuating properties.

It is important to know the frequency components of the impulses that are transmitted by the human frame because it is well known that mechanical properties of some materials are extremely frequency-dependent. To determine meaningful mechanical properties of a material requires one to measure these properties under mechanical conditions as close as possible to those of the material in service (in vivo). It would be un-

reasonable to measure the static properties of a material and ascribe physiological importance to these measurements if the in service loading of the material is of a dynamic impulsive nature.

Experimental Procedure

An Endevco Model 2215 Accelerometer was securely strapped to the knee of a live, healthy human. Cloth straps and adhesive tape were used to ensure that the accelerometer was situated as tightly as possible just above the left medial condyle of the femur (Figure 74). The subject then ran in place at a frequency of about one per second. The subject was barefooted and was careful to impact his heel so that the accelerometer would pick up a reasonable signal. The output of the accelerometer was fed into a Kistler Model 504 Charge Amplifier and the output of this was fed into an oscilloscope (See Figure 75). A typical acceleration trace is shown in Figure 76. This was found to be exactly reproducible.

Results and Discussion

The acceleration trace depicted is very indicative of the shape of the mechanical impulse transmitted through the knee during running in place. Notice that the rise time of the first sharp peak is about 1.0 millisecond. If this is taken to be a sine wave, this corresponds to a frequency of 250 Hz. The peak is in fact slightly sharper than a sine and appears to resemble a triangular wave. This suggests that there are Fourier components in the impulse that are of much higher frequency than 250 Hz.

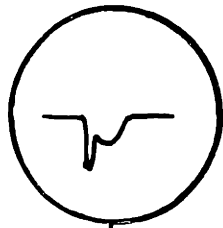


Figure 74: Placement of accelerometer above left medial condyle of femur.



rometer above left med .

OSCILLOSCOPE



CHARGE
AMPLIFIER

ENDEVCO 2215
ACCELEROMETER STRAPPED
OVER LEFT MEDIAL CONDYLE

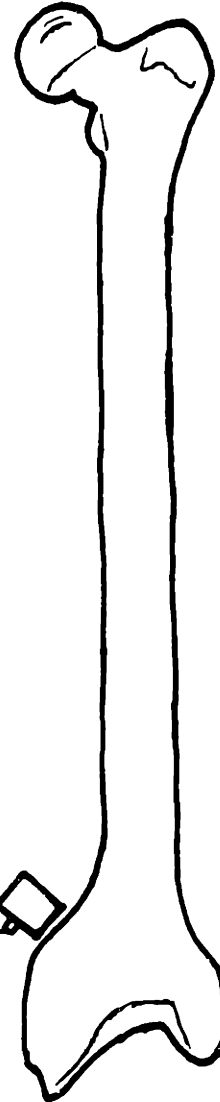


Figure 75: Schematic of instrumentation used in study.

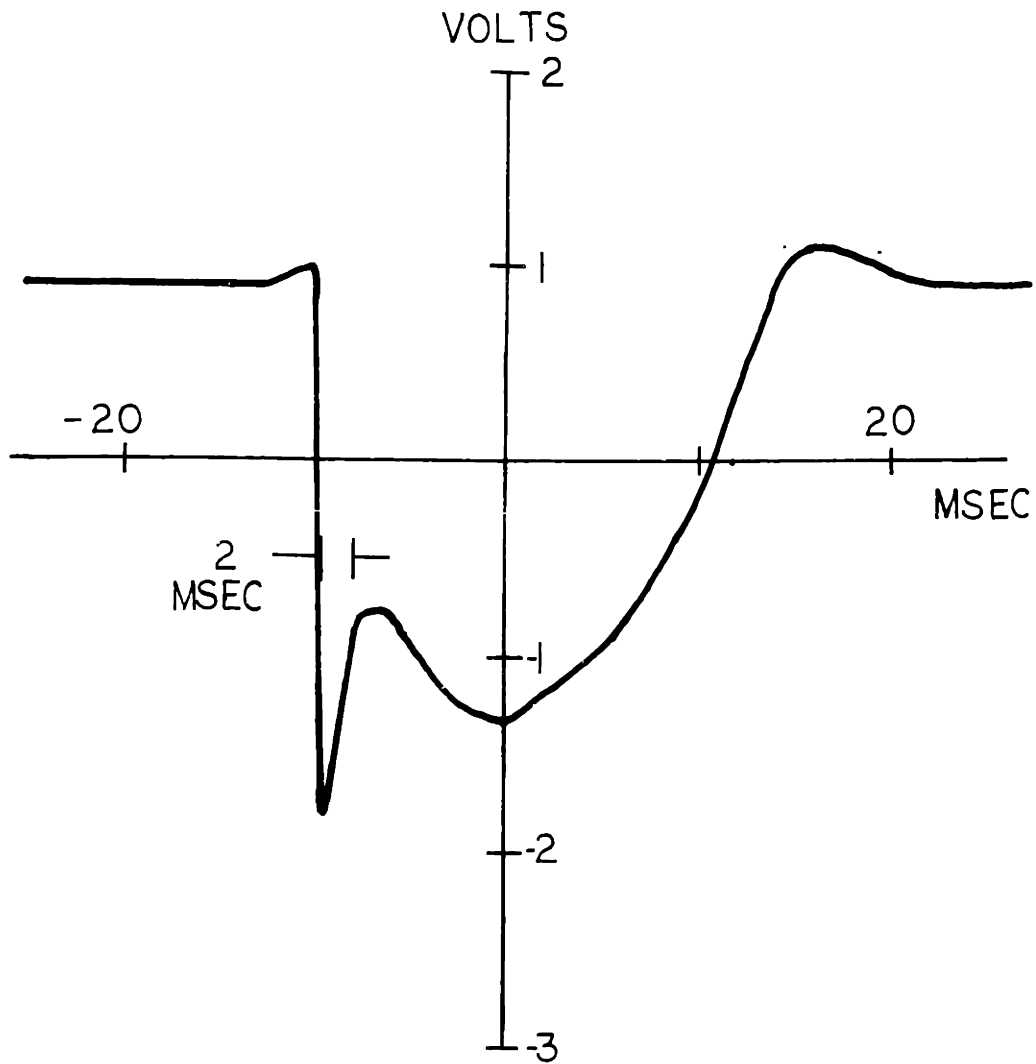


Figure 76: Typical plot of voltage output from accelerometer versus time for one step during running. The trace consists of two peaks, one sharp and one broad. Both correspond to frequencies in the low audio range, 250 and 10 Hz, respectively.

One may ask if running in place on the heel is really physiological. This method was chosen because it produced sharp, very reproducible traces in the experiment. The position of the accelerometer on the femur insures that some of the impulse is lost in the skin and soft tissue, and that the trace is only indicative of what is being transmitted through the knee. A change in the mode of running would be expected to alter both amplitudes and frequencies. It was found that even during normal walking the same general shape of the trace was produced, but with the first sharp peak severely attenuated. The suggestion is made that the sharp peak (probably at a slightly different frequency) is indeed present in the weight-bearing area of the knee during walking but is not picked up because of the placement of the accelerometer away from this area.

The broad peak in the trace corresponds to a frequency of 10 to 20 Hz. This was reproduced exactly during normal walking. This is not a pure sine wave either, and therefore has higher-frequency Fourier components. Thus in a strictly physiological situation, the mechanical impulse has a rise-time in the range of 1 to 10 milliseconds with higher-frequency components.

Conclusions

The mechanical impulses transmitted through the human knee under physiological conditions have rise times of the order of 1 millisecond. This corresponds to a steady-state dynamic load at 250 Hz. These impulses are found to have even higher-frequency components associated with them. Thus the hypothesis that the lower leg is capable of transmitting high-frequency impulses to the femur is verified.

APPENDIX B

CONSTANTS FOR CALCULATION OF MODULUS OF CERAMIC TEST
SPECIMEN IN SECTION IV

$$V = 134 \text{ volts; } \frac{1}{2}CV^2 = 2.34 \times 10^{-5} \text{ in-lbs}$$

$$E_1 = 7.7 \times 10^6 = E_3$$

$$l_1 = 0.125 \text{ inch, } A_1 = 0.197 \text{ in}^2, V_1 = 0.0246 \text{ in}^3$$

$$l_2 = 1.0 \text{ inch, } A_2 = 0.1 \text{ in}^2, V_2 = 0.1 \text{ in}^3$$

$$l_3 = 0.080 \text{ inch, } A_3 = 0.1 \text{ in}^2, V_3 = 0.008 \text{ in}^3$$

$$F = 85 \text{ lb.}$$

$$E = 7.2 \times 10^5 \sigma$$

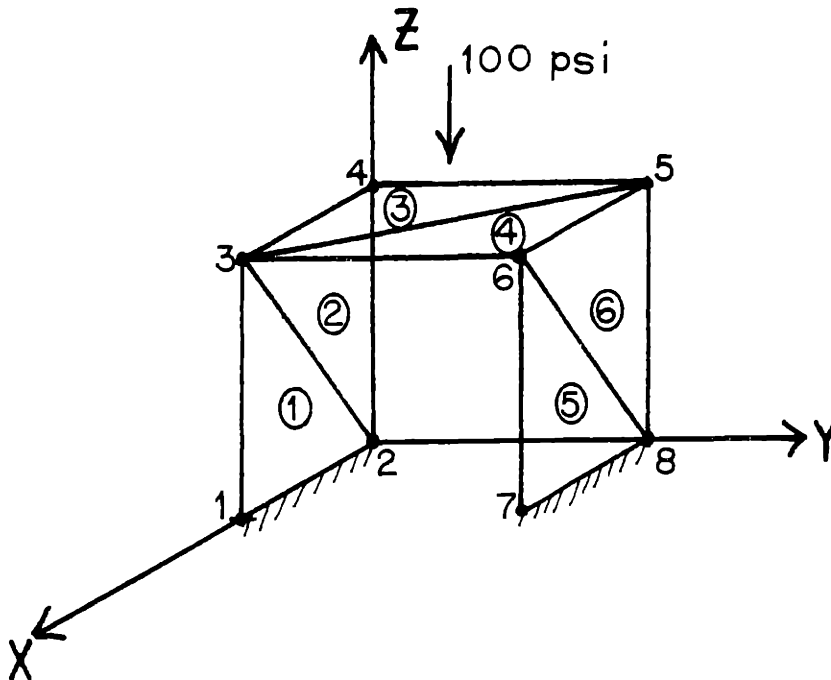
APPENDIX C

SAMPLE COMPUTER RUN FOR A SIMPLE PROBLEM

```

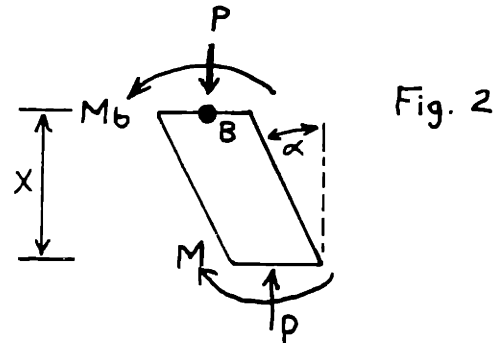
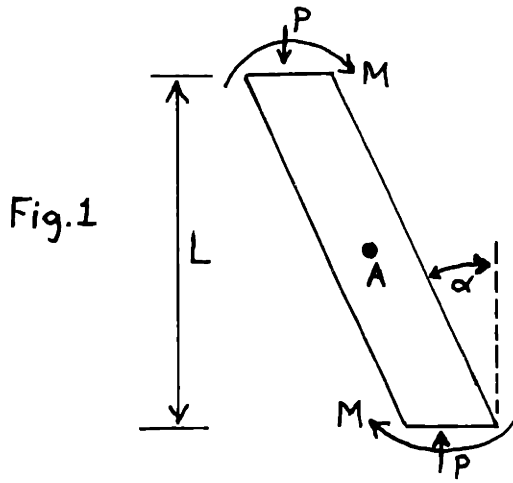
STRUDL 'SIMPLE PROBLEM' 'BONE ANALYSIS'
TYPE SPACE FRAME
DEBUG ALL
DUMP TIME
JOINT COORDINATES
1 1. 0. 0. S
2 0. 0. 0. S
3 1. 0. 1.
4 0. 0. 1.
5 0. 1. 1.
6 1. 1. 1.
7 1. 1. 0. S
8 0. 1. 0. S
ELEMENT INCIDENCES
1 3 2 1
2 2 3 4
3 3 5 4
4 5 3 6
5 6 8 7
6 8 6 5
UNITS LBS INCHES
ELEMENT PROPERTIES
1 TO 6 TYPE 'PBST' THICKNESS 0.003
CONSTANTS E 2000000.0 ALL
POISSON 0.3 ALL
LOADING 1 'TOP'
ELEMENT LOADS
3 TO 4 SURFACE FORCES GLOBAL PY -100.0
GLOBAL SURFACE FORCES
STIFFNESS ANALYSIS WITH REACTIONS NIP 3
LIST DISPLACEMENTS, STRESSES, STRAINS, FORCES, REACTIONS, ALL
FINISH

```



APPENDIX D

FREE-BODY DIAGRAM FOR INCLINED TRABECULA



To keep the inclined trabecula in a stable equilibrium there could be an external shear force or moment providing lateral support. The latter is assumed to provide the total amount of support needed to keep the trabecula from leaning over. It is evident that from Figure 1:

$$\sum F = P - P = 0$$

Summing the components of the moments about the center point A of the trabecula:

$$\sum M = 2P \frac{L}{2} \tan \alpha - 2M = 0$$

$$M = \frac{PL \tan \alpha}{2}$$

Therefore, at any point B along the trabecula given by the vertical distance x , (Figure 2) the moment equilibrium is as follows:

$$\sum M = Px \tan \alpha - M + M_b = 0$$

$$M_b = \frac{PL \tan \alpha}{2} - Px \tan \alpha$$

$$M_b = P \tan \alpha \left(\frac{L}{2} - x \right)$$

Thus, the internal bending moment in the trabecula is a function

of $(L/2 - x)$, and is a maximum at $x = 0, L$.

X. REFERENCES

1. Hans Elias, Three-Dimensional Structure Identified from Single Sections, *Science* 174, 3 December 1971, pp. 993-1000.
2. K. Piekarski, Fracture of Bone, *J. Appl. Phys.* 41, (1970), p. 217.
3. W. Bloom and D. W. Fawcett, A Textbook of Histology, W. D. Saunders Co., 1968, p. 224.
4. G. L. Kehl, The Principles of Metallographic Laboratory Practice, McGraw-Hill, 1949, Chapter 1.
5. Robert T. DeHoff and Frederick N. Rhines, Quantitative Microscopy, McGraw-Hill, 1968, pp. 56-58.
6. H. M. Frost, Preparation of Thin Undecalcified Bone Sections by Rapid Manual Technique, *Stain Technology* 33, (1958), pp. 273-277.
7. H. M. Frost, Staining of Fresh, Undecalcified, Thin Bone Sections, *Stain Technology* 34, (1959), pp. 135-146.
8. J. Wulff, The Structure and Properties of Materials, Vol. III, John Wiley, New York, 1965, pp. 198-199.
9. John D. Ferry, Viscoelastic Properties of Polymers, John Wiley, New York, 1961, pp. 41-43.
10. Elias D. Sedlin, A Rheological Model for Cortical Bone. A Study of the Physical Properties of Human Femoral Samples, *Acta Orthopædica Scandinavica, Supplementum 83 to Vol. 36*, 1965, pp. 45-51.
11. F. G. Evans, Stress and Strain in Bones, Charles C. Thomas Publisher, Springfield, Illinois, (1957).
12. James H. McElhaney and Edward F. Byars, Dynamic Response of Biological Materials, ASME Publication 65-WA/HUF-9 (1965).
13. James McElhaney, Nabih Alem, and Verne Roberts, A Porous Block Model for Cancellous Bone, ASME Publication 70-WA/BHF-2 (1970).
14. J. Galante, W. Rostoker, and R. D. Ray, Physical Properties of Trabecular Bone, *Calc. Tiss. Res.* 5, (1970), pp. 236-246.
15. Fred R. Rollins, Jr., Evaluation of Elastic Constants from Ultrasonic Reflection Measurements, *Int. J. of Nondestruct. Test.* 2, (1970), pp. 261-265.
16. Sidney B. Lang, Elastic Coefficients of Animal Bone, *Science* 165, (1969) pp. 287-288.

17. W. Abendschein and G. W. Hyatt, Ultrasonics and Selected Physical Properties of Bone, Clin. Orthopaedics and Rel. Res. 69 (1970) pp. 294-301.
18. Reference 10, pp. 61-68.
19. Albert H. Burstein and Victor H. Frankel, The Viscoelastic Properties of Some Biological Materials, Annals of the N.Y. Acad. of Science 146 (1968) pp. 158-165.
20. Reference 12.
21. John M. Urist, In Vivo Determination of the Elastic Response of Bone. I. Method of Ulnar Resonant Frequency Determination, Phys. Med. Biol. 15 (1970) pp. 417-426.
22. John N. Campbell and John M. Urist, Mechanical Impedance of the Femur, A Preliminary Report, J. Biomechanics 4 (1971) pp. 319-322.
23. S. A. V. Swanson and M. A. R. Freeman, Is Bone Hydraulically Strengthened? Med. & Biol. Eng. 4 (1966) pp. 433-438.
24. John D. Ferry, Viscoelastic Properties of Polymers, John Wiley, New York, 1961.
25. Edwin R. Fitzgerald and Alan E. Freeland, Viscoelastic Response of Intervertebral Disks at Audiofrequencies, Med. & Biol. Eng. 9 (1970) pp. 459-478.
26. Reference 25, p. 459.
27. Reference 24, Chapter 2.
28. Reference 24, Chapter 14, p. 310.
29. E. R. Fitzgerald, Mechanical Resonance Dispersion in Crystalline polymers at Audio-Frequencies, J. Chem. Phys. 27 (1957) pp. 1190-1193.
30. E. R. Fitzgerald, Dynamic Mechanical Properties of Polyvinyl Stearate at Audio-Frequencies, Journal of Applied Physics 29 (1958) pp. 1442-1450.
31. E. R. Fitzgerald, Crystalline Transitions and Mechanical Resonance Dispersion in Vinyl and Ethyl Stearate, Journal of Chem. Physics 32 (1960) pp. 771-786.
32. E. R. Fitzgerald, Mechanical Resonance Dispersion in Metal at Audio-Frequencies, Physical Review 108 (1957) pp. 690-706.
33. E. R. Fitzgerald, Mechanical Resonance Dispersion in Quartz at Audio-Frequencies, pp. 765-784; Mechanical Resonance Dispersion in Single Crystals, Physical Review 112 (1958) pp. 1063-1075.

34. Reference 25, pp. 474-476.
35. E. R. Fitzgerald, Particle Waves and Deformation in Crystalline Solids, Interscience Publishers, New York, 1966.
36. Reference 28, p. 42.
37. Bruce D. Wedlock and James K. Roberge, Electronic Components and Measurements, Prentice-Hall, 1969, p. 39.
38. Reference 24, pp. 456-457.
39. J. Wulff, The Structure and Properties of Materials, Vol. III, John Wiley, New York (1965) p. 231.
40. Reference 24, p. 310.
41. J. C. Wall, S. Chatterji, J. W. Jeffrey, On the Origin of Scatter in Results of Human Bone Strength Tests, Med. & Biol. Eng. 8 (1970) pp. 171-180.
42. Reference 13, p. 4.
43. W. Bonfield and C. H. Li, Deformation and Fracture in Bone, J. Appl. Phys. 38 (1966) pp. 2450-2455.
44. Reference 17, p. 299.
45. J. W. Smith and R. Walmsley, Factors Affecting the Elasticity of Bone, J. Anat. 93 (1970) pp. 294-301.
46. Jack L. Wood, Dynamic Response of Human Cranial Bone, J. Biomechanics 4 (1971), pp. 1-12.
47. Reference 12, pp. 4-6.
48. Reference 13, p. 4.
49. F. Gaynor Evans and Seong Bang, Differences and Relationships Between the Physical Properties and the Microscopic Structure of Human Femoral, Tibial, and Fibular Cortical Bone, Am. J. Anat. 120 (1967), p. 81.
50. J. D. Currey, The Mechanical Properties of Bone, Clin. Orthopaedics and Rel. Res. 73 (1970), pp. 210-220.
51. Eric L. Radin, I. L. Paul, and M. Lowy, A Comparison of the Dynamic Force Transmitting Properties of Subchondral Bone and Articular Cartilage, J. Bone and Joint Surgery 52-A (1970), p. 451.
52. Reference 12, p. 5.
53. Reference 10, pp. 52-60.

54. Melvin J. Glimcher and Stephen M. Krane, The Organization and Structure of Bone, and the Mechanism of Calcification, Harvard-MIT Musculo-Skeletal Block handout.
55. Reference 22, p. 321.
56. Reference 21, p. 421.
57. J. Wulff, The Structure and Properties of Materials, Vol. I-IV, John Wiley, New York, 1965.
58. J. Galante, W. Rostoker, and R. D. Ray, The Physical Properties of Trabecular Bone, Calc. Tiss. Res. 5 (1970), pp. 236-246.
59. J. McElhaney, Nabih Alem, Verne Roberts, A Porous Block Model for Cancellous Bone, ASME Publication 70-WA/BHF-2 (1970).
60. R. T. DeHoff and F. N. Rhines, Quantitative Microscopy, McGraw-Hill (1968).
61. E. L. Radin, J. W. Pugh, R. S. Steinberg, H. G. Parker, R. M. Rose, Trabecular Microfractures in Response to Stress: The Possible Mechanism of Wolff's Law, Accepted by Sicot Proceedings.
62. F. Gaynor Evans, Stress and Strain in Bones, Charles C. Thomas Publisher, Springfield, Illinois (1957), pp. 111-129.
63. J. Wolff, Ueber die Innere Architectur der Knochen und ihre Bedeutung fur de Frage vom Knochenwachstum, Virchow's Arch. Path. Anat. 50 (1870), pp. 389-453.
64. Joseph Trueta, Studies of the Development and Decay of the Human Frame, W. B. Saunders, Philadelphia, 1968, p. 316.
65. Reference 60, p. 49.
66. Reference 60, p. 79.
67. Reference 60, pp. 279-280.
68. J. Gurland, The Measurement of Grain Contiguity in Two-Phase Alloys, Trans. Met. Soc. AIME, August 1958, p. 452.
69. Eric L. Radin, Igor L. Paul, Marc J. Tolkoﬀ, Subchondral Bone Changes in Patients With Early Degenerative Joint Diseases, Arth. and Rheum. 13 (1970), pp. 400-405.
70. Arthur F. Kip, Fundamentals of Electricity and Magnetism, McGraw-Hill, New York, 1962, p. 86.
71. Reference 70, p. 69.

72. J. F. Nye, Physical Properties of Crystals, Oxford University Press (1967), p. 136.
73. Piezoelectric Technology Data for Designers, The Clevite Corporation, Piezoelectric Division, 232 Forbes Road, Bedford, Ohio, 44146, (1965), p. 33.
74. Elias D. Sedlin, A Rheological Model for Cortical Bone, *Acta Orthopædica Scandinavica*, Supplementum 83 to Vol. 36, 1965, p. 61.
75. Marc J. Tolhoff, S.M. Thesis, Department of Mechanical Engineering, MIT, 1971.
76. C. Gudmundson, Oxytetracycline-Induced Fragility of Growing Bones, An Experimental Study in Rats, *Clin. Orthop.* 77 (1971), p. 284.
77. Mervyn G. Hardinge, Determination of the Strength of the Cancellous Bone in the Head and Neck of the Femur, *Surg., Gyn., and Obstetrics* 89 (1949), pp. 439-441.
78. R. Miegel, R. Steinberg, T. Sikri, M. Monroe, personal communication.
79. Harold M. Frost, Dynamics of Bone Remodelling, Chapter 18 of Bone Biodynamics, Little, Brown, and Company, Boston (1964), pp. 316-318.
80. J. McElhany, N. Alem, V. Roberts, A Porous Block Model for Cancellous Bone, ASME Publication 70-WA/BHF-2 (1970).
81. Hans Elias, Three-Dimensional Structure Identified from Single Sections, *Science* 174, 3 December 1971, pp. 996-997.
82. E. D. Dyson, C. K. Jackson, W. J. Whitehouse, Scanning Electron Microscope Studies of Human Trabecular Bone, *Nature* 225 (1970), pp. 957- 959.
83. Dorland's Illustrated Medical Dictionary, W. B. Saunders Co., Philadelphia, 1965, p. 1598.
84. Benno Kummer, Photoelastic Studies on the Functional Structure of Bone, *Folio Biotheoretica* 6 (1966), p. 31.
85. Reference 84, p. 39.
86. W. Bloom and D. W. Fawcett, A Textbook of Histology, W. B. Saunders Co., 1968, pp. 256-257.
87. Eric L. Radin, Igor L. Paul, Current Comment: Joint Function, *Arth. and Rheum.* 13 (1970), pp. 276-279.
88. Eric L. Radin, Igor L. Paul, Failure of Synovial Fluid to Cushion, *Nature* 222 (1969), pp. 999-1000.

72. J. F. Nye, Physical Properties of Crystals, Oxford University Press (1967), p. 136.
73. Piezoelectric Technology Data for Designers, The Clevite Corporation, Piezoelectric Division, 232 Forbes Road, Bedford, Ohio, 44146, (1965), p. 33.
74. Elias D. Sedlin, A Rheological Model for Cortical Bone, *Acta Orthopædica Scandinavica, Supplementum 83 to Vol. 36*, 1965, p. 61.
75. Marc J. Tolkoff, S.M. Thesis, Department of Mechanical Engineering, MIT, 1971.
76. C. Gudmundson, Oxytetracycline-Induced Fragility of Growing Bones, An Experimental Study in Rats, *Clin. Orthop.* 77 (1971), p. 284.
77. Mervyn G. Hardinge, Determination of the Strength of the Cancellous Bone in the Head and Neck of the Femur, *Surg., Gyn., and Obstetrics* 89 (1949), pp. 439-441.
78. R. Miegel, R. Steinberg, T. Sikri, M. Monroe, personal communication.
79. Harold M. Frost, Dynamics of Bone Remodelling, Chapter 18 of Bone Biodynamics, Little, Brown, and Company, Boston (1964), pp. 316-318.
80. J. McElhany, N. Alem, V. Roberts, A Porous Block Model for Cancellous Bone, ASME Publication 70-WA/BHF-2 (1970).
81. Hans Elias, Three-Dimensional Structure Identified from Single Sections, *Science* 174, 3 December 1971, pp. 996-997.
82. E. D. Dyson, C. K. Jackson, W. J. Whitehouse, Scanning Electron Microscope Studies of Human Trabecular Bone, *Nature* 225 (1970), pp. 957- 959.
83. Dorland's Illustrated Medical Dictionary, W. B. Saunders Co., Philadelphia, 1965, p. 1598.
84. Benno Kummer, Photoelastic Studies on the Functional Structure of Bone, *Folio Biotheoretica* 6 (1966), p. 31.
85. Reference 84, p. 39.
86. W. Bloom and D. W. Fawcett, A Textbook of Histology, W. B. Saunders Co., 1968, pp. 256-257.
87. Eric L. Radin, Igor L. Paul, Current Comment: Joint Function, *Arth. and Rheum.* 13 (1970), pp. 276-279.
88. Eric L. Radin, Igor L. Paul, Failure of Synovial Fluid to Cushion, *Nature* 222 (1969), pp. 999-1000.

89. Albert H. Burstein, Bernard W. Shaffer, Victor H. Frankel, Elastic Analysis of Condylar Structures, ASME Publication 70-WA/BHF-1 (1970), pp. 10-11.
90. George Piotrowski and George A. Wilcox, Jr., The STRESS Program: A computer Program for the Analysis of Stresses in Long Bones, J. Biomechanics 4 (1971), pp. 497-506.
91. A. E. H. Love, The Mathematical Theory of Elasticity, Cambridge University Press, 1927.
92. J. P. Timshenko and J. M. Goodier, Theory of Elasticity, McGraw-Hill, New York, 1970.
93. O. C. Zienkiewicz, The Finite-Element Method in Engineering Science, McGraw-Hill, London, 1971.
94. Robert M. Hackett, Viscoelastic Stresses in a Composite System, Polymer Eng. and Science 11 (1971), pp. 220-225.
95. P. E. Chen, Strength Properties of Discontinuous Fiber Composites, Polymer Eng. and Science, 11 (1971), pp. 51-56.
96. Reference 93, Section 2.4, pp. 26-28.
97. Robert D. Logcher, et al., ICES STRUDL II, Vol. I - Frame Analysis, Research Report R68-91 (1968); and Vol. II - Additional Design and Analysis Facilities, Research Report R70-77 (1971), Department of Civil Engineering, Massachusetts Institute of Technology.
98. McDonnell - ECI ICES STRUDL USER'S MANUAL FOR PBST FINITE ELEMENT, Engineering Computer International, Inc., 1073 Massachusetts Avenue, Cambridge, Massachusetts 02138.
99. Charles H. Norris and John Benson Wilbur, Elementary Structural Analysis, McGraw-Hill, 1960, pp. 558-566.
100. Reference 84, p. 32.
101. G. N. Savin, Stress Concentration Around Holes, Pergamon Press, 1961, p. 305.
102. Reference 101, p. 73.
103. Reference 101, p. 321.
104. J. Wulff, The Structure and Properties of Materials, Vol. III, John Wiley, Section 7.3, pp. 145-148.
105. Daniel C. Drucker, Introduction to Mechanics of Deformable Solids, McGraw-Hill, 1967, Chapter 16.
106. Stephen H. Crandall and Norman C. Dahl, An Introduction to the Mechanics of Solids, McGraw-Hill, 1959, p. 406.

107. Raymond J. Roark, Formulas for Stress and Strain, McGraw-Hill, 1943, p. 293.
108. Reference 106, p. 292.
109. Hiroshi Yamada, Strength of Biological Materials, Williams and Wilkins Co., Baltimore, 1970, pp. 19-34.
110. J. D. Currey, The Mechanical Properties of Bone, Clin. Orthopaedics and Rel. Res. 73 (1970), p. 217.
111. F. G. Evans, Relation of the Physical Properties of Bone to Fractures, ASOS Instruct. Course for Lecturers 18 (1961), pp. 110-121.
112. F. G. Evans, Stress and Strain in Bones, Charles C. Thomas Publisher, 1957, Chapter 14, pp. 176-202.
113. R. D. McLeish and S. Habboobi, Strain Gauge Techniques for Cadaveric Bone, Engineering in Medicine 1 (1972), p. 37.
114. F. G. Evans, Biomechanical Studies of the Musculo-Skeletal System, Charles C. Thomas, Springfield, Illinois, 1961, Chapter 3.
115. Reference 80.
116. Harold M. Frost, Introduction to Joint Biomechanics, Henry Ford Hospital Bulletin 8 (1960), p. 422.
117. Reference 82.
118. Reference 105, p. 423.
119. M. A. R. Freeman, W. H. Day, and S. A. V. Swanson, Fatigue Fracture in the Subchondral Bone of the Human Cadaver Femoral Head, Med. & Biol. Eng. 9 (1971), p. 625.
120. Joseph Trueta, Studies of the Development and Decay of the Human Frame, W. B. Saunders, Philadelphia, 1968, p. 336.
121. L. C. Rosenberg, Chemical Basis for Histological Use of Safranin Red-0 in the Study of Articular Cartilage, Presented to the Orthopedic Research Society, January 1970, Chicago, Illinois.
122. Eric L. Radin, Igor L. Paul, Marc J. Tolkoff, Subchondral Bone Changes in Patients With Early Degenerative Joint Disease, Arth. & Rheum. 13 (1970), pp. 400-402.
123. Reference 122, p. 403.
124. Eric L. Radin, Igor L. Paul, Robert M. Rose, Hypothesis: Role of Mechanical Factors in the Pathogenesis of Primary Osteo-Arthritis, The Lancet 1 (1972), pp. 519-522.

125. Harold M. Frost, Introduction to Joint Biomechanics, Henry Ford Hospital Bulletin 8 (1960), p. 430.
126. Caspar Wistar, A System of Anatomy, Vol. I, H. C. Carey and I. Lea Publishers, Philadelphia, 1825, p. 2.
127. E. L. Radin, I. L. Paul, M. Lowy, A Comparison of the Dynamic Force Transmitting Properties of Subchondral Bone and Articular Cartilage, J. Bone and Joint Surgery 52-A (1970), pp. 444-456.
128. E. L. Radin, I. L. Paul, Does Cartilage Compliance Reduce Skeletal Impact Loads? The Relative Force-Attenuating Properties of Articular Cartilage, Synovial Fluid, Periarticular Soft Tissues, and Bone, Arth. & Rheum. 13 (1970), pp. 139-144.
129. Charles E. Crede, Shock and Vibration Concepts in Engineering Design, Prentice-Hall, Inc., 1965, p. 128.
130. Reference 129, p. 135.
131. Reference 125, pp. 421-423.
132. M. A. R. Freeman, W. H. Day, and S. A. V. Swanson, Fatigue Fracture in the Subchondral Bone of the Human Cadaver Femoral Head, Med. & Biol. Eng. 9 (1971), pp. 619-629.
133. Reference 120, p. 342.
134. James M. Morris and Loren D. Blickenstaff, Fatigue Fractures - A Clinical Study, Charles C. Thomas, Springfield, Illinois, 1967.
135. Reference 134, p. 6.
136. Joseph P. Weinmann and Harry Sicher, Bone and Bones: Fundamentals of Bone Biology, The C. V. Mosby Co., St. Louis, 1947, pp. 121-122.
137. L. C. Johnson, H. T. Stradford, R. W. Geis, J. R. Dineen, E. R. Kerley, Hostogenesis of Stress Fractures, Armed Forces Institute of Pathology Lectures, 1963.
138. Reference 134, p. 8.
139. Reference 134, pp. 66-75.
140. Reference 134, p. 139, 147.
141. K. Piekarski, Fracture of Bone, J. Appl. Phys. 41 (1970), pp. 215-223.
142. Reference 122.

143. J. Trueta, Studies on the Etiopathology of Osteoarthritis of the Hip, *Clin. Ortho.* 31 (1963), pp. 13-15.
144. J. C. Runkle, J. W. Pugh, R. M. Rose, The Mechanical Behavior of Single Trabeculae, in preparation.
145. R. E. Reed-Hill, Physical Metallurgy Principles, D. Van Nostrand, Princeton, 1967, p. 559.
146. Harold L. Frost, Presence of Microscopic Cracks In Vivo in Bone, *Henry Ford Hospital Med. Bulletin* 8 (1960), pp. 23-35.
147. John M. Jurist, In Vivo Determination of the Elastic Response of Bone -- II. Ulnar Resonant Frequency in Osteoporotic, Diabetic, and Normal Subjects, *Phys. Med. Biol.* 15 (1970), pp. 427-434.
148. Reference 79.
149. Reference 24, Chapters 6 - 9.
150. Reference 25, pp. 462-463.
151. E. L. Radin, I. Paul, R. Rose, Hypothesis: Role of Mechanical Factors in the Pathogenesis of Primary Osteoarthritis, *The Lancet* 1 (1971), pp. 519-522.
152. A. R. Mettam, Comments in Symposium on Biomechanics, *Instit. of Mech. Eng., London*, 1959, p. 44.
153. R. K. White, The Rheology of Synovial Fluid, *J. Bone & Joint Surg.* 45-A (1963), pp. 1004-1090.
154. E. L. Radin, I. L. Paul, M. Lowy, A Comparison of the Dynamic Force Transmitting Properties of Subchondral Bone and Articular Cartilage, *J. Bone and Joint Surg.* 52-A (1970), pp. 444-456.
155. E. L. Radin, I. L. Paul, Does Cartilage Compliance Reduce Skeletal Impact Loads? The Relative Force-Attenuating Properties of Articular Cartilage, Synovial Fluid, Periarticular Soft Tissues and Bone, *Arth. and Rheum.* 13 (1970), pp. 139-144.

BIOGRAPHICAL NOTE

The author was born in Chicago, Illinois, on January 4, 1946. He grew up in Richmond, Virginia, and attended public schools there, graduating from John Marshall High School in June 1964.

After entering MIT in September 1964, he received his Bachelor of Science degree in June 1968, in Metallurgy and Materials Science. During the summers of his undergraduate career, he was employed at the Metallurgical Research Division of Reynolds Metals Company in Richmond, which gave him an invaluable opportunity to apply the concepts studied at MIT.

In September 1968 the author enrolled as a graduate student in the Department of Metallurgy and Materials Science at MIT. He worked for three years as a teaching assistant in physical metallurgy and structure-properties courses, and found himself enthralled with teaching. During this time he began his research in biological materials, and found the contacts with people in the medical profession very exciting.

During his career at MIT, the author was president of the Student Metallurgical Society and the MIT Graduate Student Council. He was also very active on the departmental Graduate Metallurgy Committee and Undergraduate Curriculum Committee. For one year he also served on the American Society for Metals Young Members' Committee (a national committee), and co-chaired an art exhibit entitled "Materials Used with Imagination" at the 1970 Metals Show in Cleveland. He is a member of the ASM, the AIME, The Society of the Sigma Xi, Phi Lambda Upsilon Honorary Chemical Society, and Theta Chi Social Fraternity.

On June 21, 1969, he was married to the former Barbara Seward Hellegers of Rutherford, New Jersey, and has cherished her support and understanding in his professional and social endeavors.